ALEXANDRE LEONDARIDIS

Universidade de São Paulo
Escola Politécnica

INFLUENCE OF SEPIOLITE ADDITION ON THE PHYSICAL AND MECHANICAL PROPERTIES OF FIBRE-REINFORCED CEMENT

São Paulo 2006

ALEXANDRE LEONDARIDIS

INFLUENCE OF SEPIOLITE ADDITION ON THE PHYSICAL AND MECHANICAL PROPERTIES OF FIBRE-REINFORCED CEMENT

Dissertation presented at the Polytechnic Faculty of the São Paulo University in order to obtain the degree in engineering

Area:
Materials and metallurgical engineering department

Supervisor:
Prof. Antonio Carlos Viera Coelho

São Paulo
2006

Acknowledgments

First, I would like to thank Prof. Antonio Carlos Viera Carlos, the director of this project, for giving me the opportunity to participate in such a challenging research study.

I would also like sincerely thank Dr. Cleber Dias for its day to day assistance for shearing his knowledge with me and for his precious technical advice. Without his participation, the completion of this work would not have been possible.

I would personnally like to thank Miss Kelly Kodama for assisting me in the daily experiment and the dissection of my results.

Mr Rui Barbosa de Souza has been invaluable to me throughout his technical know-how. Without him, the realisation of my experiments would not have successfull.

Finally, I want to give a special thanks to the whole staff of the Microstructural Department of Civil Engineering within the Polytechnic Faculty, for their happiness which made the work easier.

Abstract

This study is part of a project aiming at analysing the behaviour and properties of PVA cellulose fibre-reinforced cement, and has been conducted in the Microstructural Department of Civil Engineering within the Polytechnic Faculty of the University of Sao Paulo. This project was born from the necessity of substituting asbestos fibres from the fibre cement product. In the light of this, the project allows the study of the influence of the addition of new materials in the fibre cement composite. Remarkable results were obtained thanks to the sepiolite addition, especially on the fresh state study where an augmentation of the strain and the load capacity of the material has been outlined.

Resumo

Este estudo é parte de um Projeto de Pesquisa, conduzido no Laboratório de Microestrutura do Departamento de Engenharia Civil da Escola Politécnica da Univesidade de São Paulo, que tem por objetivo a análise do comportamento e das propriedades de produtos de fibro-cimento à base de PVA e fibra de cellulose. Esse projeto nasceu da necessidade de substituição das fibres de amianto nos produtos de fibro-cimento. Tendo esse enfoque, o projeto procurou estudar o efeito da adição de novos materiais no compósito de fibro-cimento. Resultados muito interessantes foram obtidos graças à adição de sepiolita, especialmente no estado fresco, onde o aumento da resistência mecânica do material pôde ser observado.

Figures

Tables

Table of contents

1. Introduction

1.1.Generalities

The fibre-reinforced cement is made from hydraulic cement, discontinuous fibres as well as other additives. Since 1900, with the development of the first real widely used composite, asbestos cement, its popularity never stopped to increase. In particular, it is used for corrugated sheets destined for the building industry; targeting the manufacturing and the residential sector. A broad range of applications involve the utilization of fibres cement sheets, roof covering, cladding, façade coating, construction of walls ... Its popularity is due to the numerous applications of this material and the easiness of production. Indeed, since the beginning of asbestos cement production, the Hatscheck process remains the most common way to produce fibres cement corrugated sheets. The principle of this process is quite simple: first fresh planar fibres cement sheet are formed according to this process, and then they are undulated by simple deposit of the fresh fibre cement sheet on a corrugated mould.

The main drawback in the corrugated sheet fabrication is the apparition of cracks when the sheets reach their final undulated shape, thus ruining their physical and mechanical properties. This is caused by the low plastic strain capability of the material used. This has become a real issue since the prohibition of asbestos in most of the countries.

Indeed, unreinforced cementitious material is brittle, characterised by low tensile strength and low tensile strain capacities. However, it holds out an excellent durability, a good compression resistance and a low cost. This can explain the keen interest for reinforced cementitious materials nowadays. A lot of fibres are commonly used to reinforce cement matrix, steel fibres, glass fibres, synthetic or natural fibres. The most common one used to be asbestos.

Asbestos is a general name given to a variety of crystalline fibrous silicates. This material gained popularity because it holds out optimal isolating, chemical resistance, mechanical resistance and thermal properties. Asbestos fibres also show an excellent interaction with the Portland cement, which is a real asset. Its compatibility with the Hatschek process seems to be unbeatable, since it is an excellent flocculating agent. The lack of asbestos caused the loss of fine cement particles during the Hatschek process through the big cylinder aiming at forming the fibre cement film. This resulted in the decrease of productivity

of the Hatsckek process, as well as dramatic loss of final product's mechanical properties. Moreover, asbestos fibres' low cost justifies its utilisation in numerous fibre cement products.

The prohibition of asbestos in most of the countries of the world forced the creation of numerous research projects aiming at finding new materials capable of replacing asbestos fibres. At first, the majority of the conducted projects focused on the simple substitution of asbestos fibres by a large variety of other new fibres, but considered only their mechanical, chemical or dimensional characteristics. Most of these replacements were unsuccessful, never leading to properties similar to the ones obtained with asbestos. Indeed, the fibre cement composite thus created behaved differently during the process of fabrication, resulting in a product with poor mechanical properties, due to high porosity and bad fibres-matrix interactions. Consequently, researchers turned their efforts towards ideas other than a simple fibre substitution. Modifications of the cement matrix combined with the substitutions of asbestos fibres by alternative ones were experimented in order to decrease the alkalinity of the environment, improve the fibre-matrix interactions and increase the compatibility with the Hatschek process. The addition of cellulose fibres in the cement matrix is largely used nowadays; because of its high compatibility with the Hatschek process, particles retention properties during the filtration stage and its low cost. The line of research nowadays concerns the addition of new fibres to the cellulose reinforced matrix, in order to improve the mechanical properties and the durability of the fibre cement product. In particular, Polyvinyl Alcohol (PVA) fibres are commonly used to reinforce the fiber cement composite and show great potential in the substitution of asbestos.

When using this type of fibres, an appropriate flocculating agent is required to guarantee proper particle retention and to control the dewatering speed rate during the Hatschek process. This is a crucial aspect in order to obtain a fibre cement product with fine mechanical properties. Nowadays in the industrial sector, the quality of the Cellulose-PVA fibre cement depends mainly on the flocculating agent as well as its optimal amount addition. According to current literature on the subject, a polymer from the family of the polyacrilamides is commonly used with an amount of about 0,1% of weight. But this flocculating agent remains very expensive, and many have studied its potential substitution with a cheaper one.

1.2.Objectives and study context

This study is part of a project aiming at analysing the behaviour and properties of cellulose fibre cement, and has been conducted in the Microstructural Department of Civil Engineering within the Polytechnic Faculty of the University of Sao Paulo. This project was born from the necessity of substituting asbestos fibres from the fibre cement product. In the light of this, the project allows the study of the influence of the addition of new materials in the fibre cement composite. The laboratory is equipped with installations that allow a perfect simulation of the fabrication process and an adequate characterization of the fibre cement composite. Moreover, the team involved in this project remains the same, which makes possible the transmission of knowledge and provides the tools to conduct an efficient research.

This research aims at studying the influence of a specific type of clay called sepiolite on the physical and mechanical behaviour of PVA-cellulose fibre cement.

Two kinds of sepiolite are used in this work, the first one commercially called Tolsa originates from Spain, and the other one called Dolsan is from Turkey. Sepiolite is known for its remarkable superficial properties and hence a flocculating behaviour is expected. A possible bridging effect between the fibres and the cement matrix can make it an interesting additive to the fibre cement composite.

A quantitative study has been conducted to emphasize the effect of the addition of sepiolite on the physical mechanical properties of PVA-cellulose fibre cement sheet.

The first part of this report reviews the basic notion of fibre cement with a specific section on PVA-cellulose reinforcement. It also presents simple notions about colloidal systems, which are crucial to understand the flocculation phenomenon. A synthesis is done about the principal sepiolite characteristics as well as a brief presentation of the industrial Hatschek process.

The second part deals with the materials and the methods used during the study. A physical characterization of each material has been conducted and all the results are gathered in annex for commodity reason. A detailed description of the sample preparation including the

casting stage is presented. And finally, a description of the different mechanical tests conducted on the samples is done.

The last part of the report exhibits the results and the analysis of the entire study as well as the conclusion on the investigation.

2. Bibliography

2.1.Portland cement basic notions

Portland cement is prepared by firing an original mixture of chalk ($CaCO_3$) and clays S_2AH_2 (This reduced nomenclature is specific to the cement chemistry and is detailed at the end of this part). This cement is thus named because its inventor, Jo Aspin, used a special stone coming from the Portland Island to prepare it. The firing of these components gives three products according to the following equation:

$$CHALK + CLAYS = C_3A + C_2S + C_3S$$

Most of the people think that the cement hardens by a drying. But actually it is the opposite according basically to two hydration group of reactions. The first one which is fast, causing the cement to set, takes place during the first 4 hours according to:

$$C_3A + 6H = C_3AH_6 + Heat$$

Physically, this step in the hardening of cement is materialized by the coating of the cement powder grain by a gelatinous envelope of C_3AH_6. This gelatinous envelope allows the bridging between each grain which gives birth to a network. These bounds are weak and can be easily broken but quickly form again.

The second group of reaction involves the hardening step of the cement. It starts after about 10 hours and can last more than 100 days. The two main reactions involved in stage are:

$$2C_2S + 4H = C_3S_2H_3 + CH + Heat$$
$$2C_3S + 6H = C_3S_2H_3 + 3CH + Heat$$

The main product of this reaction, $C_3S_2H_3$, is called Tobomorite gel. The hardening mechanism is quite amazing. Water penetrates into the coated cement grain through the gelatinous envelope of C_3AH_6. As the water enters into the bulk thanks to the high concentration of calcium contained in it, the pressure increases and thus high concentrated solution of C_2S and C_3S is ejected into the surrounding water. This water hydrates these

components leading to the formation of sea ursine-like spines of the Tobomorite gel. The liquid is pumped thanks to the osmotic pressure and react along the spines. It ends up when all the reactants are gone. These needle-like spines can give birth to real meshes that facilitate the hardening of the cement [1].

Reduced nomenclature:

- Lime CaO = C
- Alumina Al_2O_3 = A
- Silica SiO_2 = S
- Water H_2O = H

2.2.Fibre-reinforced cement

2.2.1. Generalities

Portland cement, like most cement, is a brittle material with a low tensile strength and strain capacities. In this measure, a corrugated sheet made only with Portland cement would not be able to fulfil its mechanical requests such as supporting the stress. But the fibres are not used to increase the strength of the cement even if sometimes a little improvement can be obtained; they are used because of their ability of controlling the cracking of cement. Thus, they improve the ductility of the material and therefore the energy absorption capacity of it.

Fibre reinforced cement can be defined as a material made from a hydraulic cement and discrete, discontinuous fibres. Fibre reinforced cements are constituted of three different phases, the matrix, the fibre and the interface matrix-fibre. All of these three phases influence the mechanical behavior of the fibre reinforced cement.
Nowadays, a wide range of fibres types is used. There are many types of fibres:

- Steel fibres
- Glass fibres
- Asbestos fibres

- Synthetic fibres (Polypropylene, Carbon fibres, Kevlar fibres, acrylic fibres, Polyvinyl Alcohol (PVA) fibres...)
- Natural fibres such as cellulose- pulp

The mechanical properties of the reinforced cement do not only depend on the fibres ones. Indeed, they depend on the shape of the individual fibres and their dispersion in the cementitious matrices.

The individual fibres can be classified according to their arrangement in the cementitious matrices. They belong either to the monofilament or to the bundle fibres group. In fibre reinforced cement, the main part played by the fibres occurs once the cracking happened. Indeed, when cracking occurs in the brittle matrix, the load is transferred to the fibres that act as bridges across cracks. Therefore, the two post-cracking functions of them are: Providing an increase of strength by transferring stresses and loads across the crack, and increasing the toughness of the composite with their energy absorption capacity.
Usually for composite materials, to estimate mechanical properties such as the strength and the modulus of elasticity, the "rule of the mixtures" can be applied. Assuming that the two components are linear elastic and the bond between them is perfect, the modulus of elasticity E_c and the first crack stress σ_{mu} of the composite can be expressed as followed:

$$E_c = E_m V_m + \eta_l \eta_\vartheta E_f V_f \quad \textit{Equation 1}$$

$$\sigma_{mu} = \sigma_m V_m + \eta_l \eta_\vartheta \sigma_f V_f \quad \textit{Equation 1}$$

where:

- E_c, E_m, E_f are the modulus of elasticity of the composite, the matrix and the fibre.
- σ_{mu} is the first crack stress of the composite in tension
- σ_m is the tensile strength of the matrix without fibre reinforcement
- σ_f is the stress in the fibre at the first crack strain
- V_m and V_f are the volumetric fractions of the matrix and the fibres
- η_l and η_ϑ are the longitudinal and oriental efficiency factors in pre-cracked zone

As said previously, a significant contribution of the fibres is obtained in the post-cracking zone. This is obvious on *Equation 1* and *Equation 2* as V_m is much higher than V_f (typical values are around 5%). Thereby, in the post-cracking zone the effect of the matrix is negligible, thus the *Equation 2* can be reconsidered to estimate the tensile strength σ_{cu} of the fibre reinforced cement:

$$\sigma_{cu} = \eta_l \eta_\vartheta \sigma'_f V_f \quad \textit{Equation 2}$$

where:

- η_l and η_ϑ are the longitudinal and oriental efficiency factors in pre-cracked zone
- σ'_f is the tensile strength of the fibre
- V_f is the volumetric fraction of the fibres

The toughness is also an important propriety for sheet of fibre reinforced cement. It is directly linked with the ability of absorbing energy during impacts. These sheets are often submitted to impacts either during the utilization or during transport.

All these mechanical improvements to the brittle cementitious matrix are the result of the fibre-cement interaction. Two phenomena are controlling these improvements: how the stress is transferred from the matrix to the fibre and after, the bridging behavior of the fibre across the cracked matrix. Depending on the interfacial characteristics, during the cracking of the brittle matrix, the fibre can either break or be pulled out. The energy required for the latter is greater. To understand the pull out mechanism, considerations must be done for the pre-cracking zone and the post cracking zone separately.

During the pre-cracking stage, the fibre and the matrix are perfectly bonded i.e. the displacement involved during the deformation are geometrically coherent. Thus, the mechanism running the pre-cracking stage is the elastic stress transfer. A non uniform shear stress is distributed along the interface in order to distribute the load between the fibre and the matrix.

During the post-cracking stage, debonding between the matrix and the fibre occurs. A relative difference of displacement exists between the two components of the composite, and the dominant mechanism controlling this stage is the frictional slip. Frictional stress is

uniformly distributed along the interface. Ultimate strength and strain are determined by this stage.

A typically interfacial shear stress x displacement can be obtained *Figure 1*.

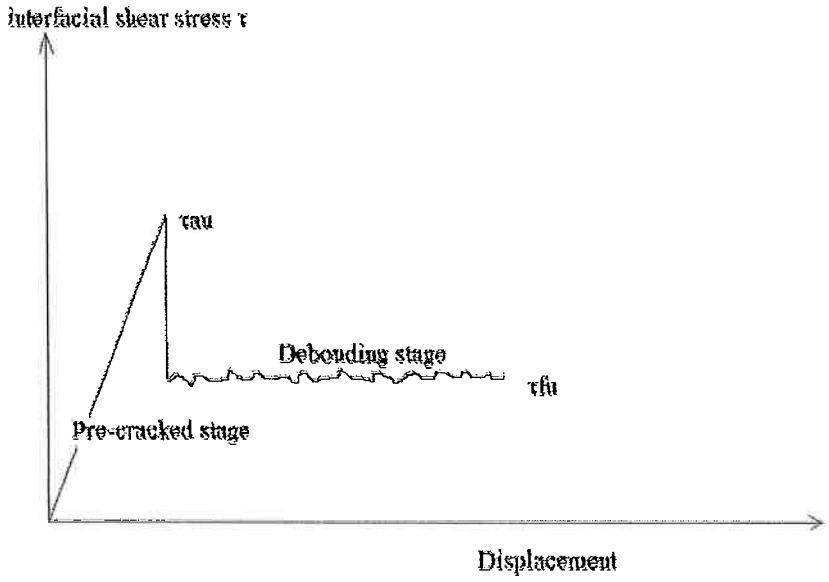

Figure 1- Ideal interface shear stress-displacement curve

τ_{au} represents the shear bond strength and τ_{fu} the maximum frictional shear stress interface. The values of these shear stresses depend on the properties of the cementitious matrix, of the fibre but mostly of the interface characteristics [2].

2.2.2. *Cellulose and PVA fibres*

As said in the introduction, the success of asbestos-cement is based on the excellent compatibility of asbestos fibres with the Portland cementitious matrix and the mechanical properties obtained. Indeed, asbestos fibres possess a high modulus of elasticity as well as high strength. The great affinity of asbestos fibre with Portland cement matrix allows a good dispersion of the bundle. Asbestos fibres are highly compatible with Hatschek process which guarantees an easy production of asbestos fibre cement sheet. The only inconvenient is low toughness of the cement composite.

Since the discovery of health damage caused by asbestos fibres, nowadays their replacement is subjected to many studies. In particular, their substitution by cellulose and Polyvinyl Alcohol (PVA) fibres is of great interest. Cellulose fibres have lower mechanical properties than asbestos fibres, lower strength and stiffness but they can increase the strain capacity. They are highly compatible with the Hatschek process and can be used for total or partial substitution of asbestos fibres [2].

High strength PVA fibres are also being developed for asbestos replacement. After surface treatment of the polymer in addition with its natural hydrophilic behavior (due to the presence of hydroxyl groups) a good affinity with cement matrix can be obtained: strong bond and excellent dispersion. Cement matrix reinforced with PVA fibres can present similar mechanical properties to those of asbestos-cement, especially for the toughness and the strength. They present a good resistance to alkali environment and preserve their mechanical properties through time. Their drawback is low adaptability to the Hatschek process. In this measure, their volume addition is limited. Therefore, they are often used in addition with other natural fibres to balance this inconvenience [3].

Fibre cement reinforced with cellulose and PVA fibres generally present a lower mechanical strength but a higher toughness than asbestos-cement. In addition, it shows a higher ductility which is an asset in production of fibre cement sheets.

The following table *Table 1* presents the principal mechanical characteristics of PVA, cellulose and asbestos fibres as well as their adaptability to the Hatschek process.

Table 1- Properties of some fibres used in the fibre cement production

Fibres	Tensile strength (MPa)	Modulus of elasticity (GPa)	Ultimate strain	Resistance to alkali environment	Adaptability to the Hatschek process
Asbestos	3100	162	2,0-3,0	Good	Good
Cellulose	300-500	10	_	Bad	Good
PVA	900-1300	20-35	10-20	Good	Bad

2.3.Colloidal systems and zeta potential

2.3.1. Colloidal systems presentation

One refers to a colloidal system when one of the fundamental states (solid, liquid, gas) is dispersed in another and when the dimension of the dispersed state is microscopic. In our study, we will focus more on solid in suspension in liquid solution. These colloidal systems have great practical properties.

These particles in solution can have different behavior, they can be dispersed or in some specific circumstances, they may adhere to one another and form aggregates of successively increasing size *Figure 2*. This process is called flocculation and the aggregates thus formed flocs. These flocs can sediment in the base solution confining smaller particles present in the solution. A third phenomenon, called coagulation, can appear if the aggregates become denser. In the literature, the terms of coagulation and flocculation are often confused. Actually, the word of flocculation is kept for a long distance particles interaction, involving lower energy minimum, while coagulation is used when the interfaces are in contact which involves relatively high attraction energy. Furthermore, flocculation is said to be a reversible process while coagulation is irreversible [5].

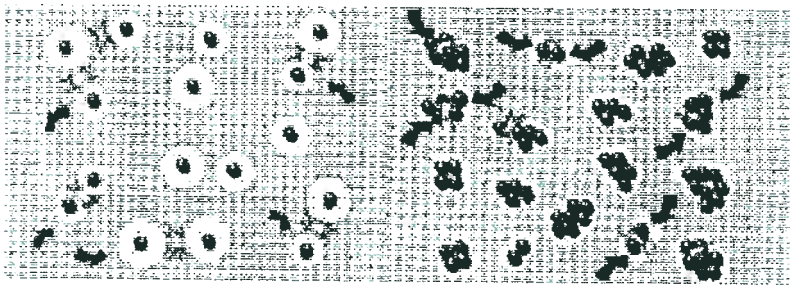

Figure 2- Dispersed and aggregated system

2.3.2. Colloidal system and the DVLO theory

DVLO theory deals with the stability of a particle in a solution. DVLO theory is thus named in honor of the four scientists who developed it in the 40's, Derjaguin, Verwey, Landau and Overbeek. This theory defends that the stability of a particle in solution depends

on its total potential energy function V_{total}. The total potential energy function is the sum of several competing contributions.

$$V_{total} = V_A + V_R + V_S \quad \textit{Equation 4}$$

V_S is the potential energy induced by the solvent, it only has a small influence on the total potential energy. The two main contributions are the ones caused by the attractive and repulsive forces resulting in the two potentials V_A and V_R. They can operate at long distance and have a strong effect on the total potential energy in comparison with V_S. V_A and V_R can be expressed as followed:

$$V_A = -\frac{A}{12.\pi.D^2} \quad \textit{Equation 5} \text{ and } V_R = 2.\pi.\varepsilon.a.\zeta^2 e^{-kD} \quad \textit{Equation 6}$$

where A is the Hamaker constant, D the particle separation, a the particle radius, π is the solvent permeability, k a function of the ionic composition and ζ the zeta potential.

This theory assumes that the stability of the colloidal system is determined by the sum of the Wan Der Waals attractive forces (V_A) and the repulsive forces (V_R) contributions. The repulsive forces come from the electrical double layer around each particle and the Brownian motion phenomenon. Indeed, the particles approach each other due do the Brownian motion provoking their repulsion because of their electrical double layer. An energy barrier is thus created preventing two particles approaching one another and adhering together. But if the collision between to particles is sufficiently energetic to overcome this barrier, the attraction forces can link the two particles together and the phenomenon of coagulation appears. Therefore, if the energetic barrier is high enough, meaning that the repulsive forces are strong, the colloidal system will resist to the flocculation phenomenon and the particles will remain well dispersed [5].

In the following scheme *Figure 3*, the force is repulsive at long distance with a maximum corresponding to the V_m energetic barrier discussed previously. If the Brownian motion thermal agitation is not enough to overcome this barrier, the repulsive forces will impede the two interfaces to get close enough to make the forces become attractive. Thus, with a high barrier the system will remain dispersed [4].

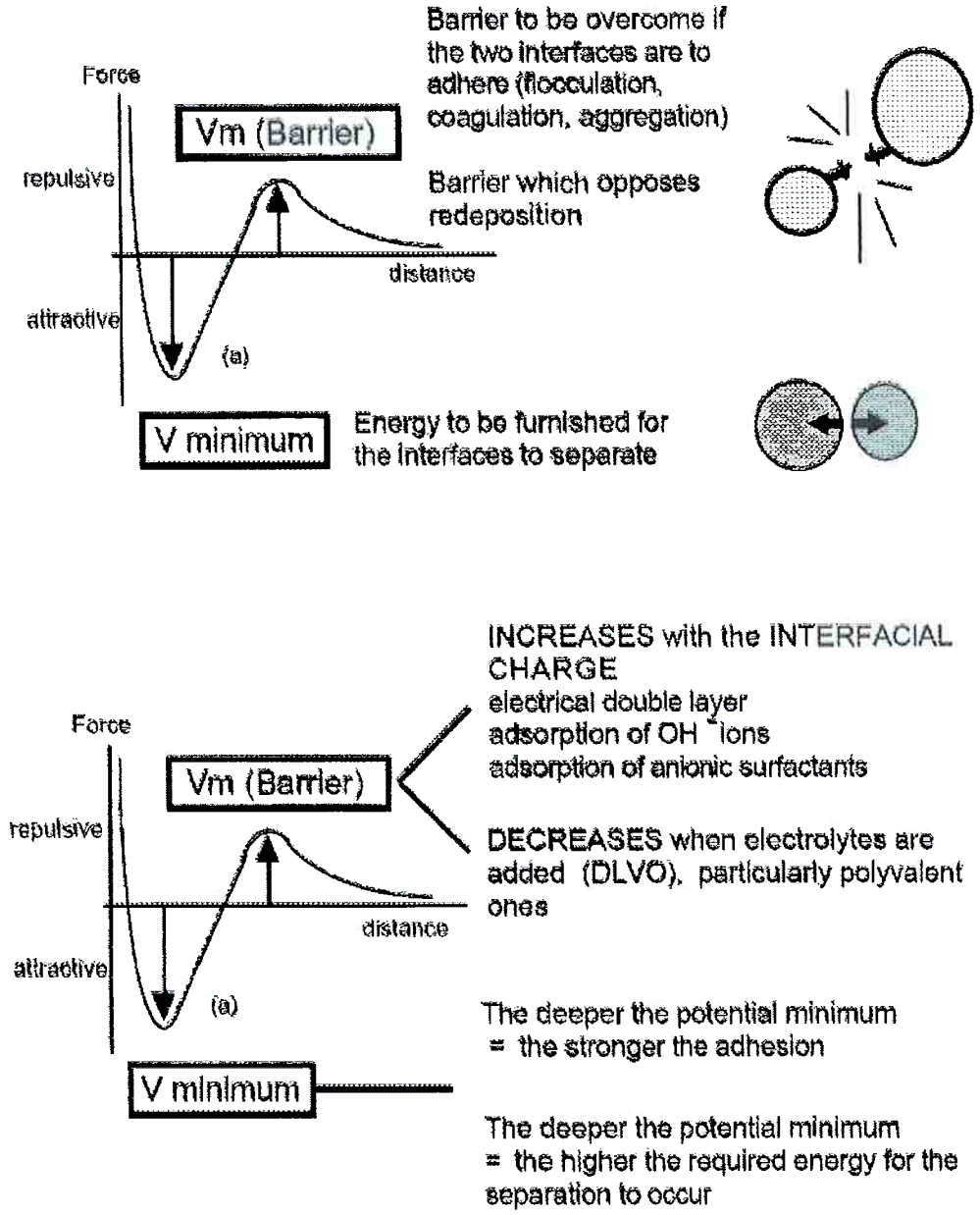

Figure 3- Scheme resuming the DVLO theory concepts

2.3.3. Zeta potential definition

It is important to understand the environment of the particle to give a proper definition of the zeta potential. When the particle surface presents a net charge, the surrounding of the particle is modified, resulting in the increase of counter ions concentration (ions of opposite charge that of the particle surface). An electrical double layer is thus created around each particle of the system. The layer is composed of two different parts, an inner region called the Stern layer and an outer layer called the diffuse layer. In the Stern layer, the ions are strongly

bound to the surface. Within the outer layer the particles and the counter ions form a real entity moving together. The potential zeta is defined as the potential at the external boundary of the diffuse layer. The following scheme *Figure 4* describes a typical electrical double layer around a spherical particle [5].

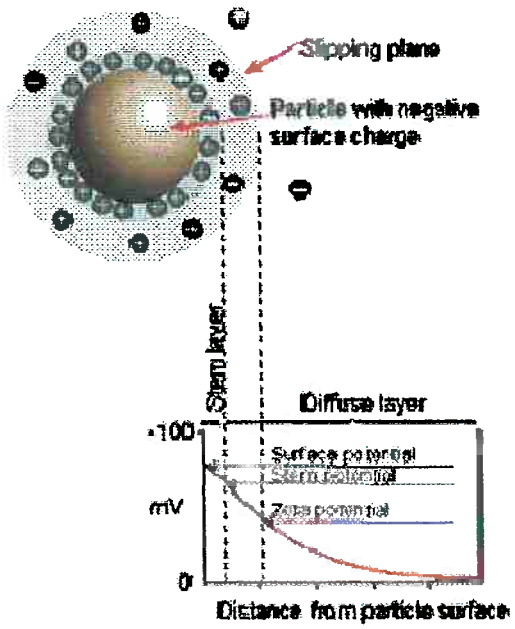

Figure 4- Schematic representation of the zeta potential

2.3.4. Zeta potential and stability of colloidal systems

The zeta potential determines the stability of the colloidal system. If the particles in suspension have a large negative or positive zeta potential, they will repel each other giving birth to a perfectly well dispersed suspension. In another hand, if the potential is equal or close to zero, the particle tendency is to come together, because there are no repulsive forces preventing the flocculation/coagulation phenomenon. It is common to consider that if the zeta potential magnitude is situated between -30 mV and 30 mV, flocculation or coagulation will happened.

Three main factors can affect the zeta potential:

- pH
- conductivity of the solution
- particle concentration

The more the pH is elevated the more the particle tends to have negative charges and vice versa. The pH where the zeta potential is null is called the isoelectric point. At this point the suspension is least stable [5].

The thickness of the electrical double layer is a function of the ions concentration and from the ionic strength. The higher the ionic strength is the more the electrical double layer is compressed. The valency of the ions influences the thickness layer too. A divalent or trivalent cation will compress more the electrical double layer than a monovalent cation. The adsorption of specific ions by the particle can modify consequently the superficial charge and thus moving the isoelectric point.

In high salt concentration, the zeta potential is reduced and can lead to a secondary minimum much weaker in potential curve as it is shown on the following scheme *Figure 5*.

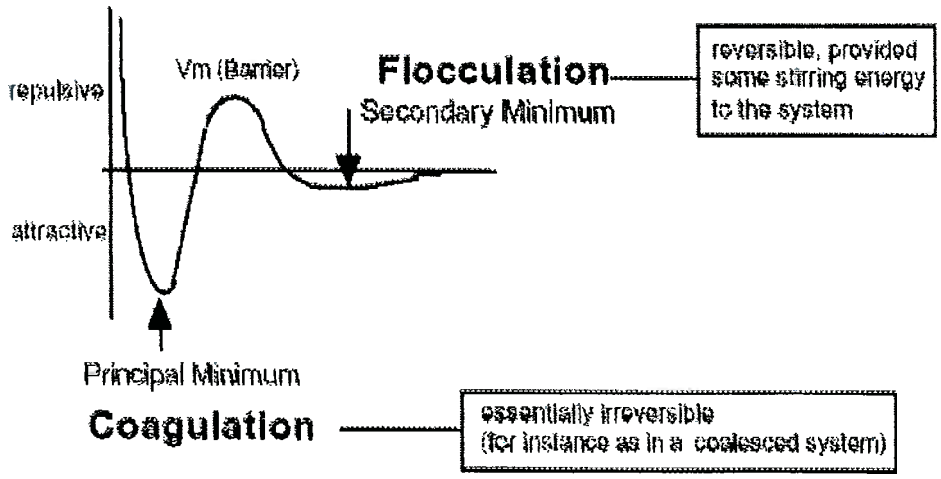

Figure 5- Secondary minimum situation

The flocs thus created are stable enough to resist to the Brownian thermal motion, but can be reversely dispersed with a simple agitation [4].

2.4.The sepiolite and its properties

2.4.1. Introduction

Sepiolite belongs to the clay family known as sepiolite-palygorskite. Clays can be considered as extremely small particles. Sepiolite is used in a wide range of applications thanks to three types of properties which are:

- Sorptive properties
- Rheological properties
- Filler properties
- Catalytic properties

In our study, the properties which are really important are the three first ones. To understand the origin of these properties, it is necessary to detail the sepiolite structure and also to the surface properties such as the cation exchange capacity (CEC) as well as its specific surface area. Surface characteristic are determinant to understand the behavior of sepiolite suspension in different electrolytes [6].

2.4.2. Structure

Commonly, sepiolite appears as larges bundle of crystalline fibres. It adopts a compact soft porous macroscopic appearance. But it can also presents a lump form like the one found in Turkey. The fibre dimension can vary considerably to 0,2 to 2 μm in length, 100 to 300 Å in width and a thickness of 50 to 100 Å. The fibrous structure of the sepiolite is constituted of talc-like ribbons with two sheets of tetrahedral silica units, each ribbons is linked thanks to oxygen atoms to an octahedral sheet of magnesium composed of eight cations. The silicon sheets are continuous and after every six tetrahedral units, the direction of these tetrahedral units is inverted. The octahedral sheet of magnesium is discontinuous at each inversion which gives birth to channels in the longitudinal direction. These channels of 3,6 * 10,6 Å of section can contain water and other fluid molecules. Sepiolite can contain a large amount of water which can be classified in three groups according to its location:

- Absorbed water bonded by hydrogen bonds at the external surface or into the channels which in this case is called zeolitic water.
- Crystal water bonded with octahedral cations at the edge of the central ribbon, therefore completing their coordination.
- Constitution water or hydroxyl groups.
- A typical formulation of the sepiolite molecule can be given thanks to the Brauner and Preisinger model:

$$(Si_{12})(Mg_8)(O_{30})(OH_4)(OH_2)_4 8H_2O$$

The following scheme *Figure 6* shows the structure of the sepiolite.

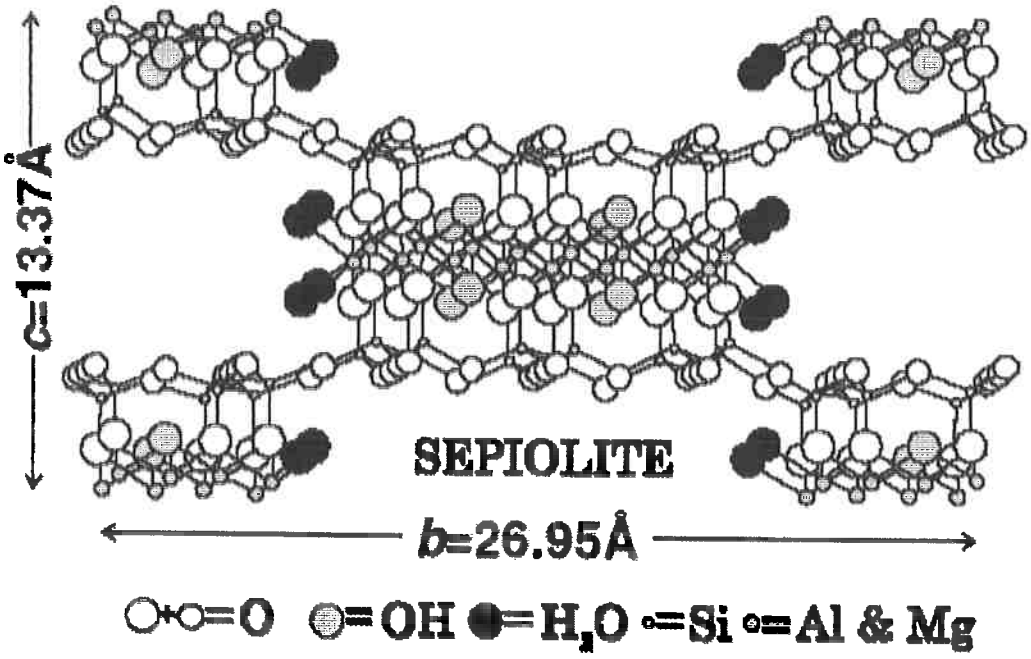

Figure 6- Schematic structure of sepiolite according to Brauner and Preisinger model, 1956

Lots of formulae show a small substitution of Si^{4+} by Al^{3+} or Fe^{3+} in the tetrahedral sheet, which cause a deficiency of charges on the sepiolite surface [7].

2.4.3. *Specific surface area and Cation Exchange Capacity (CEC) of the Sepiolite*

Many measures of the specific surface area of the sepiolite have been done, and quiet a wide range of values can be found in the literature, depending on the methods used to make these measurements. The molecule used to measure the specific surface area can either be adsorbed on the external surface or penetrate the intra-crystalline channels. The specific surface area of sepiolite increases as the temperature is increased and as the zeololitic water is removed, thus liberating free spaces The specific surface area of the sepiolite computed with structural models (Brauner and Preisinger model for instance) is approximately of 800-900$m^2.g^{-1}$. But usual BET N_2 measurements show values more around 340 $m^2.g^{-1}$ [6].

The cation exchange capacity (CEC) is a measure of the total number of sites available for ion exchange of positively charged ions, i.e. cations, or the total amount of exchangeable cations. The cation exchange capacity of sepiolite values, found in the literature, vary greatly according to different crystalline compositions of the sepiolite. A typical value done by the ammonium acetate method is around 25 meg/100g. The cation exchange capacity of sepiolite is due to the deficiency of charges caused by the trivalent ions substitution of Si^{4+} in the tetrahedral sheet and by broken bounds at the edge of the fibre. This deficiency can be compensated by adsorbed cations from the solution [6].

2.4.4. *Sorptive characteristics*

Sepiolite possesses several sorption active centers on its surface:

- The oxygen atoms present in the tetrahedral sheet.
- Water molecules in coordination with magnesium at the edge of the central octahedral sheet which can be linked thanks to hydrogen bond to sorbed molecules.
- Silanol groups along the tetrahedral sheets of the molecule. These silanol groups are created by the break of Si-O-Si bonds. The residual charge thus created can be balanced by accepting a proton or a hydroxyl molecule.

Moreover, as described above, sepiolite possesses a great surface area thanks to the zeolitic channels. Combined with the numerous sorption active centers, sepiolite can adsorbed a large amount of water and other polar substances. Sepiolite can retain up to 200% to 250% of its weight in water [7].

2.4.5. Rheological behaviour of sepiolite suspensions

Sepiolite particles have a needle like structures and often appear as bundles. Dispersion of these bundles can easily be done in water and other high or medium solvent. Once dispersed in the liquid, it forms a structure of randomly intermeshed elongated particles, which is maintained by physical interference and hydrogen bonding, and entraps the liquid, increasing the viscosity of the suspension. The dispersion efficiency and the rheological properties of sepiolite suspension depend on several factors such as the concentration of solid, the agitation process or the pH. In aqueous environment (medium of high polarity), the rheological behaviour of the sepiolite suspension is influenced by several factors:

- Concentration of sepiolite
- Shear stress applied during the dispersion process
- pH
- electrolyte

As the concentration of the sepiolite increases, the viscosity of the suspension increases remarkably, resulting in a non-Newtonian fluid and even forming gels.

Disagglomeration is obtained thanks the application of a shear stress. The viscosity of the suspension increases with the shear rate but also with the shearing time [6].

The pH does not affect much the suspension of sepiolite over a wide range of values around 8. According to Alkan et al. [9] the isoelectric point of the sepiolite was found around 6,6. An increase of the solution pH results with an increase of the negative charge of the sepiolite and a decrease of the zeta potential which at pH 9 is about -43 mV. The increase of negative charge can be attributed to the adsorption of HO^- onto the positive centers and a deprotonation of surface hydroxyl group.

The electrolyte can quite modifies the rheological behaviour of the sepiolite suspension. According to a study conducted by Alkan and al., divalent cations such as Ca^{2+} for instance, are able to decrease the zeta potential of sepiolite (becoming less negative) and in high concentration, even cause a charge reversal. This can lead to a flocculation phenomenon of the sepiolite suspension. In another hand, monovalent cations have not a great effect on the zeta potential of the sepiolite; in high concentration they decrease it compressing its electrical double layer, but addition of such cations never leads to charge reversal. Therefore, dispersed suspension of sepiolite remains stable in monovalent cations electrolyte [9].

3. Materials and methods

3.1. Material description and characterization

This section deals with the characterization of the materials used for this study. For the validity of a survey, it is crucial to have precise data on the components in relation with the study. These components are:

- The Portland cement CPII
- The filler limestone
- The cellulose fibres
- The PVA fibres
- The microsilica
- The two types of sepiolite (Turkish and Spanish)

All these materials (expect the sepiolite) were provided by Infibra, a company that produces fiber cement corrugated sheet in the state of São Paulo and which collaborated with our team.

Each material was submitted to specific test according to its nature. The powder materials such as the cement, the limestone and the microsilica were submitted to:

- A chemical analysis to determine their exact composition

- A granulometric distribution measurement
- X-ray diffraction
- BET analysis to estimate the specific area
- Density measurement thanks to a helium pictometer

Two different kinds of sepiolite were studied, a Turkish one commercially called Dolsan and a Spanish one named Tolsa. Both have a granular aspect, with brown coloration for the Tolsa and a milky coloration for the Dolsan. Each one was submitted to a nitrogen BET analysis, X-ray diffraction, a density measurement and also to rheological study to understand the behavior of sepiolite suspension.
The Annex I gathers all the characterization data.

3.2.Samples composition

To study the effect of the addition of sepiolite on the fibre reinforced cement, three different compositions were chosen for the samples. The composition of the sample of reference (the one free of sepiolite), is a typical industrial one used in the industry for the production of PVA / cellulose reinforced cement sheet. The two others samples contain the two different kind of sepiolite that we are interested in this study.
Table 2 presents these compositions:

Table 2- Samples weight pourcentage composition

Components	Weight composition (%)		
	Reference	**Tolsa**	**Dolsan**
Cement	64,00	63,36	63,36
Limestone	26,20	25,94	25,94
Active Silica	5,00	4,95	4,95
Sepiolite Tolsa	0,00	1,00	0,00
Sepiolite Dolsan	0,00	0,00	1,00
Cellulose fibres	3,00	2,97	2,97
PVA fibres	1,80	1,78	1,78
Total	100,00	100,00	100,00

The optimal amount of sepiolite added was chosen according to the result given by the flocculation study.

3.3.Methodology

This section describes the methodology used in this study. The fibre reinforced cement sheets were cast according to a process that simulates to a laboratory scale, the one used in the industry: The Hatschek process. This process is based on a vacuum dewatering of the dissolved fibre cement in a quadratic metallic recipient which is able to create suction at its base. The mixture is composed of 30% of solid in weight in suspension in water. The pressure created by the vacuum allows the dewatering of the fibre cement mixture.

Once, the fibre cement sheets prepared, they were tailored for the different mechanical tests requested in this study. Two different mechanical tests were done on the samples according to the properties of interest. First, each fresh fibre cement samples, thus molded, were tested under tensile. Then after 28 days of hardening, each sample was submitted to a bending test.

3.3.1. Properties studied

It is important to define the physical and the mechanical properties that are important to study the behavior of fibre cement sheet. Like it has been said previously, the fibre cement is studied in its fresh and hardened condition. We can distinguish the properties extracted from these two conditions.

Thus, the following properties are resulting from the study of the fresh fibre cement:

- The Stress-strain relation (given by the tensile test)
- The tensile strength (given by the tensile test)
- The strain at the fracture (given by the tensile test)
- The humidity of the sheet
- The dewatering rate during the casting of the fibre cement sheet

The properties of the hardened fibre cement are:

- Modulus of Elasticity (MoE)
- The Modulus of Rupture (MoR)
- Toughness

The knowledge of these different properties will allow the conclusion on the benefit of the added sepiolite on the physical and mechanical fiber cement properties.

3.3.2. Samples preparation and casting

The mixtures were realized thanks to an electrical agitator which guaranties the agitation of 2000 rpm. The different components were added gradually to allow an adequate homogeneity in a 3l capacity recipient with 1290 ml of water (corresponding to 30% of solid) *Figure 7*. The component where added according to the following sequence:

- Cellulose fibres (3mn of agitation)
- PVA fibres (3mn)
- Microsilica (1mn)
- Limestone + Cement (3mn)
- Sepiolite (3mn)

Figure 7- Some steps of the fibre cement solution preparation: addition of cellulose, blending of cellulose, blending of PVA +Cellulose, addition of sepiolite (from left to right and from up to down)

The addition of sepiolite required a specific preparation *Figure 8*. Indeed the sepiolite was added after a pre-dispersion step. Gels of sepiolite were prepared thanks to an electrical mixer which allowed an agitation of 3000 rpm of the suspension. The gels were composed of 5% in weight of sepiolite which was enough to guaranty a good viscosity. The study of the rheological behavior of the sepiolite suspension were done previously to determine the right amount of sepiolite necessary to create a gel with the adequate viscosity.

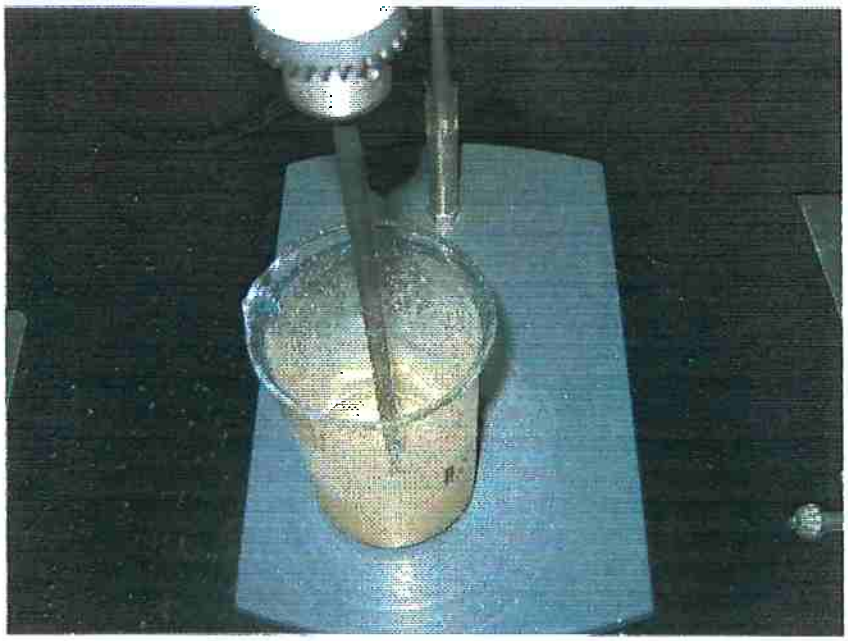

Figure 8- Sepiolite gel preparation

Once the fibre cement mixture ready the casting process could begin. The mixture was transferred in the casting device *Figure 9*. The mixture was spread out with a spatula to reach a good homogeneity of the fibre distribution in the cement sheet. Simultaneously, the vacuum suction was activated under a pressure of 3 atm. Thus the dewatering process of the fibre cement began. After 150 seconds of suction, the process was stopped, thus forming the fibre cement sheet. The cement sheets have humid solid appearance with dimensions determined by the ones of the mold, 200*200mm, and with a thickness which varies between 6 mm and 8 mm according to their respective composition. Indeed, some compositions possess better water retention capacity which brings on an augmentation of the sheet volume.

Figure 9- Vacuum dewatering device connected to a Kitasato container

The vacuum-dewatering device is connected to a Kitasato recipient of 4 l capacity, aiming at collecting the water. The recipient is set up on electronic balance, which is connected to a computer, allowing the in-situ measurement of fibre cement mixture dewatering rate *Figure 9*.

For each fibre cement composition, five sheets are molded, two for mechanical test on the fresh state and the other three for the hardened state *Figure 10* . The sheets for the tensile test are cut according to a precise normalize shape. The cutting stage is realized thanks to an original device which allows an easy removing of the samples.

Figure 10- Example of fresh cast fibre cement sheet

Once the fibre cement sheet cast, they were pressed individually under 3,2 Mpa, which simulates the pression applied by the cylinder of Hatschek mechanical device. After that, the sheets were placed into plastic box to avoid any moisture variation.

3.3.3. Mechanical tests

a. Tensile test

The tensile tests were done on Instron 5569 device. The tensile device was set up to test samples of low resistance as the fresh fibre cement ones. Samples are fixed tanks to a system of plastic clasps *Figure 11*, which avoid any damage on them.

Figure 11- Plastic clasps allowing a smooth holding of the sample

The tensile tests were done under a minimal load permitted with this device, 1000 N with a strain speed of 2 mm/mn. Typical load/displacement curves were obtained and analyzed in the next part of the report. 8 samples were tested for each formulation giving enough data to infer a general behavior, i.e. the maximum load, tensile strength and the strain at maximum load. *Figure 12* shows a sample during the tensile test.

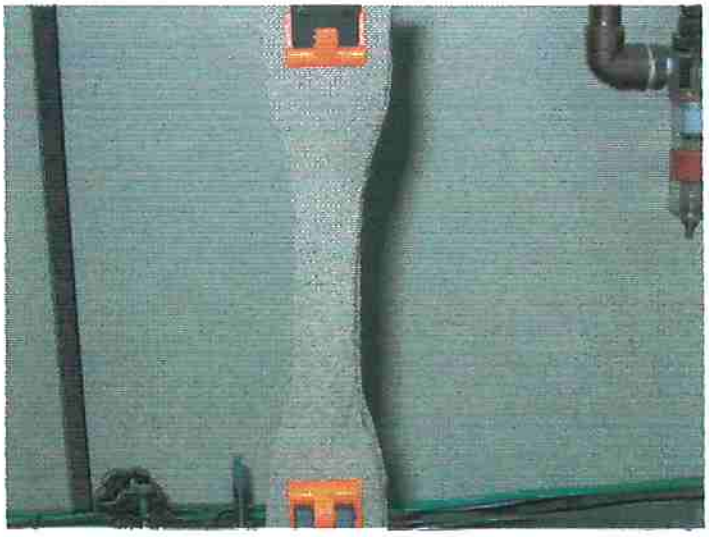

Figure 12- Sample during tensile test

After being tested, each sample was submitted to a process of accelerated drying during 7 mn in the microwave. The measurement of the weight sample before and after drying allowed the calculation of the percentage of humidity in it:

$$H(\%) = \frac{m_{humid} - m_{dry}}{m_{humid}}.100 \quad \textit{Equation 7}$$

where:

- m_{humid} is the sample weight before drying
- m_{dry} is the sample weight after drying

b. Bending test

Three fibre cement sheets, for each composition, were reserved for the hardened state mechanical characterization. After being molded, these sheets were placed in a plastic bag for 48 hours to create a water-saturated atmosphere. After that, more than 90% of the cement reactions already have occurred, and the fibre cement sheets presented solid rigid aspect. According to the fibre cement bending test standards, the samples (4 per sheets) were immerged in water during 28 days. Once the sample saturated in water, the bending test were done with a speed of 1,5mm/mn. For this test, precise sample dimensions are really important; they were cut to have approximately 40*160mm section. But before each test, the sample dimensions are measured to allow a precise calculation of the characteristics of interest such as modulus of elasticity, toughness...

To measure the flexure extension, a linear variable differential transformer (LVDT) was used. ***Figure 13*** shows a schematic representation as well as a picture of the bending test.

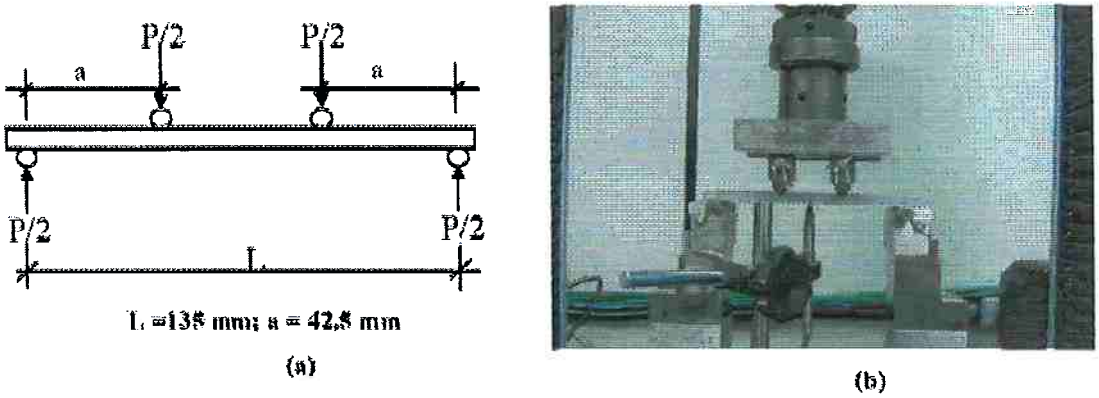

Figure 13- (a) scheme of the 4 points bending test, (b) picture of the bending test

compare properly each sample. A bench of four agitators in series is used to compare the effect of different quantity of sepiolite in solution, as shown on the following scheme *Figure 14*.

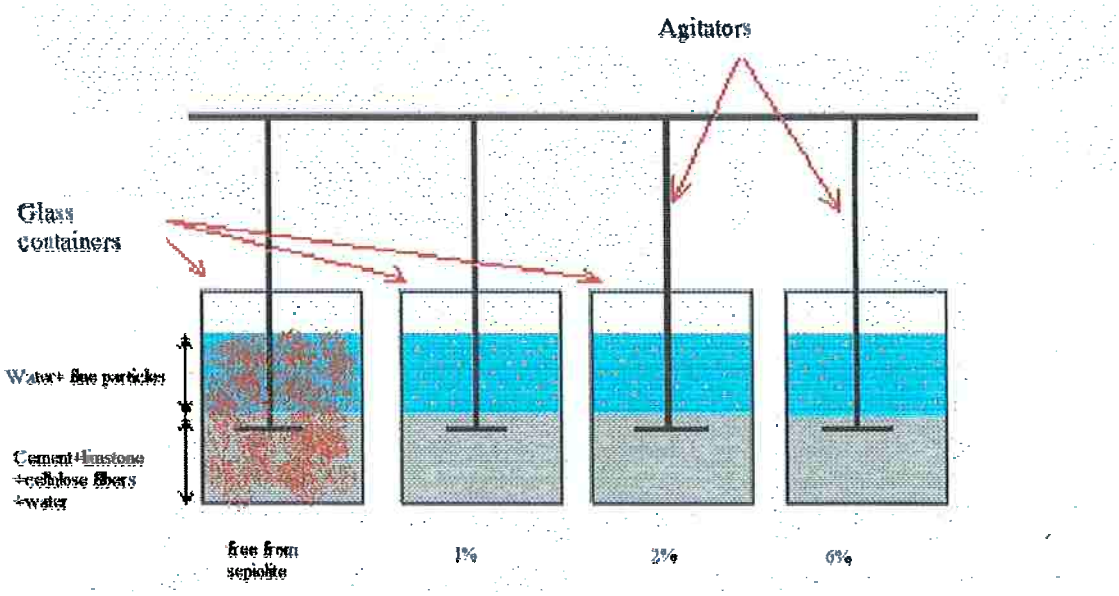

Figure 14- Schematic representation of the flocculation test

First the fibre cement solutions were prepared without adding sepiolite. The mixture of cement, limestone and fibres were agitated at 70 rpm for 30 mn. The sepiolite addition steps in only at the ultimate stage of the fibre solution preparation according to the industrial procedure.

After 30mn of agitation, the sepiolite was finally added to the fibre cement mixture. The agitation was increased for a couple of minutes to allow a perfect homogenization of the solution. Then, the agitation was decreased to 30 rpm to observe the decantation phenomenon. For each type of sepiolite, the pictures and movies of the bench were taken to compare the four mixtures (free from sepiolite, 1%, 2% and 6%).

4.1.3. Results and discussion

Whatsoever the quantities of sepiolite added in the fibre cement solution, the effects were immediate. Flocs formation immediately began, thus forming a dense and opaque solid bulk. After a few minutes, flocs began to settle giving birth to a solid bulk of a viscous aspect in the bottom of the container. The water on the top of flocs thus settled, was more or less translucent depending on the quantity of sepiolite addition. The flocculation phenomenon was visible enough to easily enable comparison between a sample free from sepiolite *Figure 15* and the sample with sepiolite *Figure 16.*

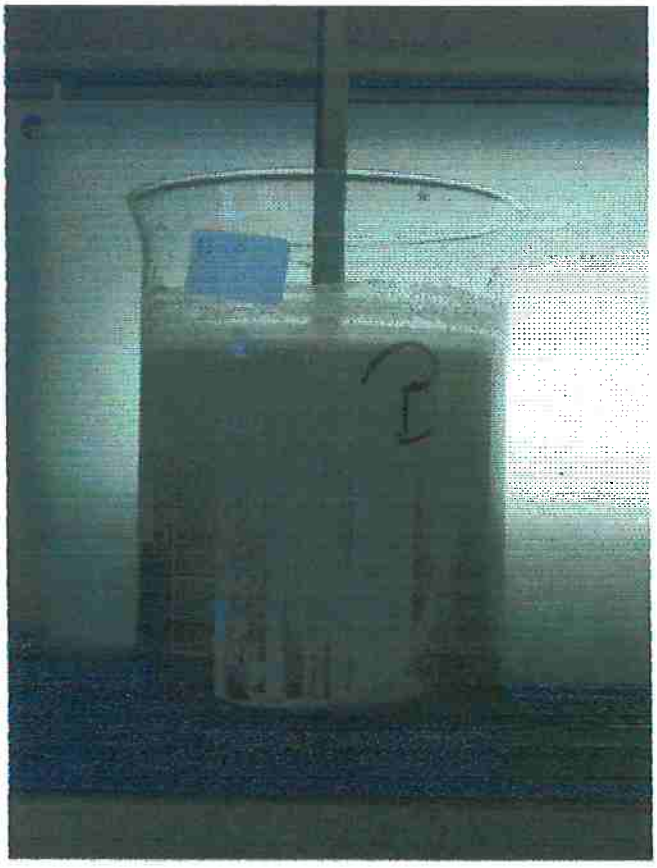

Figure 15- Fibre cement solution free from sepiolite after 15 mn of decantation

Figure 16- Flocculation phenomenon, cement solution after 1% (left) and 2% (rigth) Dolsan sepiolite addition.

No clear differences appeared between the two different kinds of sepiolite except that the water in top of the settled bulk was a little more translucent for the Tolsa than for the Dolsan. Indeed, the sedimentation rate, the settled bulk volume and the flocs size were similar for both sepiolites. Therefore in the following, no differentiation could be done for the two kinds of sepiolite and thus the discussion is valuable for both.

The only clear differences between the various fibre cement solutions were due to the variation in sepiolite quantities added. The more sepiolite is added, the bigger is the settled bulk and clearer is the top water. The following pictures illustrate well these impressions *Figure 17.*

Figure 17- Sepiolite addition effects: 1% and 2% after 15mn (picture on the left); 2% and 6% after 15mn (picture on the left)

The clearness of the top water with the 6% sepiolite addition is spectacular. Almost every particle seems to be trap into the settled bulk *Figure 17*. Another tendency can be underlined: the decantation time influences the solution aspect. The longer is the decantation time, the more the flocculation phenomenon is noticeable (bigger settled volume of flocs, clearer top water). Indeed, this is due to increased time enabling the sepiolite particles to interact with the fibre cement solution ones.

Finally, the sepiolite flocculation capacity is obvious whatever the added quantity or the type of sepiolite. In the industrial process, the flocculant addition quantity is around 0,1%. The results observed in this survey show a significant effect with 1% of addition. This quantity seems to be sufficient to obtain a good ratio efficiency/cost in adequacy with Hatscheck process. Moreover, it is important to notice that the actual industrial flocculant agent, even in small amount as 0,1%, remains much more expensive that sepiolite.

4.2.Fresh state study

4.2.1. Dewatering properties

The dewatering speed rate gives information about the permeability of the fibre cement sheet. All curves, water loss (in weight) versus time, converge toward an asymptote, which indicates the capacity of the material to retain water in its microstructure. All the dewatering data are gathered in Annex II.

Figure 18 shows the average dewatering curves of three samples (the reference ones (free from sepiolite), the Tolsa and Dolsan ones). These curves were obtained by averaging 5 series of data for each of the three compositions.

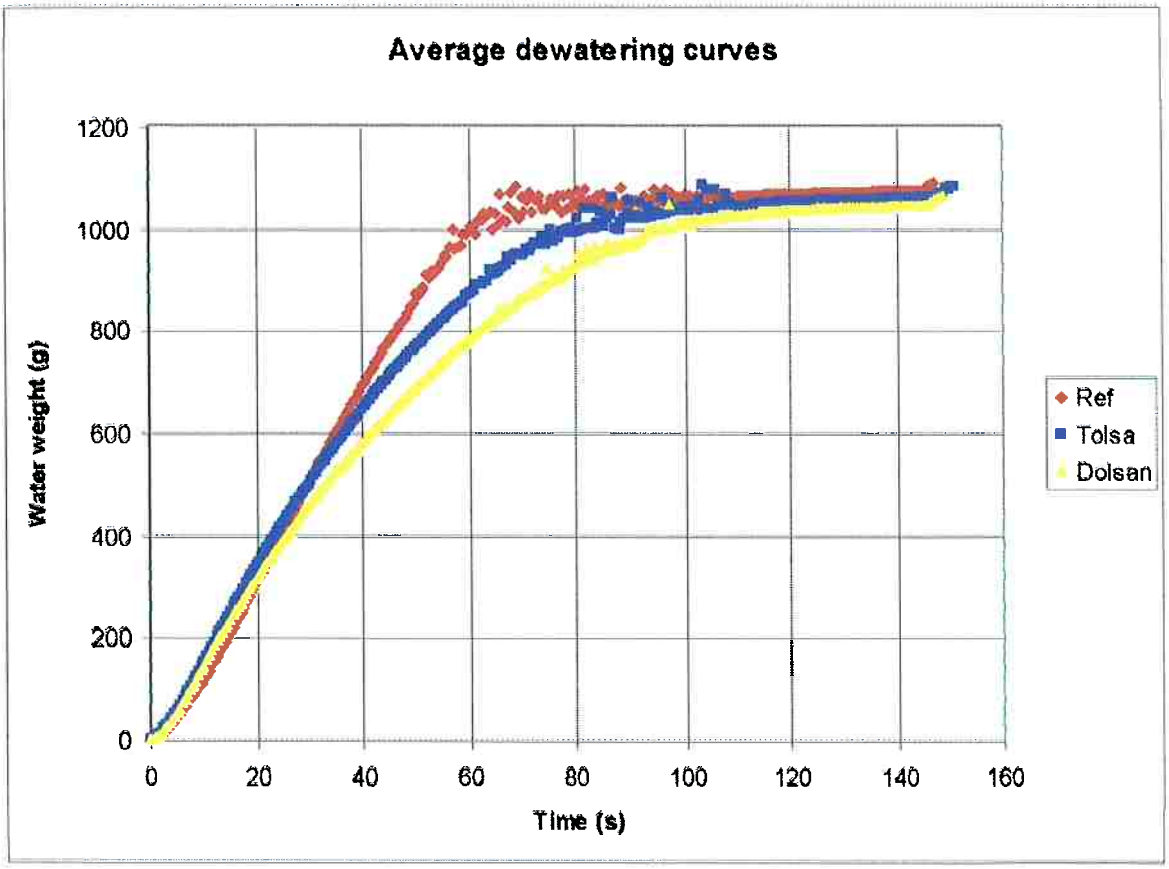

Figure 18- Dewatering curves for the three fibre cement compositions

The dewatering curves exhibit a similar shape, with a linear part during most of the process, and an asymptotic behavior at the end. The dewatering procedure is really efficient in the first part (represented by the linear shape on the curves of *Figure 18*): almost all the water that can be removed regarding the physical condition of the process (vacuum suction of 3atm), is actually removed during this period. Therefore to remove the major part of the water, it takes approximately 80 s for the sepiolite-free samples and 100 s for the samples containing sepiolite. Moreover, the dewatering speed rate is constant during this part.

The samples, which contain either sepiolite Tolsa or Dolsan, exhibit lower dewatering speed rate than the ones free from sepiolite. Indeed, the inclination of the rectilinear part is more important for the sepiolite-free samples than for the others. One can also notice a clear differentiation between the two sepiolite samples. The Dolsan ones show much lower

dewatering speed rates than the Tolsa ones. This means that the permeability of the samples with sepiolite, especially the ones with Dolsan sepiolite, is lower than the ones free of sepiolite, which signifies that the water has more difficulties to go through these samples. The following graphic, *Figure 19*, presents the linear part of the dewatering curves with their linear approximation:

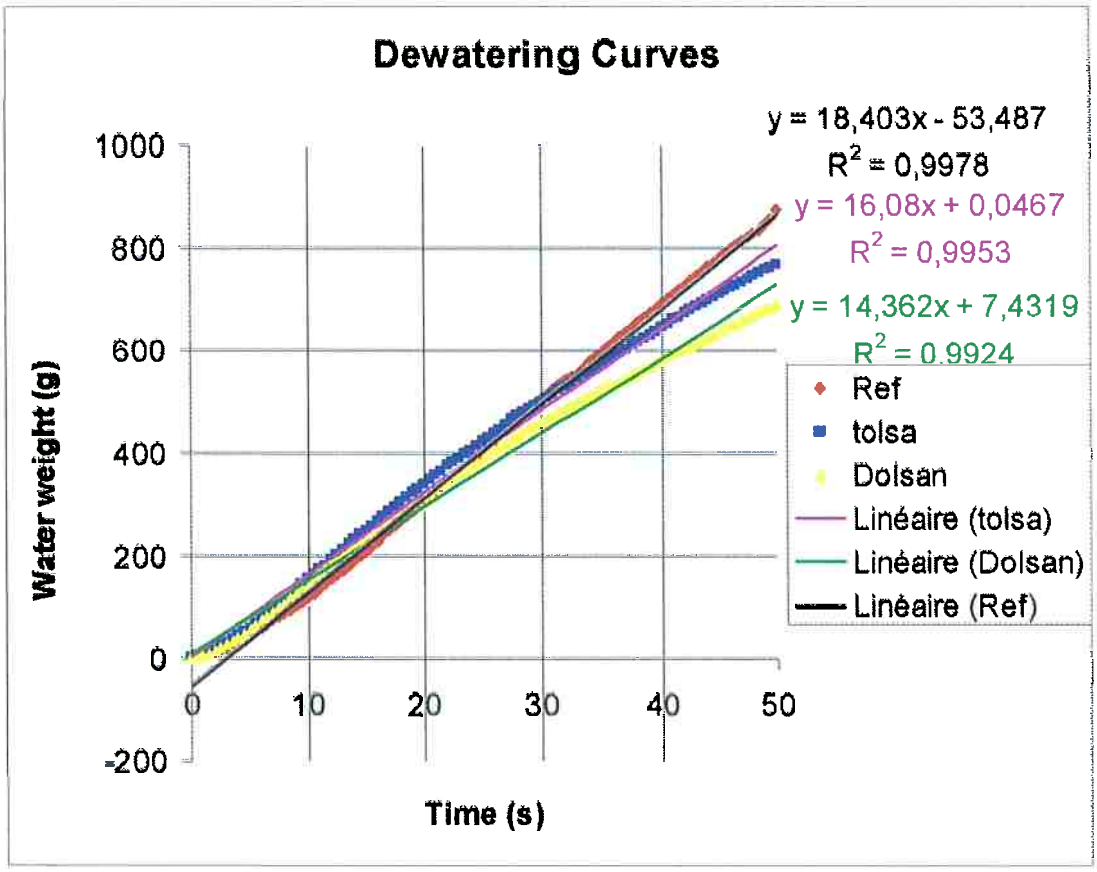

Figure 19 - Approximation of the linear part of the dewatering curves

The free sepiolite-free samples show an average dewatering rate of 18,4 $g.s^{-1}$, the Tolsa samples of 16,1 $g.s^{-1}$ and the Dolsan ones of 14,4 $g.s^{-1}$. As demonstrated in the graph in *Figure 20*, the dispersions around these average values are relatively low; this shows a relatively good constancy in the dewatering process. Indeed the reference, the Tolsa and the Dolsan samples display a standard deviation of 1,31, 0,72 and 0,40 $g.s^{-1}$ respectively.

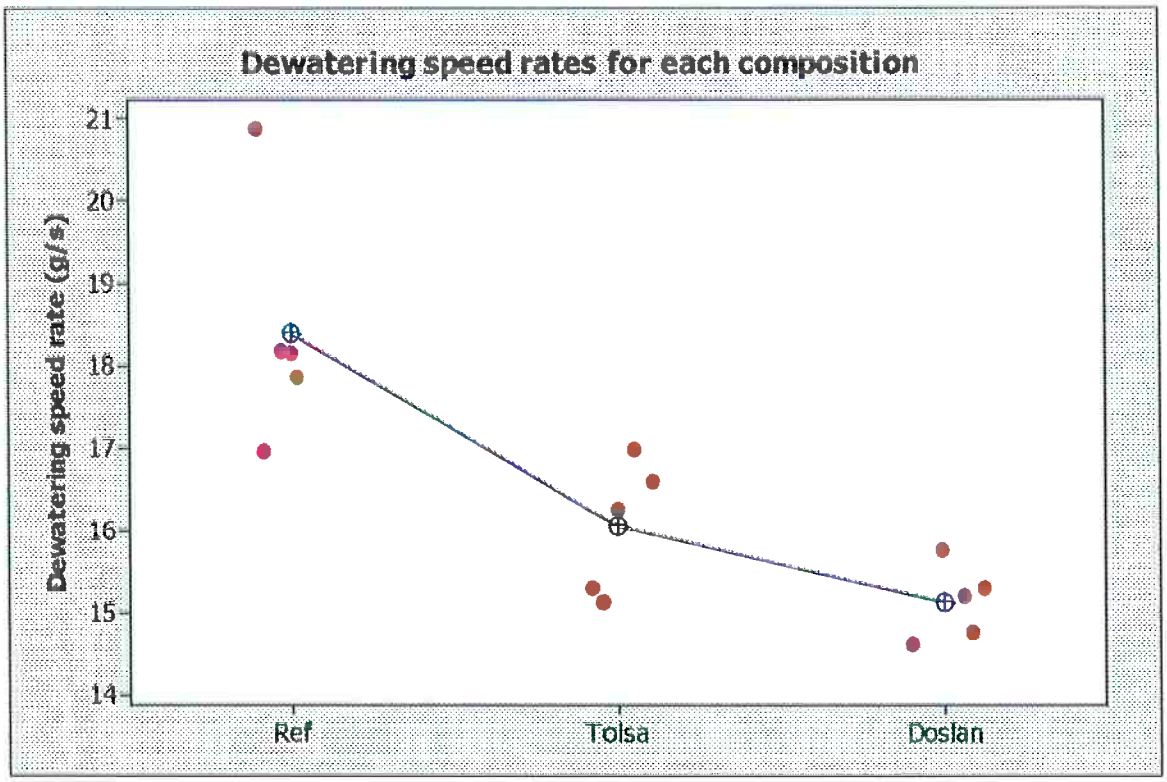

Figure 20- Dewatering speed rates for each fibre cement composition

These differences of dewatering speed rates between the samples without sepiolite and the ones containing it can easily be explained. The presence of sepiolite fibres result in the creation of a network that densifies the fibre cement, and so prevents the water to flow out easily. The divergence between the two kinds of sepiolite cannot be explained simply and requires a microstructural analysis of the fibre cement sheets, but it is surely related to the flocculation ability of the sepiolites. Indeed, the more efficient the flocculation process, the lower the dewatering speed rate.

Another important point that deserved to be examined is relative to the asymptotic part of the dewatering curves (*Figure 18*). Indeed, this part characterizes the water retention of the samples, which means the water that is going to stay into the samples after the dewatering process. The water retention cannot be directly characterized by comparing the relative position of the dewatering curve asymptotes (*Figure 18*). In fact at the end of the dewatering procedure (when reaching the asymptotic behavior), the sheets were manually pressed in order to obtain a regular planar shape. The adjustment of the balance could have been affected, thus moving the relative position of the dewatering curves. However, this did not

affect the linear part, which consequently allowed the calculation of the dewatering speed rate.

The relative humidity is determined by measuring the percentage of water that stayed into the sheet. *Figure 21* shows the relative humidity of the samples, the average value and the dispersion around it.

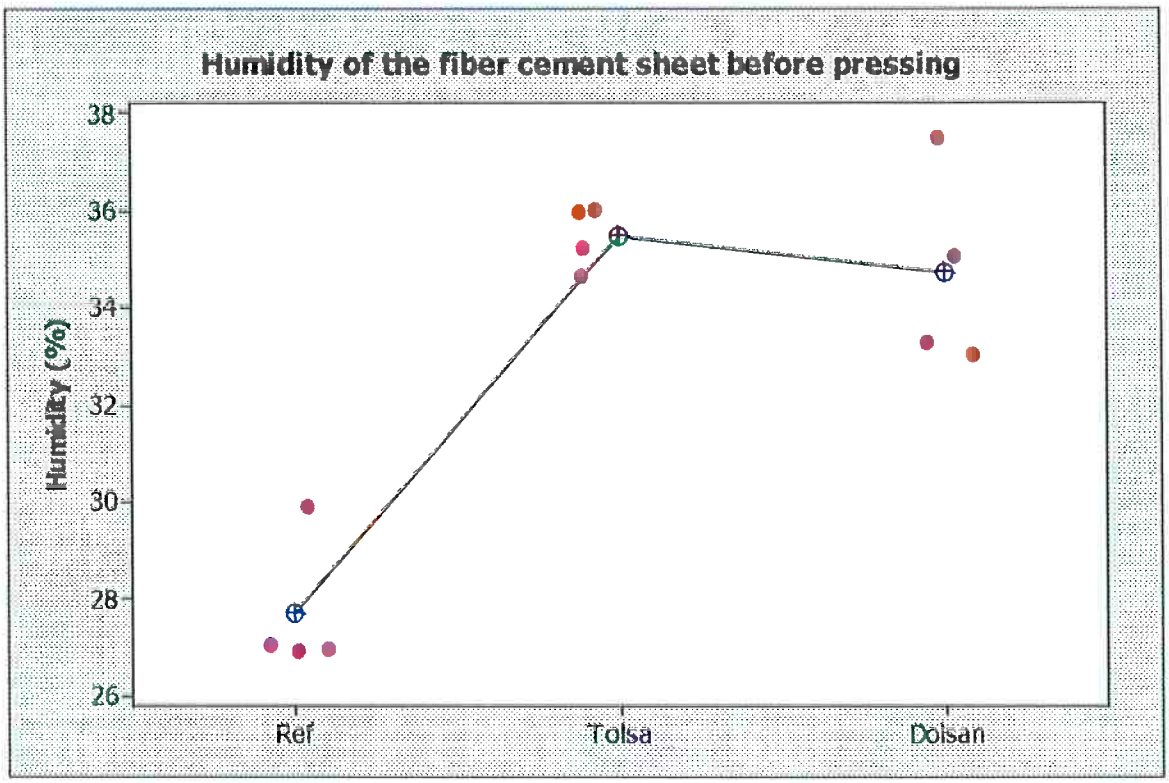

Figure 21- Relative humidity of the fibre cement sheet before pressing

The previous graph, *Figure 21*, shows that samples with sepiolite retain more water than the one without, as expected. Indeed, the Tolsa and the Dolsan samples retained an average percentage of respectively 35,4 % and 34,7 % of water, whereas the reference samples retained only 27,7%. The dispersions around these average values were relatively small around 2%, which demonstrate a good constancy in the process. These differences in the water retention capability of the samples can easily be explained. The sepiolite induces a flocculation phenomenon, and the thus formed flocs can trap the water in their bulk. Moreover sepiolite possesses a good affinity with the water thanks to its numerous sorption active centers and great specific surface area with its zeolitic channels. Therefore the water can be simply trapped by the molecule itself during its hydration.

After being cast, the fibre cement sheets are pressed, and during this stage water is expelled again. It is interesting to quantify the humidity of these sheets after pressing. The following graphic *Figure 22* depicts the relative humidity of the sheet after the pressing stage:

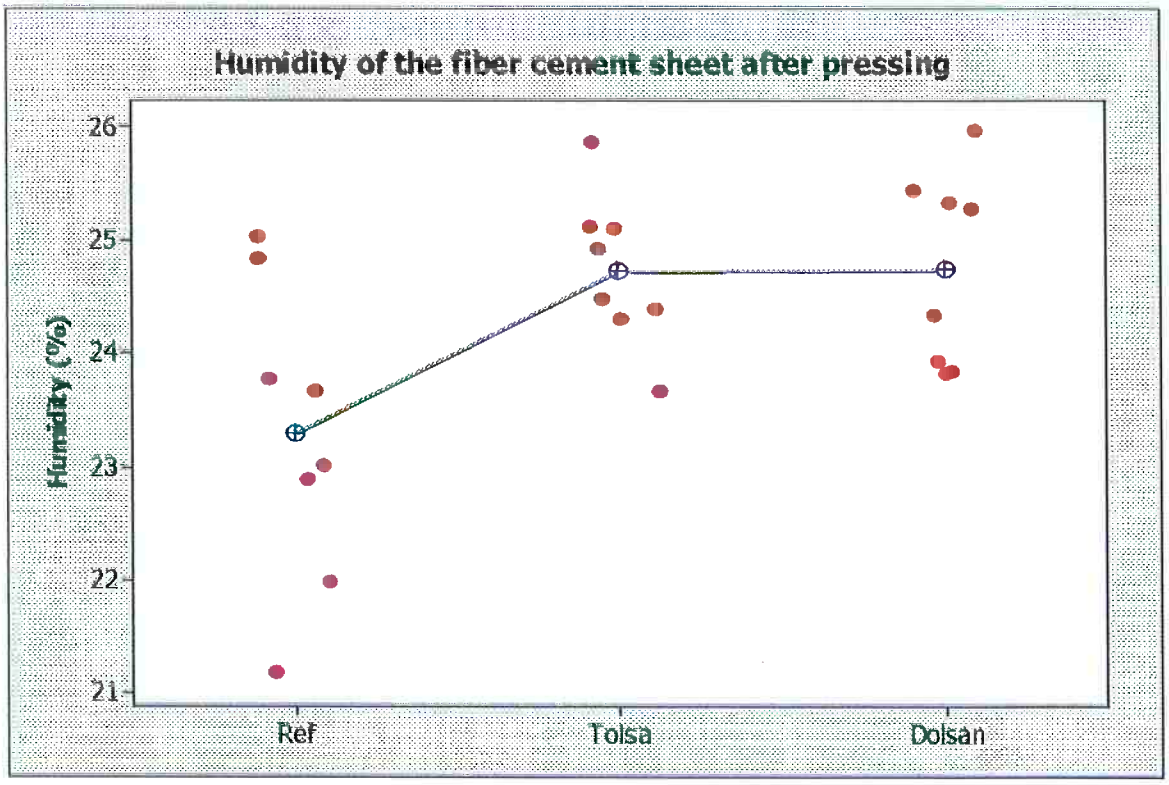

Figure 22- Relative humidity of the fibre cement sheets after pressing

Reference sheets show an average relative humidity after pressing of 23,4% whereas the Tolsa and Dolsan ones exhibit a similar value of 24,7%. This shows that during the pressing stage, the sheets containing sepiolite loose a larger amount of water than the one without. Indeed the media relative humidity of the sepiolite samples decreased from 35,4% for the Tolsa and 34,7% for the Dolsan to 24,7%, whereas the reference sheets decrease only from 27,7% to 23,4%. These values show a good constancy, indeed the standard deviations remain inferior to 1,3% (this maximum value is obtained for the reference samples). The reason of such a water loss difference between the sample with and without sepiolite come from the fact that most of the water trapped during the flocculation phenomenon is easily expelled by simple pressure on the sheets. But there still remains approximately 1,3% more water in the sheets containing sepiolite. This is due to the pressing process which is not able to evacuate the water adsorbed by the sepiolite molecules (in the zeologic channels for

instance). An addition of 1% of sepiolite thus leads to a difference of about 1,3% of relative humidity of the fibre cement sheets.

4.2.2. Tensile test

As described in the above-mentioned part methodology, 8 fresh samples per composition were submitted to conventional tensile test in order to determine interesting mechanical properties such as the maximum stress and the sample extension at maximum stress. This gives us information about the plasticity of the fibre cement sheet in function of its composition. As previously mentioned, the more the fibre cement is able to deform plastically, the lesser the risk of fissure apparition. The maximum stress and the extension were calculated by measuring the width and thickness of each samples and entering them into the Blue Hill program which allows the stress calculation at each point, thus simplifying the relation between the load and the stress.

The following graphic, *Figure 23*, illustrates the average tensile curves of the reference, the Tolsa and the Dolsan samples. They were obtained by averaging 8 series of data per composition:

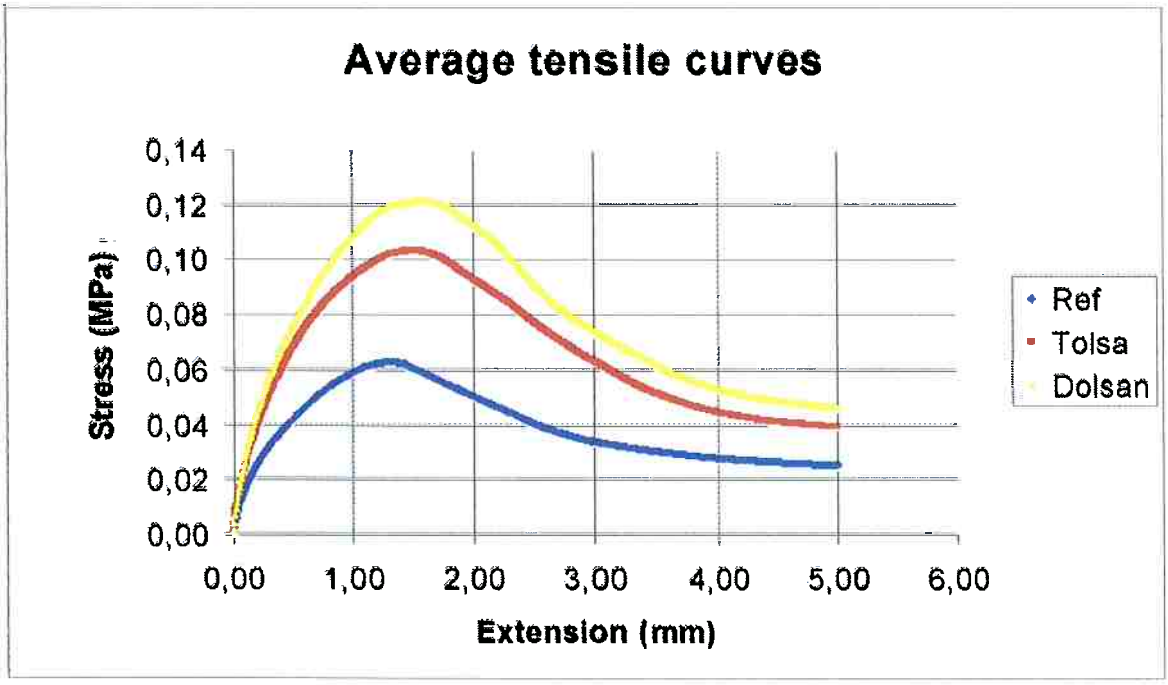

Figure 23- Average tensile curves

These curves have a similar bell shape characterized by a maximum tension. The effect of sepiolite is evidently increasing both maximum tension and extension. All the tensile test data are gathered in Annex III.

a. Maximum stress

Figure 24 emphasizes the sepiolite addition effect on the maximum stress. The reference samples present an average maximum tension at about 0,062 MPa. The added sepiolite has a significant effect, increasing largely this value. Indeed, an augmentation of 70,3% and 108,5% is obtained by adding sepiolite Tolsa and Dolsan with a value of 0,11 MPa and 0,13 MPa respectively.

The standard deviation is quite important and is approximately the same for all the samples 0,024 MPa. This underlines the need to enhance the casting process by improving the efficiency of mixing stage in order to increase the fibre distribution. The maximum stress augmentation shows the mechanical improvement obtained by adding sepiolite. This improvement illustrates the noticeable reinforcement effect of sepiolite on the fibre cement sheets.

The different values obtained between the two kinds of sepiolite cannot be explained easily. Again, microstructural investigation on the fibre cement sheet and on the sepiolites themselves had to be done. The Dolsan sepiolite could possess a better superficial interaction with cementitious matrix, which would explain the efficiency of the reinforcement. It also can be related to the morphological aspect of the sepiolite fibres, their dimension, their specific surface area... etc.

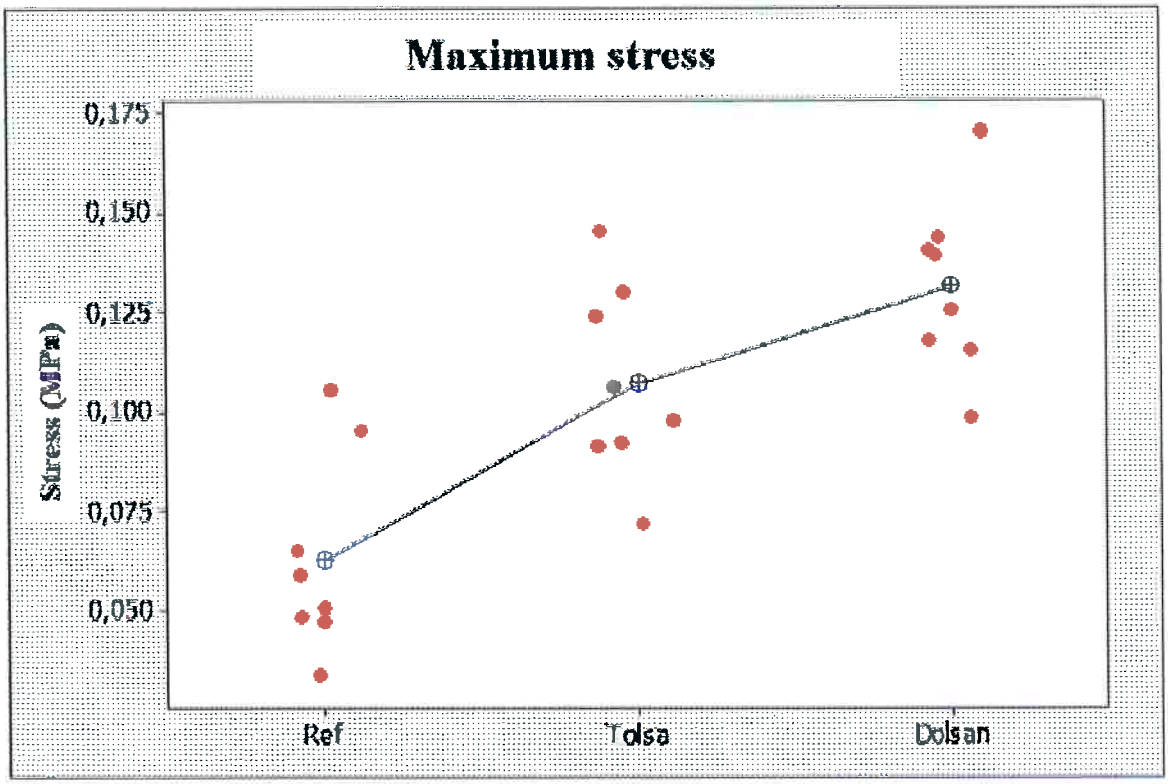

Figure 24- Maximum tensile stress of the three samples

b. Tensile extension at maximum stress

The graphic *Figure 25*, shows the results obtain by adding sepiolite on the extension at maximum stress. At first view, the effect is noticeable, with an average improvement of 21,3% and 26,8% for the Tolsa and the Dolsan samples respectively. Indeed, the average extension at maximum stress was found at about 1,36 mm, 1,65 mm and 1,73 mm respectively for the reference, Tolsa and the Dolsan samples. But as illustrated in the graph the standard deviation around these values are quite high, especially for the samples containing sepiolite, of about 0,16 mm, 0,32 mm and 0,44 mm for the reference, the Tolsa and the Dolsan samples. This reinforces the idea that a problem is encountered during the mixing process. But still, the sepiolite addition seems to have a positive effect on the plasticity of the fibre cement sheets. This is explained by the fact that the sepiolite fibres are able to create a meshing by interacting with the water molecules, retaining them in by fibre hydration. Thus, it can be said that the augmentation of the fibre cement sheets humidity thanks to the added sepiolite has a positive effect since it increase their ductility.

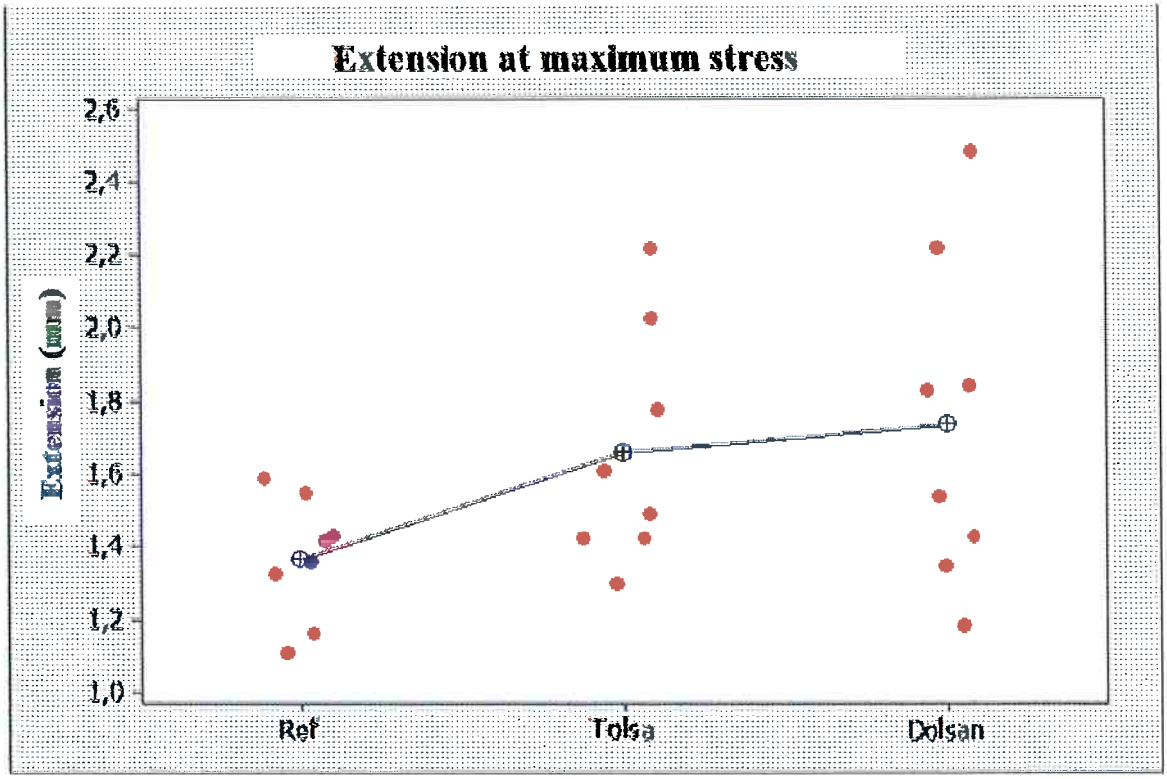

Figure 25- Extension at maximum stress for each sample

It is convenient to confound the maximum stress point with the one of first fissure apparition; actually this is not quite true. Practically, one observes a light shifting between these two. The first fracture can either occur after the maximum stress point or before. Nevertheless, it gives a good indication on the plastic deformation ability of the material.

4.3.Hardened state study

4.3.1. Bending test

The fibre cement sheets were hardened during 28 days, and cut wiht an electrical saw. For each composition, 12 samples with 40*160 mm area were cut in order to be submitted to a 4 points bending test. Before being tested, the samples were saturated in water according to the international bending test norms. This test allows the obtaining of complementary mechanical information such as the modulus of rupture which characterizes the fracture resistance of the material, the modulus of elasticity or the toughness. These mechanical properties were obtained by inserting the exact dimension of each sample in the Blue Hill program which calculated them from the flexure load versus flexure extension curves.

The following graph, *Figure 26*, displays a typical curve obtained by the 4 point bending test.

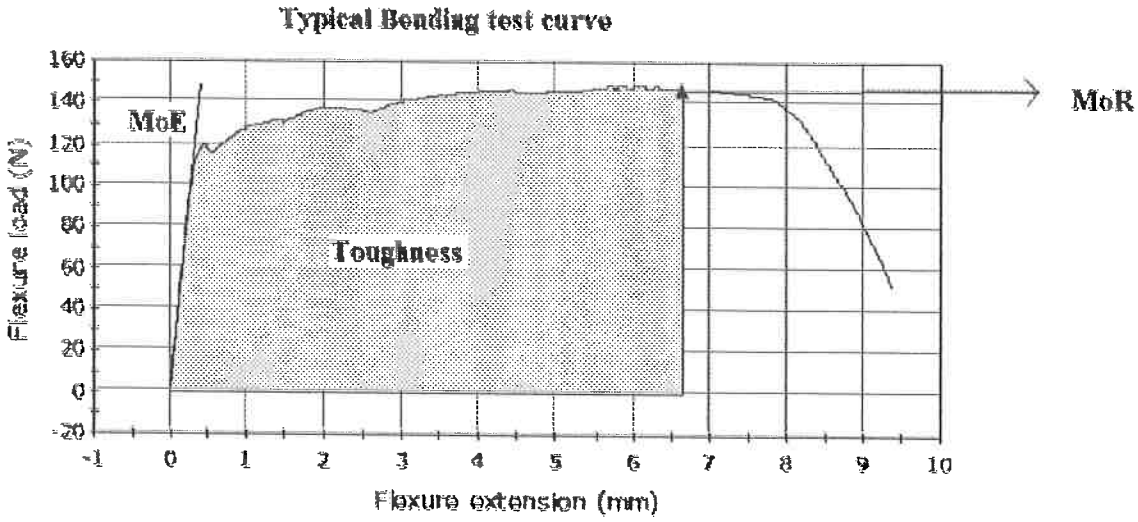

Figure 26- Typical bending test curve

The first linear part of the curve corresponding to the elastic domain, allows the calculation of the Modulus of Elasticity (MoE). The second part characterizing the plastic behaviour of the sample presents a maximum flexure load (or stress), which permits the calculation of the Modulus of Rupture (MoR). The area, in yellow on the figure, delimited by the maximum flexure load gives the toughness after calculation. All the bending test data are gathered in Annex IV.

a. Modulus of Rupture (MoR)

The following graph *Figure 27*, displays the modulus of rupture obtained for each composition, as well as their average value and dispersion. The effect of sepiolite addition is quite obvious. The reference samples exhibit an average MoR of 9,81 MPa whereas the sample containing sepiolite shows higher values. An average augmentation of 32,1% and 27,2% have been respectively found for the Tolsa and the Dolsan samples with average MoR values of 12,96 MPa and 12,48 MPa. But the calculation of the standard deviation show that these values can vary noticeably. Indeed, the MoR values show a standard deviation of respectively, 1,21, 0,91 and 1,32 MPa for the reference, the Tolsa and Dolsan samples. The variability of this value is influenced by the fibre repartition. This means that an improvement in the mixing process is required to obtain a more homogenous sequence of results.

Nevertheless it is obvious that the addition of sepiolite has a positive effect on the fibre cement resistance to fracture, and no clear differentiation can be done between the two kinds of sepiolite. This improvement is certainly due to the amelioration of the interface interaction between the PVA fibres and the cementitious matrix. Indeed thanks to its superficial properties the sepiolite fibres may be able to create a bridging effect between the cement particles and the reinforcement fibres, which increase efficiently the resistance to fracture of the composite. When we decided to add sepiolite to the fibre cement, we were seeking for this bending property.

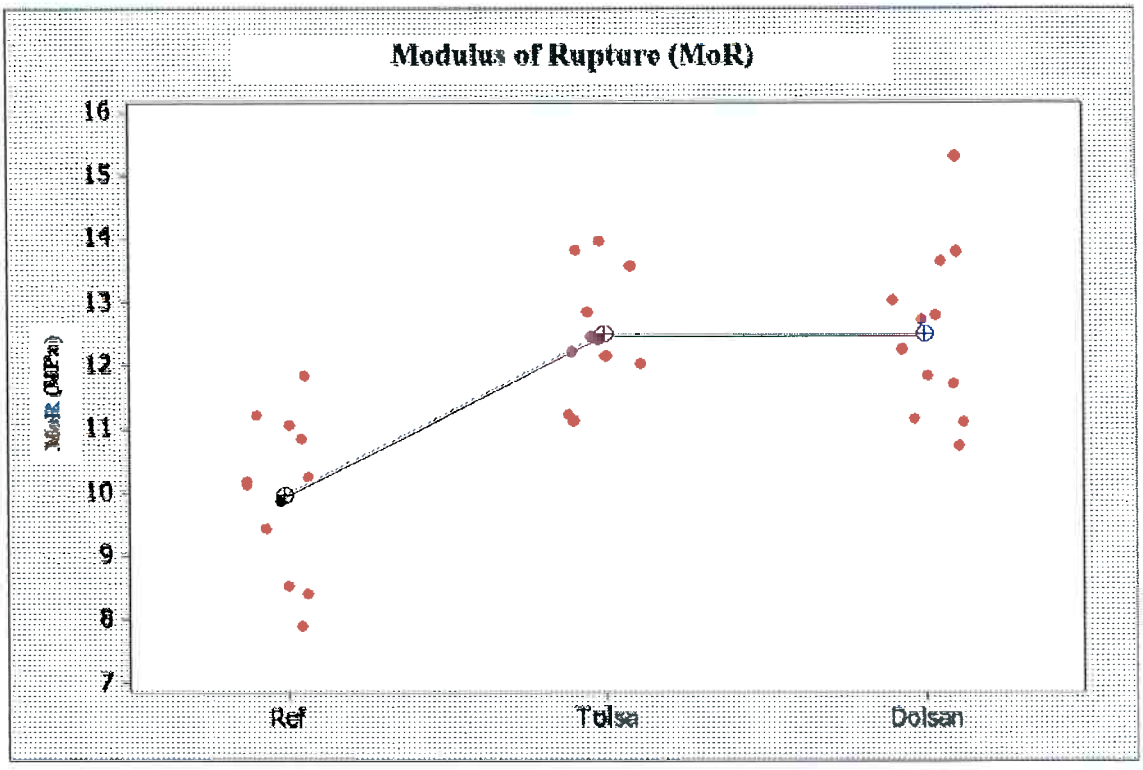

Figure 27- Modulus of Rupture (MoR) results for each composition

b. Modulus of Elasticity (MoE)

The modulus of elasticity is a property, which depends mainly of the matrix characteristics. As already said, the matrix governs the pre-cracking state, whereas the fibres govern the post-cracking state. The MoE was calculated thanks to the tangent of the flexure load versus flexure extension curve.

The following graphic *Figure 28* displays the result obtained for each composition. The results are surprising: no clear effect can be underlined. Indeed, the reference and the Dolsan samples show similar average values of MoE of 9675,4 and 9537,1 MPa respectively whereas the Tolsa presents a much higher value of 13925,6 MPa. But the standard deviations of these sequences of result are quite important of 3561 MPa for the reference samples, 1454,0 MPa and 1182,1 MPa for the Tolsa and Dolsan ones. This means that the MoE is very sensitive to any variation in the sample preparation. These results do not allow a conclusion on the effect of the addition of sepiolite on the fibre cement MoE. The Tolsa sepiolite seems to increase it whilst the Dolsan one doesn't seem to have any effect on it.

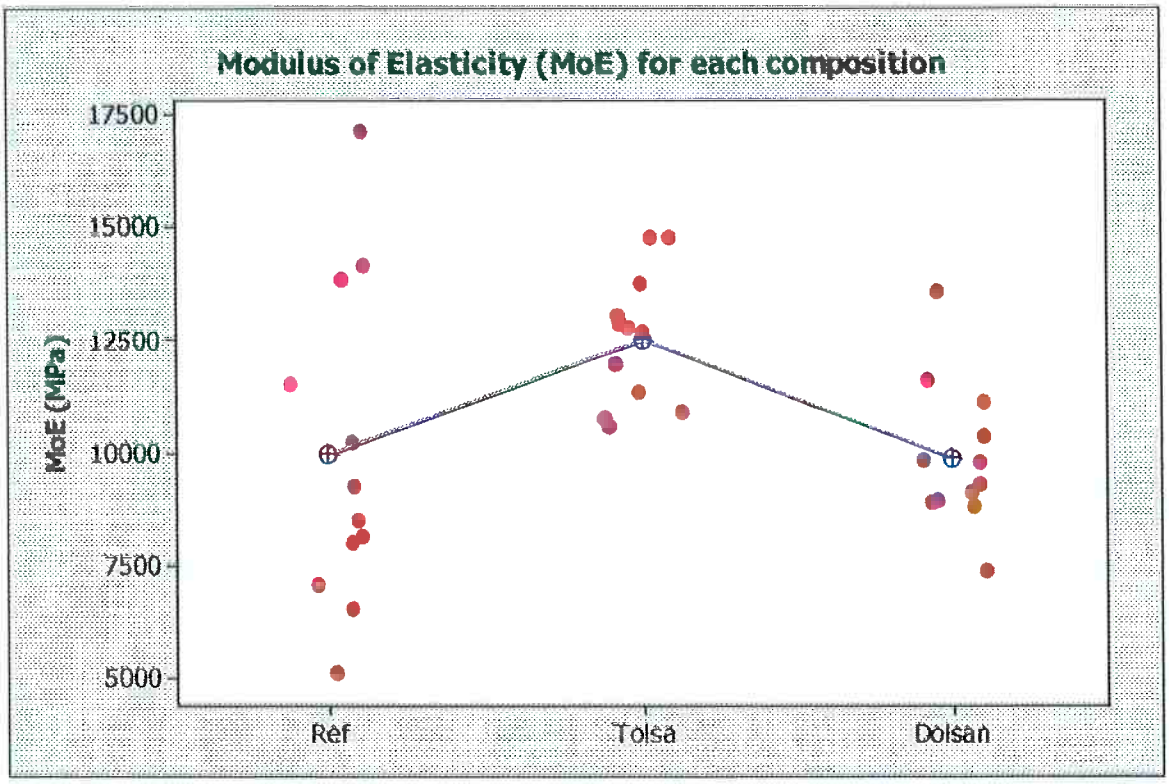

Figure 28- Modulus of Elasticity for each fibre cement sheet composition

c. Toughness

Toughness is an important mechanical property for fibre cement materials. It gives information about the material resistance to impact. In other words, it can be presented as specific fracture energy, expressed as $J.m^{-2}$. To a microscopic scale, it reflects the state of

molecules' cohesion, and is not in correlation with the hardness. The higher the toughness of the material, the less fragile it is.

Figure 29 displays the toughness of the material in relation to the composition of the fibre cement.

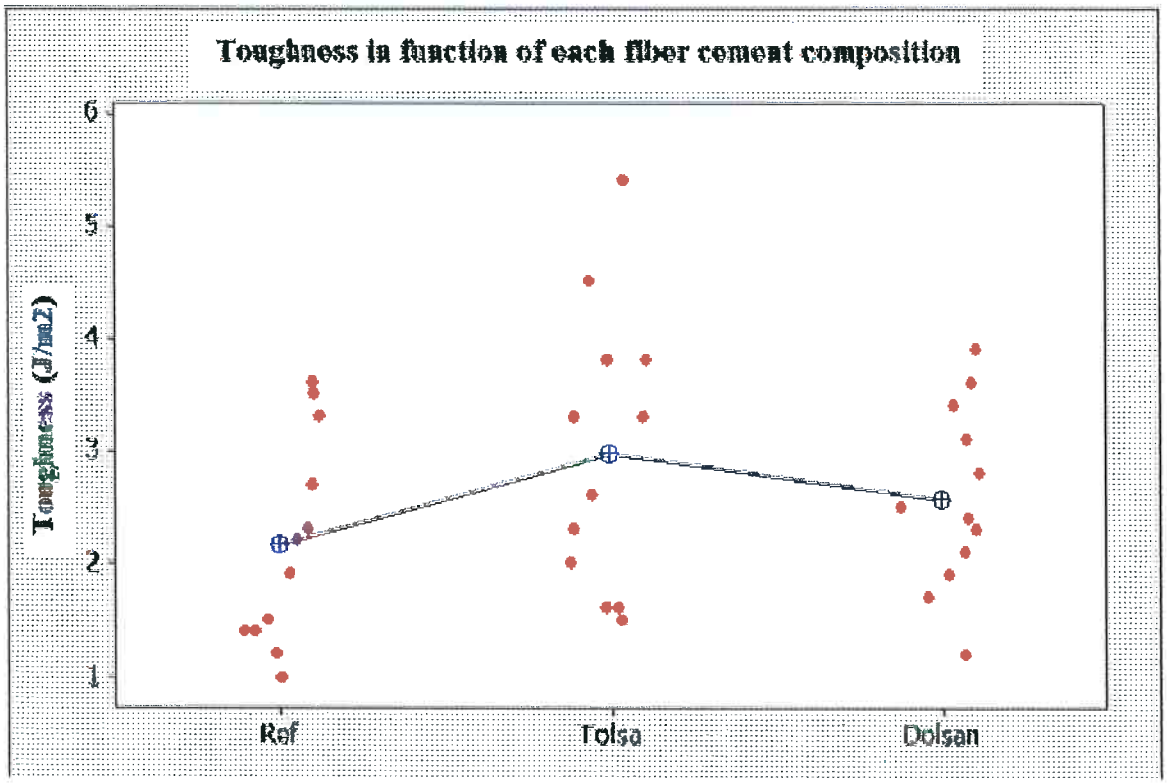

Figure 29- Toughness of each fibre cement composition

The same observations can be made on the result of toughness as the ones obtained for the modulus of elasticity. No clear tendency can be outlined, even if the Tolsa sepiolite seems to increase a little bit the average toughness value. Indeed the Tolsa samples present an average toughness of 3,4 $J.m^{-2}$ whereas the reference and the Dolsan samples exhibit lower values, respectively of 2,4 and 2,56 $J.m^{-2}$. But the calculation of the standard deviations show a great variability of this property, indeed the reference, the Tolsa and Dolsan sequence of results show values of 0,9, 1,24 and 0,8 $J.m^{-2}$ respectively. This means that no conclusion can be done on the effect of the added sepiolite on the fibre cement toughness. In the worst case, it will not decrease it, but no improvement is noticeable.

5. Conclusion

This study the goal of which was to analyse the influence of the addition of sepiolite on the physical and mechanical properties of fibre-reinforced cement sheets, gave remarkable results on numerous of points.

An addition of 1% of sepiolite to the Cellulose-PVA reinforced cement is enough to produce a suitable flocculation effect, which increases largely the efficiency of the filtration step during the casting process. This improvement enhances the capability of fine particle retention thanks to a densification of the fibre cement material. Indeed, the sepiolite molecules seem to be able to create a network within the fibre cement material preventing the water to flow easily trough it. Moreover, the fibre cement sheets containing sepiolite retain an average excess of humidity of about 1,3% compared to the sepiolite-free ones. This is due to the excellent sorptive characteristic of the sepiolite which is capable of trapping the water by hydrophilic attraction within its microstructure.

Tensile tests were performed on fresh fibre cement samples. An addition of 1% of sepiolite showed great improvement related to the statements mentioned above. Indeed, tensile curves of sepiolite samples presented maximum stress much higher than the sepiolite-free ones (improvement of 70,8 % for the Tolsa samples and 108,5 % for the Dolsan ones). This result underlines the benefit of addition of sepiolite, which enhances the interaction between the cement particles and the fibres. The tensile extension at maximum stress exhibits lower improvements with sepiolite addition but they are still noticeable. The higher water content of the fibre cement sheets with sepiolite induces an amelioration of their plasticity which is primordial to crack-preventing during their final shaping.

Four points bending test performed on hardened samples emphasized two main statements. Firstly, a large improvement was found on the Modulus of Rupture (MoR) of the samples containing sepiolite. This reinforces the idea that the sepiolite, thanks to its superficial properties, induces a bridging effect between the fibres and the cement matrix, thus strengthening it and delaying crack apparitions. The second statement comes from the high standard deviations obtained for the Modulus of Elasticity (MoE) and toughness sequences of results, avoiding a viable conclusion. This variability of the data, even found for the MoR sequences of results, expresses the lack of constancy during the laboratory scale sample

preparation. Nevertheless, the industrial process shows better constancy and would certainly solve this inconvenience.

This study analysed the effects of two types of sepiolite: a Spanish one, the commercially named Tolsa, and a Turkish one, the Dolsan. Light differences in their influence on the physical and mechanical properties of the fibre cement have been observed. However, the sepiolite Dolsan seems to present a more efficient flocculating effect, which would explain the lower dewatering speed rate and the better tensile properties exhibited by the samples containing it.

In order to further understand the phenomena involved with the addition of sepiolite to the fibre cement preparation, a micro-structural investigation is required. Thus it would be possible to characterize the meshing created by the sepiolite fibres within the fibre cement composite, allowing a better understanding of the previous physical and mechanical improvement observed.

6. References

[1] ***., ***Special topic : cements and concrete*** in: Engineering Materials,***

[2] A. BENTUR, S. MINDESS, ***Fibre Reinforced Cementitious Composites***, Elsevier Applied Science, London and New York, 1990

[3] D.J. HANNANT, Durability of Propylene Fibres in Portland Cement-based Composites; Eighteen Years of Data, in: Cement and Concrete Research V28 N12, Elsevier Science Ldt, 1998, p. 1809-1817

[4] J-L. SALAGER, ***Interfacial Phenomena in Dispersed System,*** Laboratorio FIRP Escuela de Ingeniera Quimica Universidad de Los Andes, Los Andes (Venezuela), 1993

[5] http://www.nbtc.cornell.edu/facilities/downloads/Zeta%20potential%20-%20An%20introduction%20in%2030%20minutes.pdf

[6] A. SINGER, E. GALAN, ***Palygorskite-Sepiolite Occurrences, Genesis and Uses***, in: Developments in Sedimentology 37, Elsevier, Amsterdam

[7] E. GALAN, ***Properties and Applications of Palygorskite-Sepiolite Clays***, in: Clays Mineral 31, 1996, p. 443-453

[8] T. KAVAS, E. SABAH, M. S. CELIK, ***Structural Properties of Sepiolite-reinforced Cement Composite***, in: Cement and Concrete Research 34, 2004, p. 2135-2139

[9] M. Alkan, Ö. DEMIRBAŞ, M. DOĞAN, ***Electrokinetic Properties of Sepiolite Suspensions in Different Electrolyte Media***, in: Journal of Colloid and Interface Science 281, 2005, 240-248

Annex I. Characterisation of raw materials

I.1. Chemical analysis

The following table *Table 3* indicates the weight percentage of oxides for each compound. This quantitative analysis was done by X-Ray fluorescence.

Table 3- Oxides % for each compound

Elements	Cement	Limestone	Microsilica
SiO_2	23,1	2,38	95,6
Al_2O_3	6,24	0,36	<0,10
Fe_2O_3	1,93	0,39	<0,10
MnO	<0,10	<0,10	<0,10
MgO	3,45	8,78	0,31
CaO	56,9	46,1	0,28
Na_2O	<0,10	<0,10	<0,10
K_2O	0,82	0,18	1,04
TiO2	<0,10	<0,10	<0,10
P_2O_5	<0,10	<0,10	<0,10
SrO	<0,10	<0,10	<0,10
SO_3	2,49	<0,10	<0,10
PF	4,35	42	2,91

I.2. Density and specific surface area

Table 4- Density and specific surface area of each compound

	Cement	Limestone	Microsilica	PVA fibres	Cellulose Fibers
Density ($g.cm^{-3}$)	2,972	2,691	2,176	1,356	1,2
Specific surface area ($m^2.g^{-1}$)	1,43	1,50	18,18	–	–

I.3. X-Ray Diffractometry

I.3.1. Cement CP II

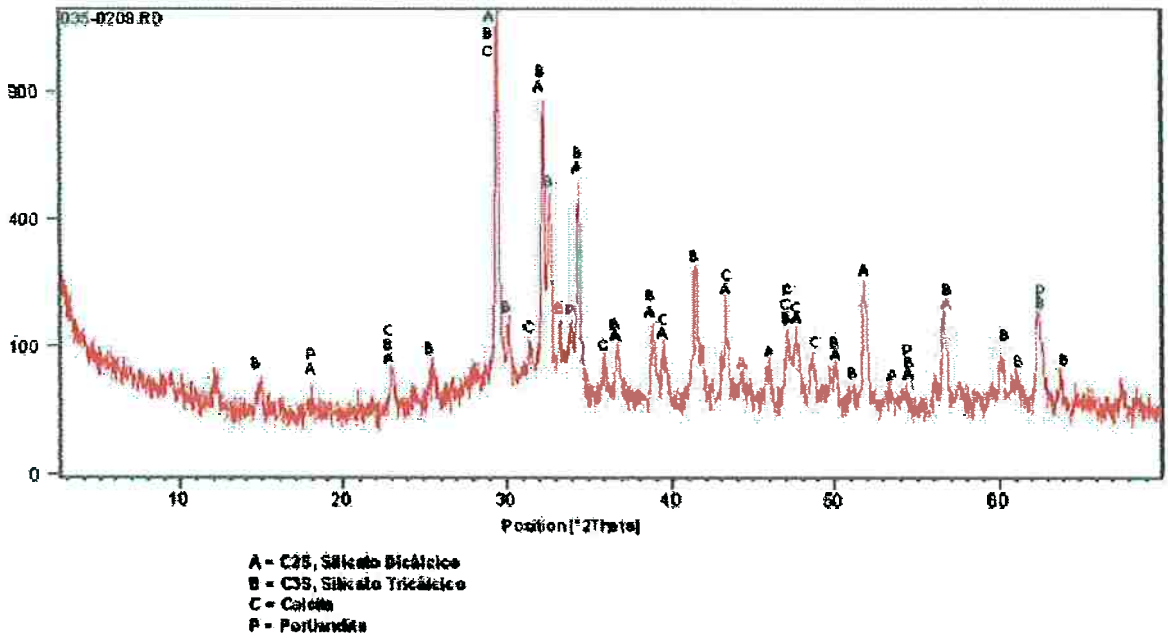

Figure 30- X-Ray diffraction of the cement CP II

I.3.2. Limestone

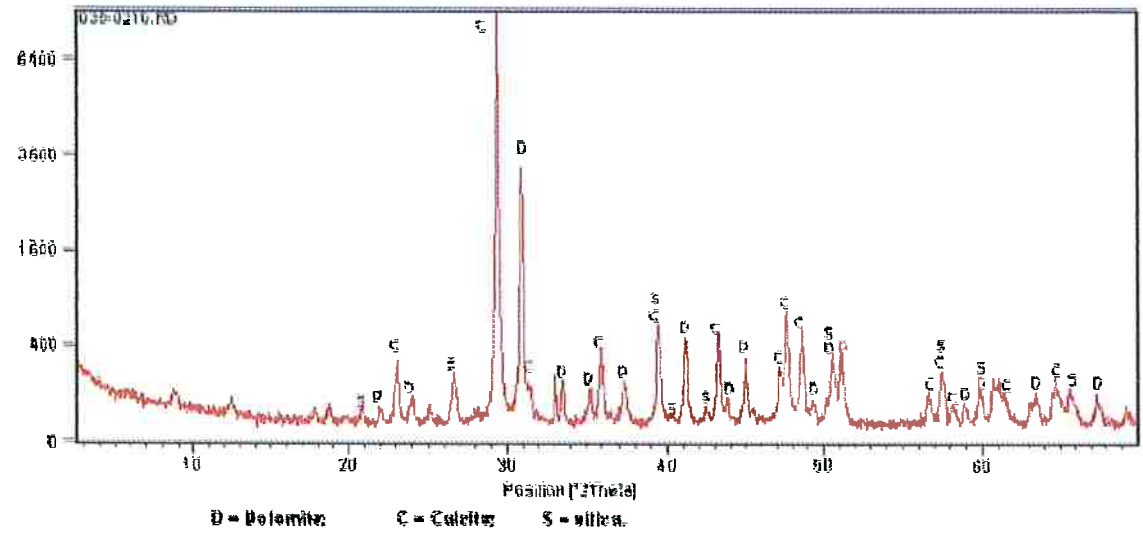

Figure 31- X-Ray diffraction of the limestone

I.3.3. Microsilica

The following diffractogram is characteristic of an amorphous structure. The microsilica is amorphous silica and thus does not possess a crystalline structure.

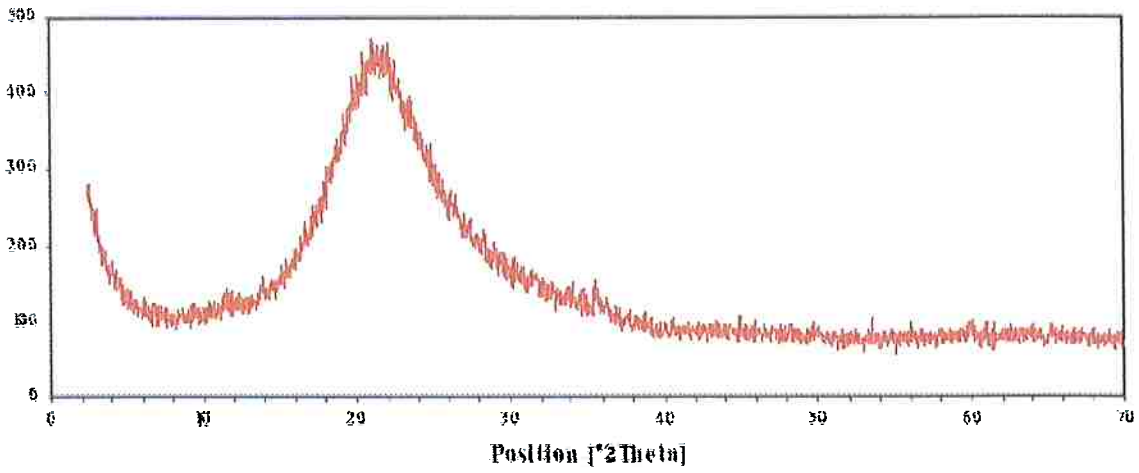

Figure 32- X-Ray diffraction of microsilica

I.3.4. Sepiolite Tolsa

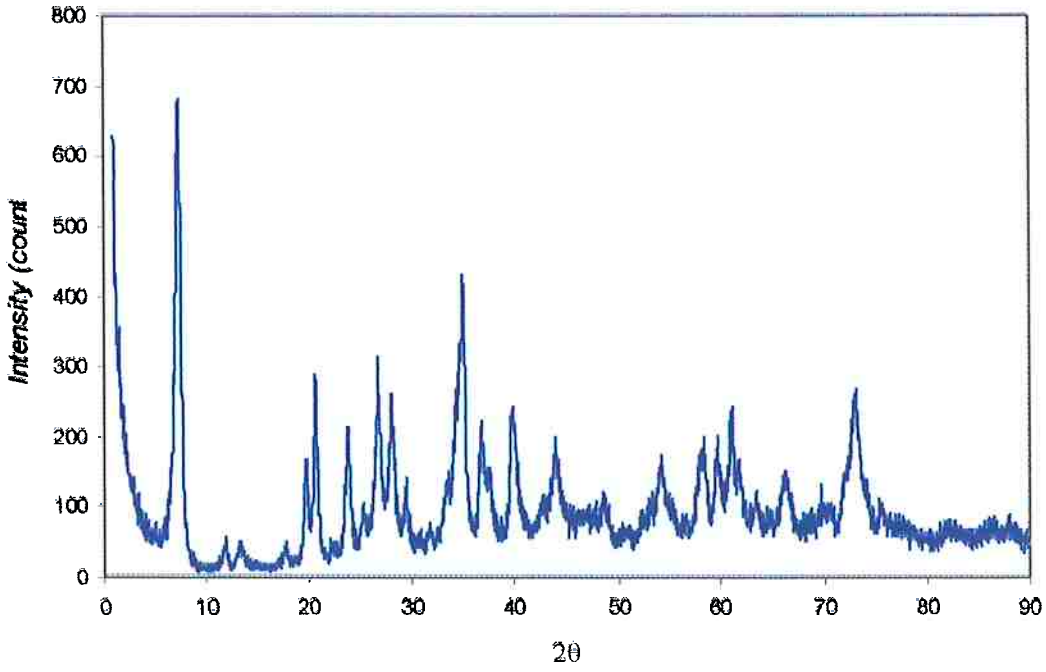

Figure 33- X-ray diffractogram of sepiolite Tolsa

I.3.5. Sepiolite Dolsan

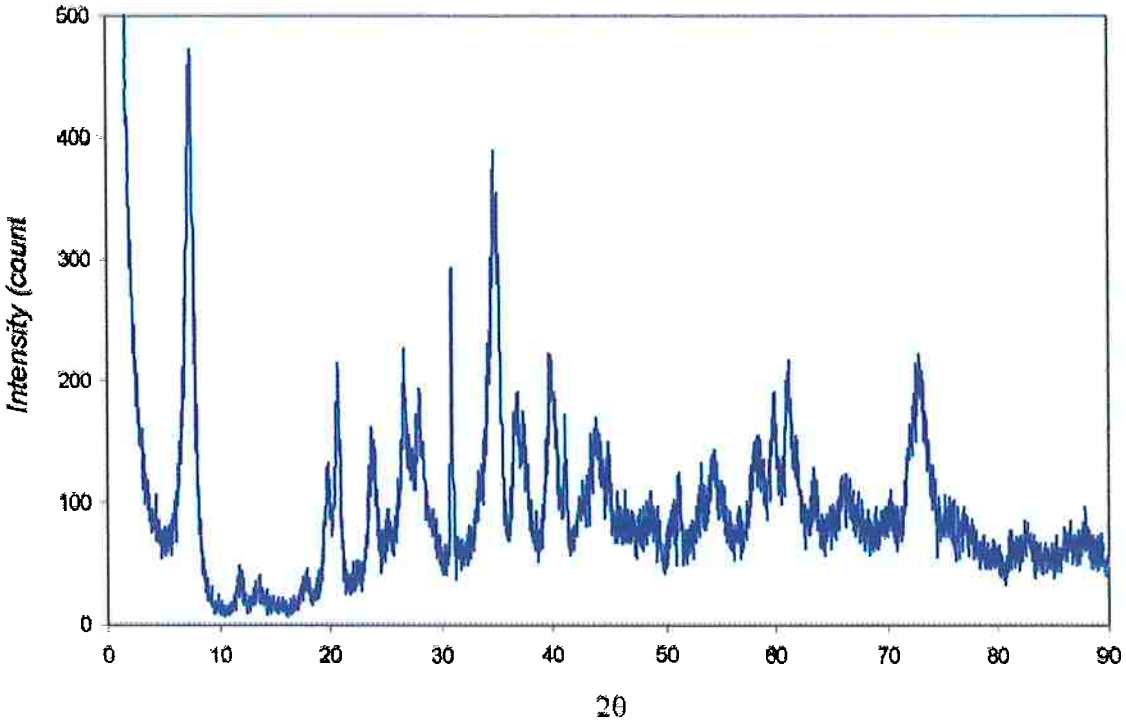

Figure 34- X-ray diffractogram of sepiolite Dolsan

I.4. Granulometric distribution

I.4.1. Cement CP II

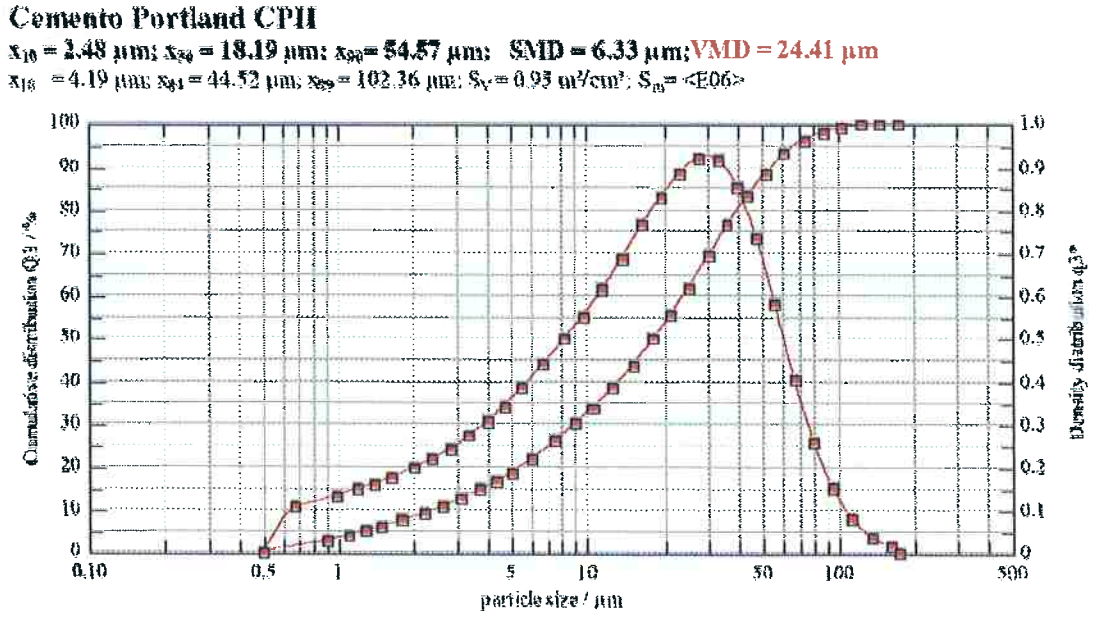

Figure 35- Cement CP II granulometric distribution

I.4.2. Limestone

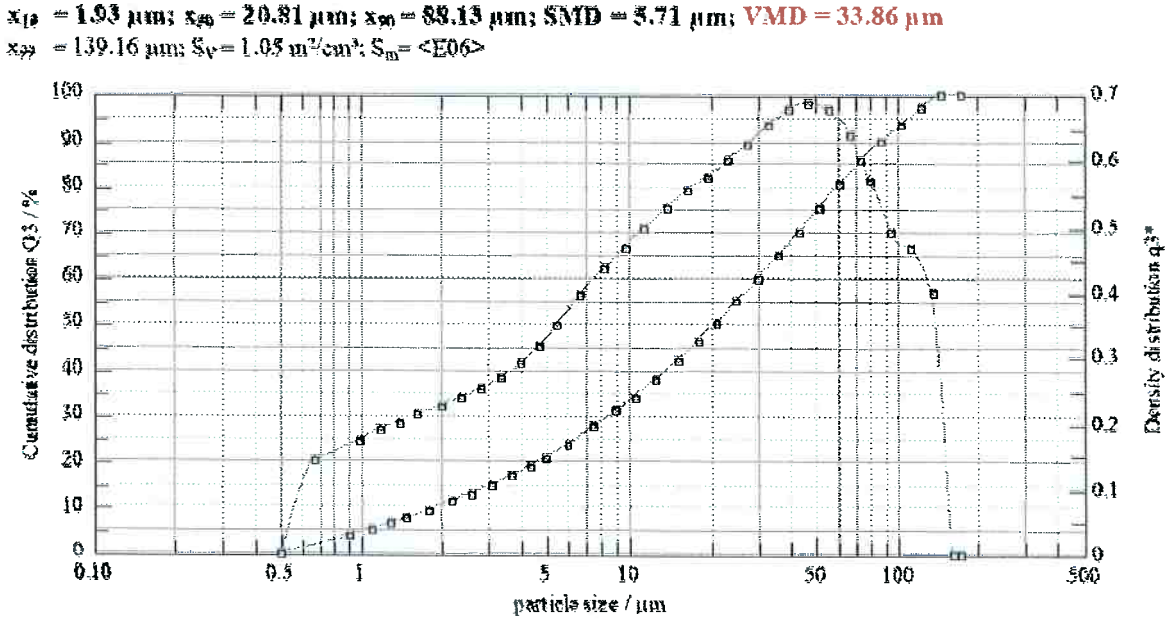

Figure 36- Limestone granulometric distribution

I.4.3. Microsilica

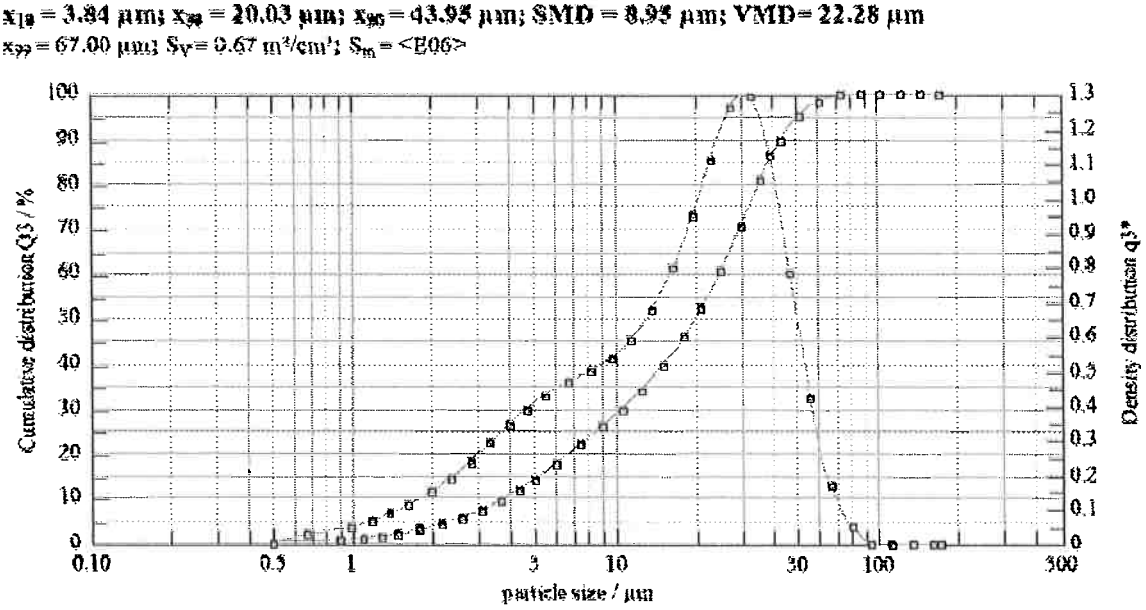

Figure 37- Microsilica granulometric distribution

I.5. Samples composition

Table 5- Samples weight % composition

Compounds	Reference (%)	Tolsa (%)	Dolsan (%)
Cement	64	63,36	63,36
Limestone	26,2	25,94	25,94
Microsilica	5	4,95	4,95
Tolsa Sepiolite	0	1,00	0,00
Dolsan Sepiolite	0	0,00	1,00
Cellulose	3	2,97	2,97
PVA	1,8	1,78	1,78
Total	100,00	100,00	100,00

Volume of the sheets = 240 cm^3

Table 6- Composition details of the reference sheets

Reference				
Compounds	**Density**	**Weight (%)**	**Volume per sheet (cm3)***	**Mass per sheet (g)**
Cement	3,1	64	81,4	252,4
Limestone	2,691	26,2	38,4	103,3
Microsilica	2,176	5	9,1	19,7
Tolsa Sepiolite	2,2	0	0	0
Dolsan Sepiolite	2,2	0	0	0
Cellulose	1,2	3	9,9	11,8
PVA	1,356	1,8	5,2	7,1
Total	-	**100**	**144**	**394,4**

*Considering a porosity of 40%

Water = 1314,83 g / 30% of solid

Table 7- Composition details of the Tolsa sheets

Tolsa				
Compounds	**Density**	**Weight (%)**	**Volume per sheet (cm3)***	**Mass per sheet (g)**
Cement	3,1	63,36	79,0	244,9
Limestone	2,691	25,94	37,2	100,2
Microsilica	2,176	4,95	8,8	19,1
Tolsa Sepiolite	2,2	1,00	1,8	3,9
Dolsan Sepiolite	2,2	0,00	0,0	0,0
Cellulose	1,2	2,97	9,6	11,5
PVA	1,356	1,78	7,7	6,9
Total	-	**100**	**144,0**	**386,5**

*Considering a porosity of 40%

Water = 1314,83 g / 30% of solid
Water for the suspension = 1210,89 g
Water for the gel = 77,29 g (5% of sepiolite in weight)

Table 8- Composition details of the Dolsan sheets

Dolsan				
Compounds	**Density**	**Weight (%)**	**Volume per sheet (cm3)***	**Mass per sheet (g)**
Cement	3,1	63,36	79,0	244,9
Limestone	2,691	25,94	37,2	100,2
Microsilica	2,176	4,95	8,8	19,1
Dolsan Sepiolite	2,2	1,00	1,8	3,9
Tolsa Sepiolite	2,2	0,00	0,0	0,0
Cellulose	1,2	2,97	9,6	11,5
PVA	1,356	1,78	7,7	6,9
Total	-	**100**	**144,0**	**386,5**

*Considering a porosity of 40%

Water = 1314,83 g / 30% of solid
Water for the suspension = 1210,89 g
Water for the gel = 77,29 g (5% of sepiolite in weight)

Annex II. Dewatering data

Table 9- Average dewatering data

Time (sec)	Reference water loss (g)	Tolsa water loss (g)	Dolsan water loss (g)
0	0	0	0
0,5	0,15	0,975	1,05
1	1,8	2,7	3,35
1,5	4,675	5,5	6,65
2	7,05	8,9	10,75
2,5	9,75	13,5	16,1
3	13,475	19,65	22,6
3,5	17,6	26,15	29
4	24,075	32,075	35,875
4,5	30,475	39,775	43,075
5	37,325	48,1	50,7
5,5	44,85	55,825	59
6	49,575	65,15	67,625
6,5	57,625	74,25	76,8
7	66,2	82,5	84,775
7,5	74,225	92,925	94
8	80,65	102,5	103,25
8,5	86,85	112,25	110,35
9	94,85	121,2	121,225
9,5	101,95	130,75	130,825
10	108,3	140,425	139,125
10,5	117,025	149,8	150,425
11	125,725	160,15	161,15
11,5	135,65	169,625	171
12	146,2	179,5	181,05
12,5	153,625	188,275	188,95
13	162,35	198	196,9
13,5	171,375	208,925	205,65
14	180,9	219,475	214,575
14,5	190,75	228,925	221,625
15	200,5	237,95	230,15
15,5	209,8	246,4	239,35
16	218,4	254,775	248,325
16,5	228,85	263,95	255,525
17	238,425	272,025	263
17,5	249,025	281,075	271,05
18	258,45	290,475	279,925
18,5	267,725	299,525	288,75

19	276,9	308,525	296,3
19,5	287,75	315,225	303,2
20	297,725	324,7	311,05
20,5	307,25	333,85	318,175
21	318,1	342	324,725
21,5	327,075	350,825	333,45
22	336,625	358,8	342,425
22,5	347,025	368,35	349,575
23	356,825	375,4	357,575
23,5	364,575	383,675	364
24	376,6	389,875	372,025
24,5	386,225	398,7	379,05
25	394,35	406,55	386,475
25,5	407,3	414	393,975
26	417,55	422,675	400,8
26,5	426,3	429,6	408,2
27	435,325	436,65	414,75
27,5	443,5	444,725	421,575
28	454,425	457,975	429,425
28,5	465,875	462,425	436,325
29	476,725	470,55	443,2
29,5	484,7	476,175	450,025
30	494,975	482,325	456,175
30,5	505,55	489,425	463,125
31	515,875	497,025	470,375
31,5	525,225	504,675	476,7
32	534,1	512,475	482,675
32,5	543,25	520,275	489,3
33	549,175	526,375	495,825
33,5	559,125	533,675	502,9
34	568,6	541,925	509,075
34,5	580,075	547,5	515,2
35	591,5	555,75	521,6
35,5	599,45	563,475	526,825
36	607,725	570,95	530,625
36,5	617,9	577,65	536,675
37	628,45	584,45	542,825
37,5	635,125	591,65	548,65
38	645,05	598,375	554,2
38,5	656,825	605,55	559,75
39	665,125	611,2	566,275
39,5	672,85	617,025	571,725
40	682,65	623,825	579,075

40,5	691,45	631,65	585,175
41	701,525	639,075	591,2
41,5	710,4	644,675	595,575
42	718,025	650,825	600,65
42,5	727,825	656,925	605,425
43	735,75	664,275	610,95
43,5	746,875	670,3	616,2
44	757,55	676,45	621,75
44,5	766,975	682,55	627,675
45	772,05	689,525	633,8
45,5	779,85	695,325	639,275
46	790,075	700,95	644,625
46,5	796,575	707,825	650,25
47	804,5	712,7	654,975
47,5	811,9	718,2	660,175
48	819,5	724,625	665,55
48,5	825,975	730,4	670,975
49	835,925	736,725	676,25
49,5	848	742,4	680,975
50	864,6	747,325	685,8
50,5	860,15	753,05	691,05
51	870,575	760,025	695,95
51,5	875,225	765,825	700,075
52	884,375	771,775	705,6
52,5	913,5	776,375	710,4
53	899,575	782,35	715,55
53,5	918,75	786,9	720,35
54	914,45	792,725	725,225
54,5	910,95	798,45	731,5
55	931,325	803,325	735,875
55,5	925,9	808,45	739,55
56	950,175	813,65	744
56,5	939,275	819,325	751,9
57	962,725	823,9	754,625
57,5	1002,6	828,25	759,025
58	955,2	832,4	763,65
58,5	958,7	837,6	768,675
59	964,425	842,65	772,95
59,5	987,225	849,875	777,075
60	996,175	856,1	782,175
60,5	989,65	858,975	786,425
61	1000,15	863,225	790,25
61,5	1002,1	873,725	794,225

62	989,4	876,5	797,9
62,5	1012,125	875,85	803,475
63	1029,825	878,925	807,275
63,5	1010,675	886	811,4
64	1028,6	904,7	813,75
64,5	1023,325	896,35	818,875
65	998,25	900,25	822,325
65,5	1028,6	904,7	842,375
66	1020,275	908,675	824,75
66,5	1047,45	912,3	833,325
67	1014,15	917,1	837,425
67,5	1026,725	920,5	841,525
68	1025,925	925,6	841,075
68,5	1073,45	929,85	848,775
69	1025,625	934,45	852,475
69,5	1078,825	940,175	864,5
70	1026,5	940,975	858,925
70,5	1068,55	941,875	862,025
71	1014,3	951,6	865,45
71,5	1052,45	952,7	867,45
72	1082,525	952,4	872,85
72,5	1015,9	956,625	876,15
73	1055,425	967,675	880,125
73,5	1068,45	967,8	882,1
74	1044,15	965,95	884,425
74,5	1049,25	966,775	886,9
75	1024,825	969,15	919,925
75,5	1039,225	993,775	892,2
76	1056,15	983	908,15
76,5	1056,175	979,025	897,325
77	1038,25	984,675	902,55
77,5	1061	987,925	904
78	1031,775	988,8	909,075
78,5	1062,2	998,2	919,375
79	1036,475	991,45	914,475
79,5	1065,525	1000,4	915,2
80	1039,25	995,1	929,8

Annex III. Tensile test data

For each of the three compositions, 8 samples were tested giving rough load versus extension curves. These curves are presented in the following without any modifications. The rough numeric data could have been displayed too but for space reason, just the remarkable points are given.

III.1. Reference samples

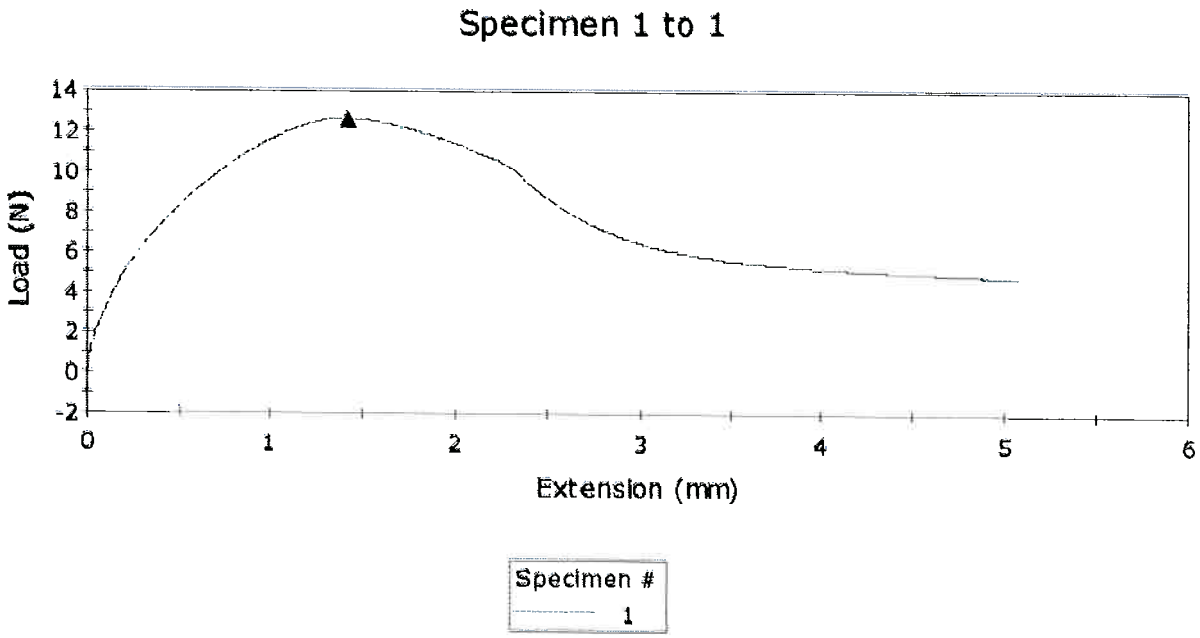

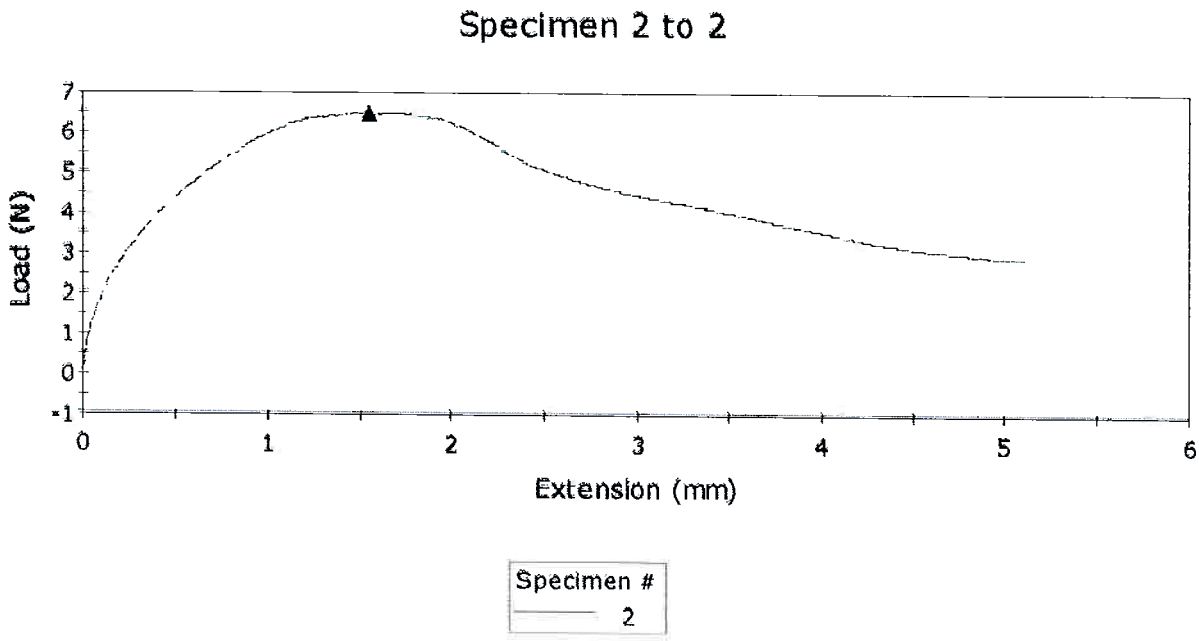
Specimen 2 to 2
Load (N)
7
6
5
4
3
2
1
0
-1
0
1
2
3
4
5
6
Extension (mm)
Specimen #
2

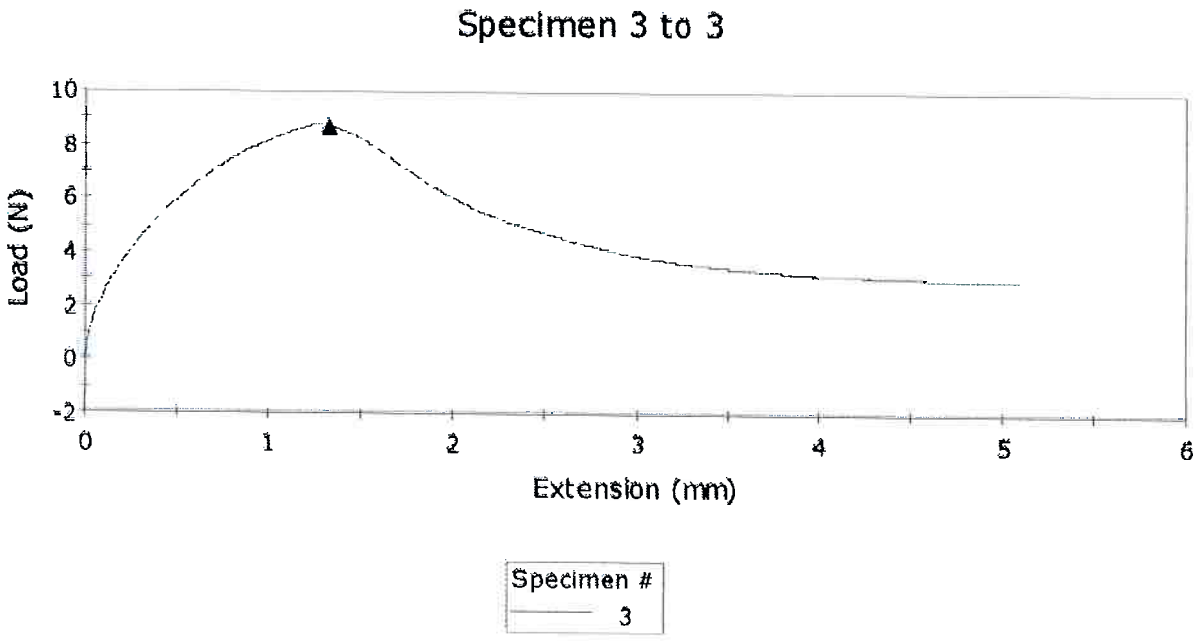
Specimen 3 to 3
Load (N)
10
8
6
4
2
0
-2
0
1
2
3
4
5
6
Extension (mm)
Specimen #
3

Specimen 4 to 4

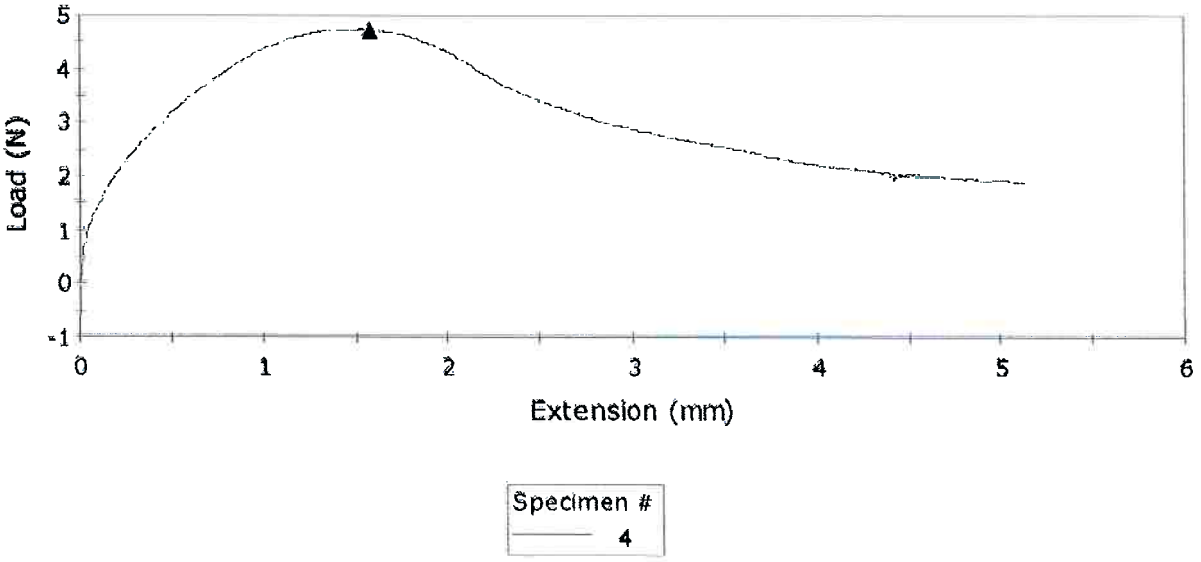

Specimen 5 to 5

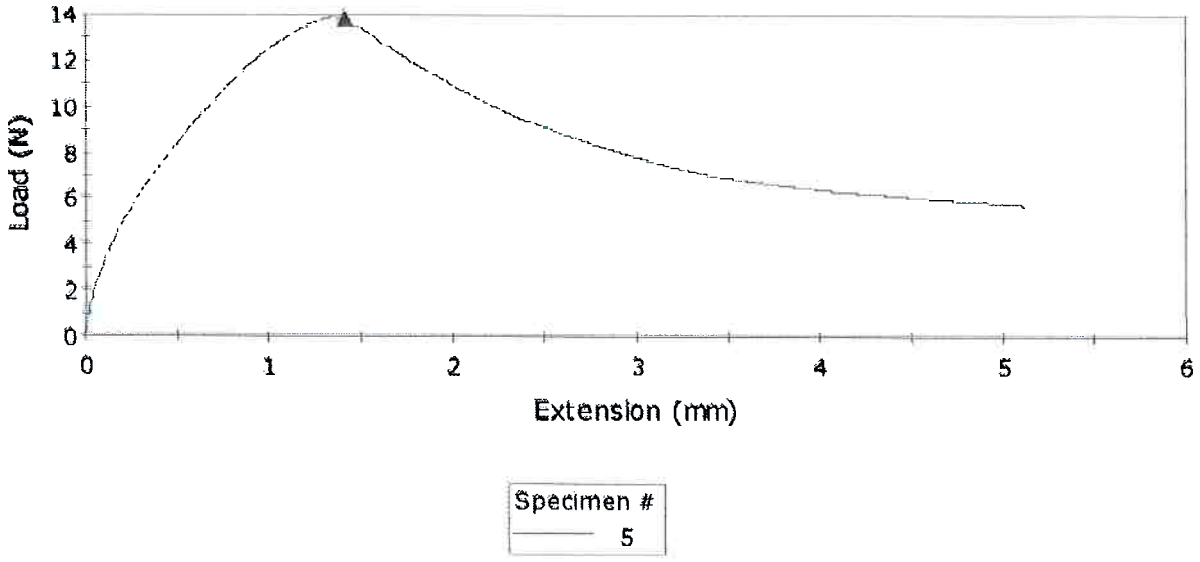

Specimen 6 to 6

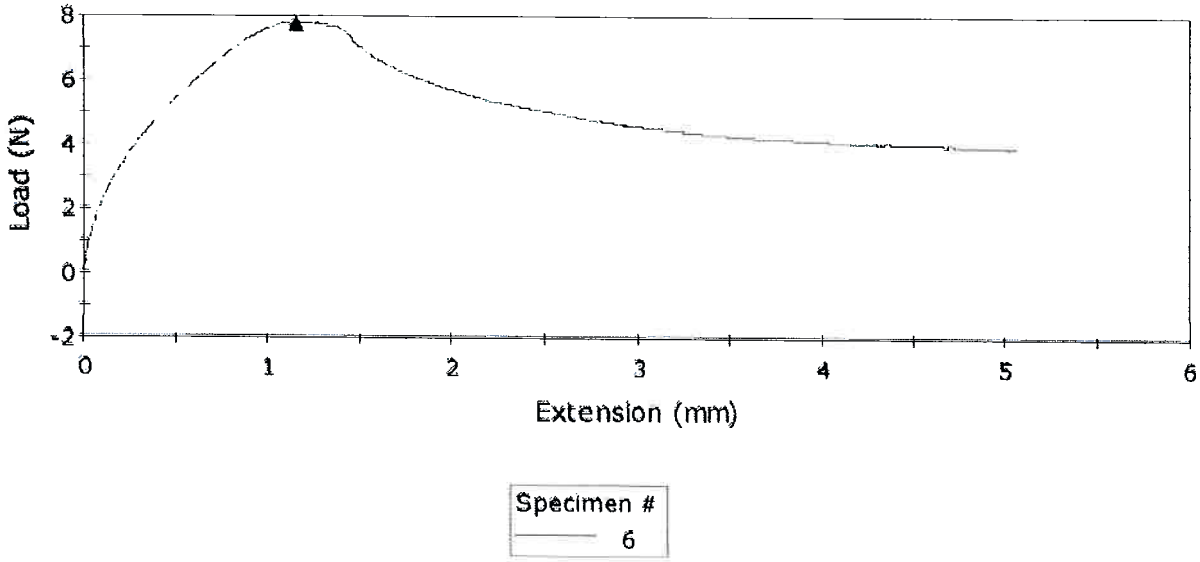

Specimen 7 to 7

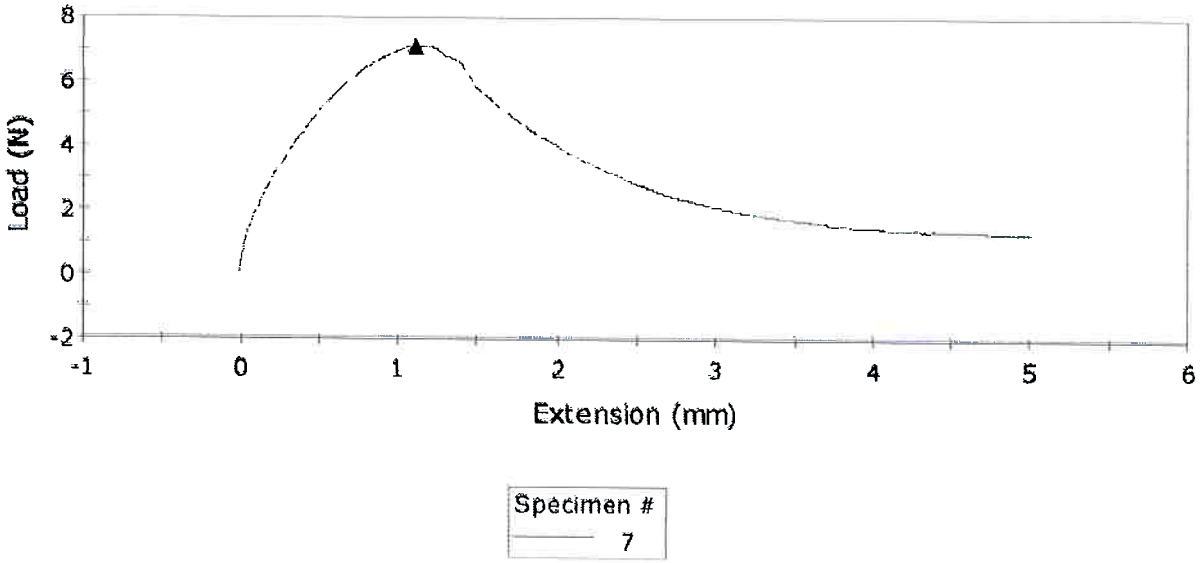

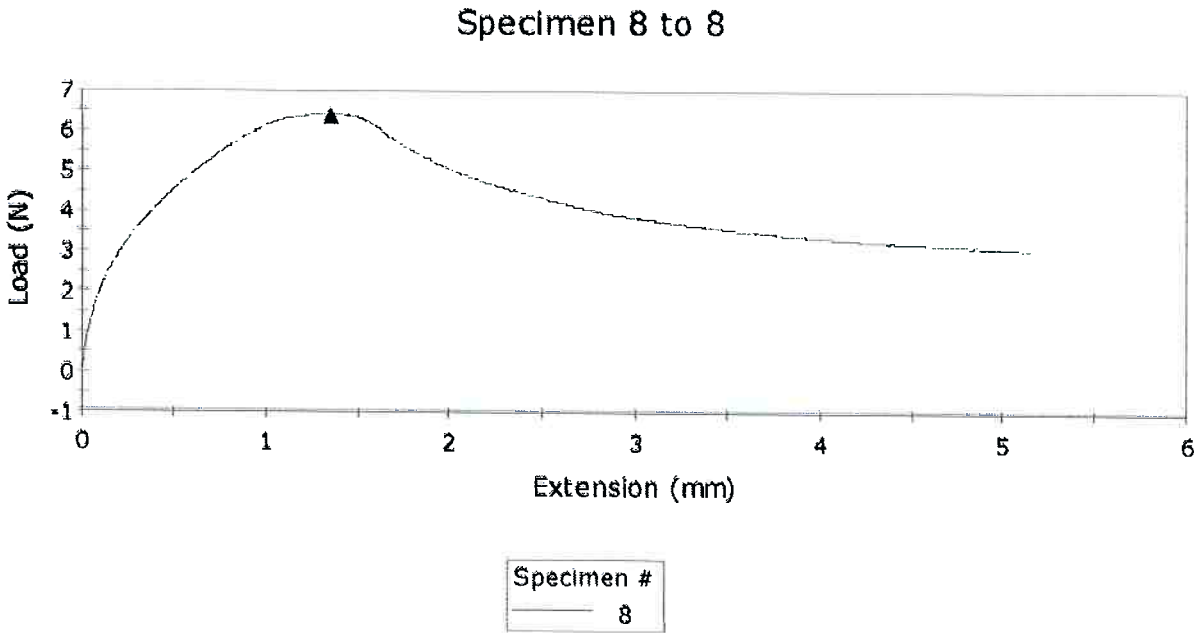

Table 10- Remarkable points of the tensile curves

	Maximum Load (N)	Tensile stress at Maximum Load (MPa)	Tensile extension at Maximum Load (mm)
1	12.55382	0.09496	1.42681
2	6.42657	0.04839	1.54687
3	8.68322	0.06480	1.32694
4	4.69364	0.03401	1.58687
5	13.82866	0.10476	1.41362
6	7.73978	0.05863	1.16037
7	7.08207	0.05059	1.11312
8	6.36513	0.04680	1.35337

III.2. Tolsa samples

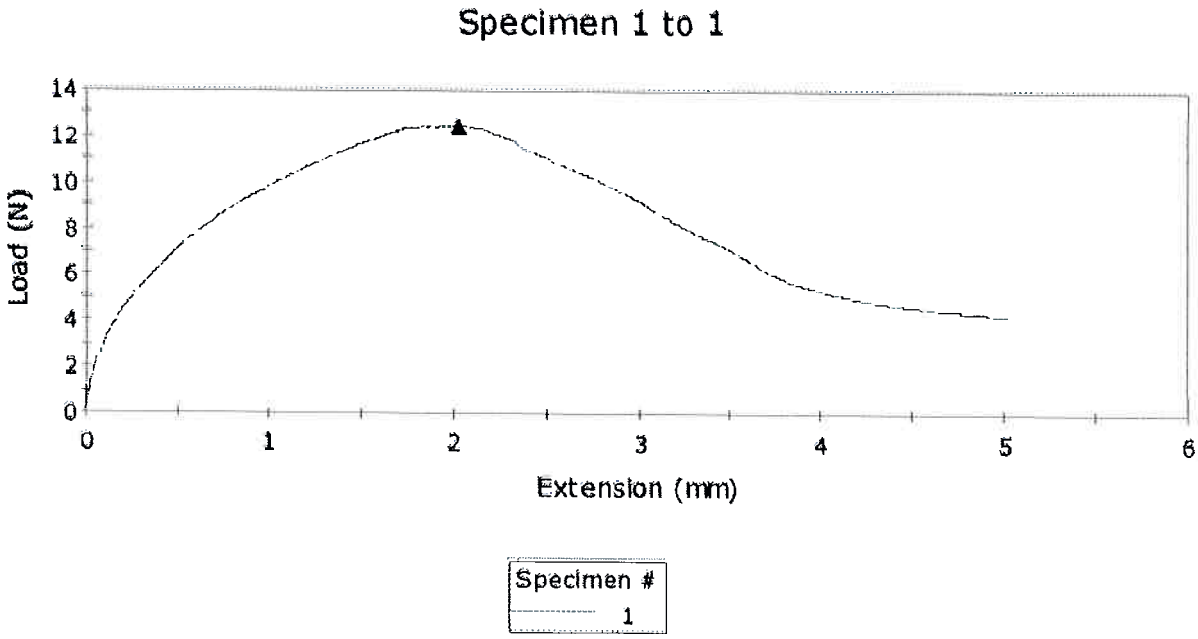

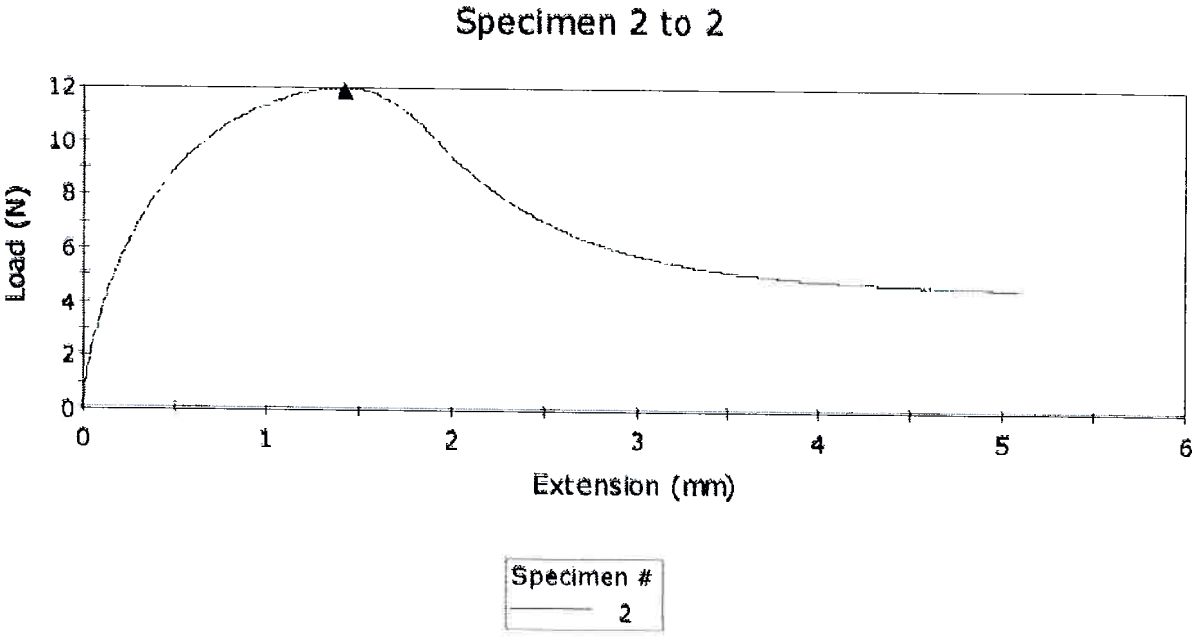

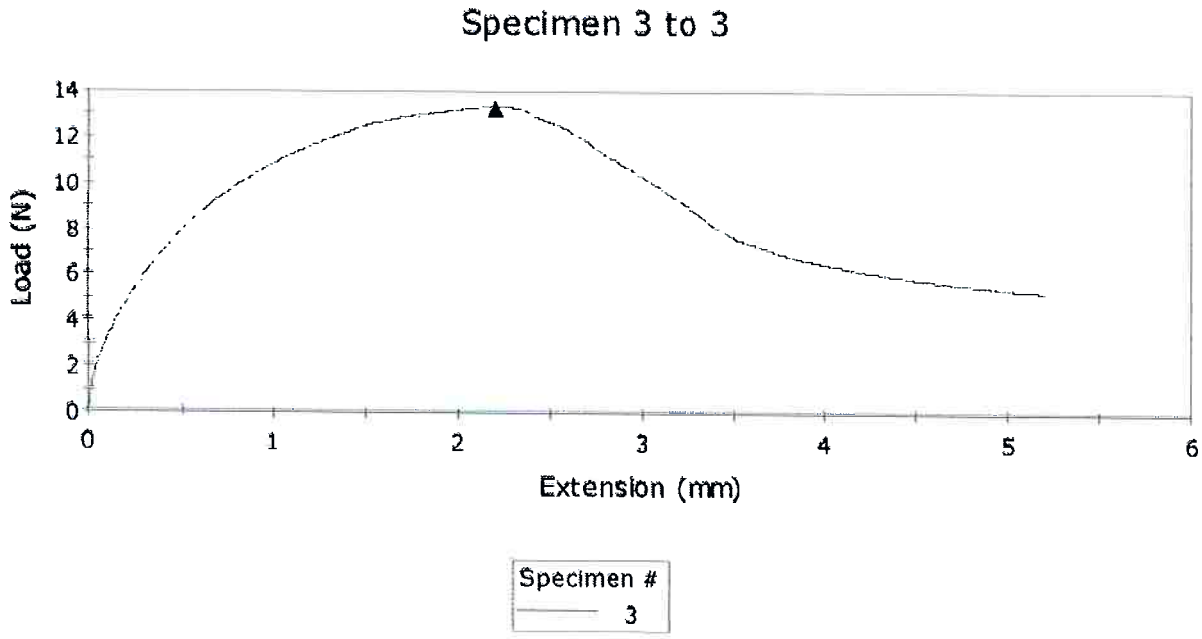
Specimen 3 to 3
Load (N)
14
12
10
8
6
4
2
0
0
1
2
3
4
5
6
Extension (mm)
Specimen #
3

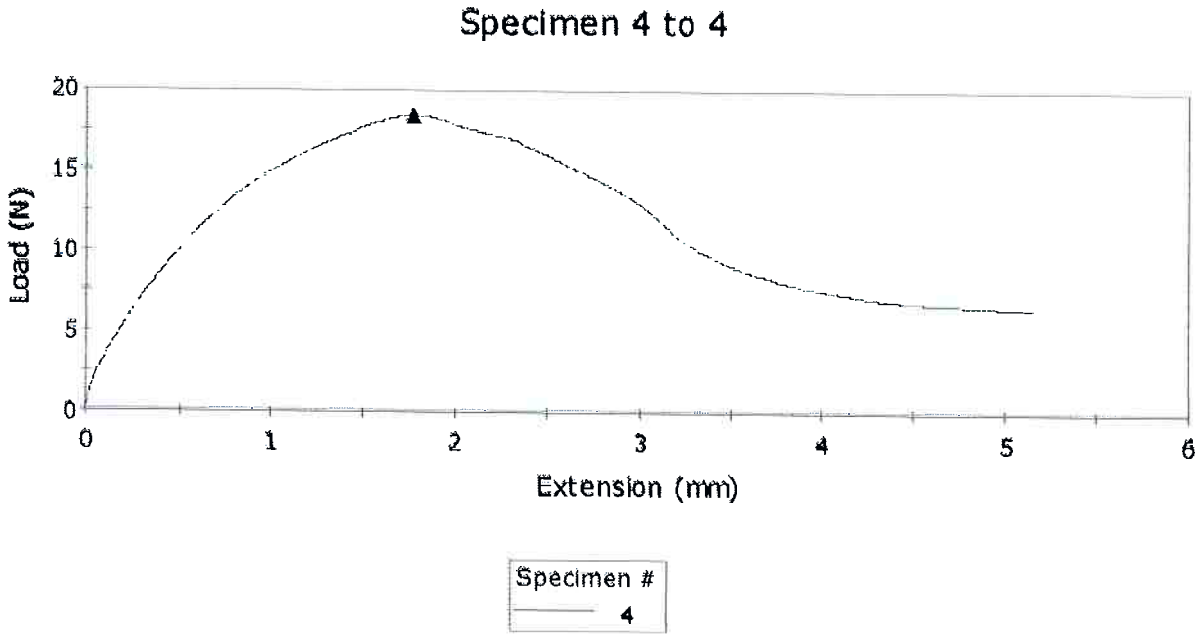
Specimen 4 to 4
Load (N)
20
15
10
5
0
0
1
2
3
4
5
6
Extension (mm)
Specimen #
4

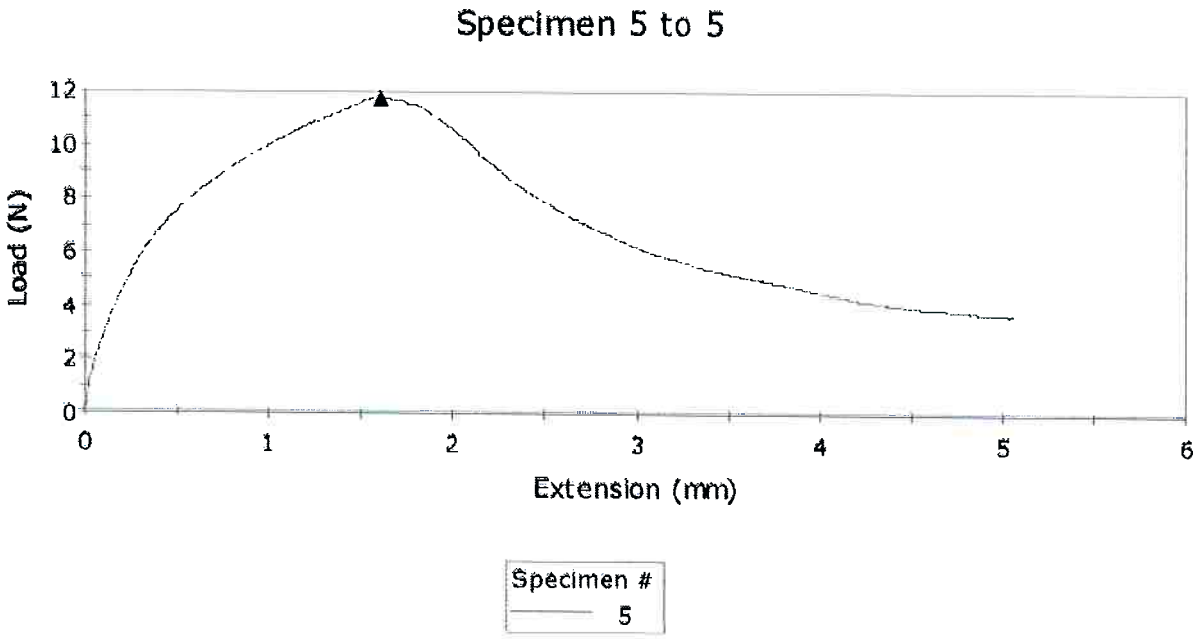
Specimen 5 to 5
Load (N)
0
2
4
6
8
10
12
0
1
2
3
4
5
6
Extension (mm)
Specimen #
5

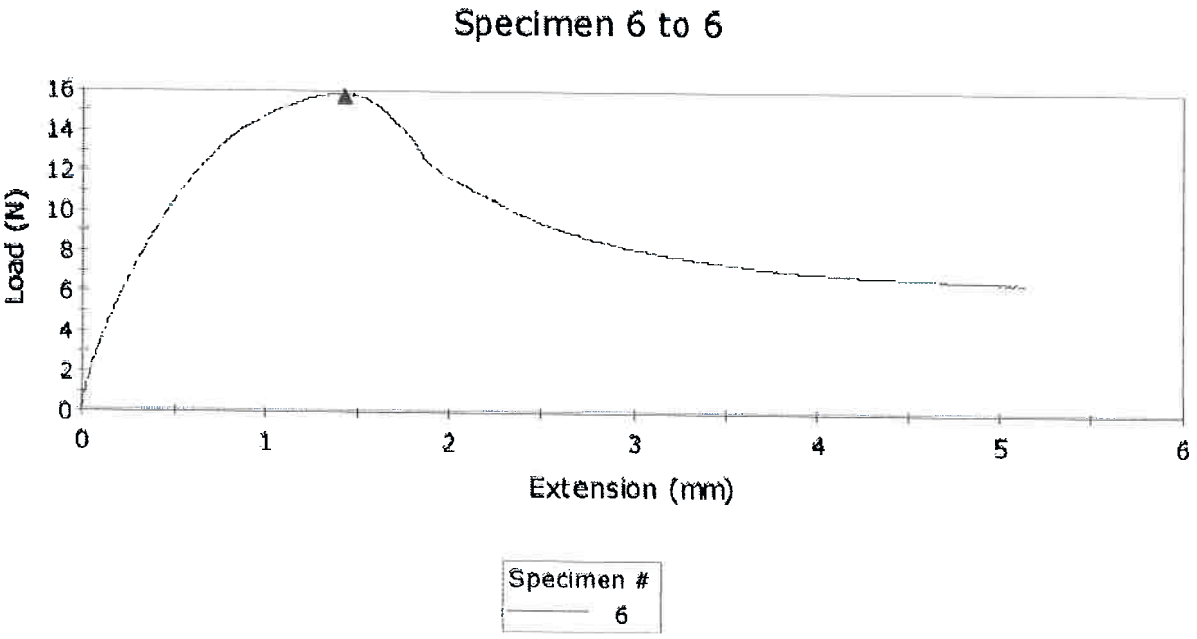
Specimen 6 to 6
Load (N)
0
2
4
6
8
10
12
14
16
0
1
2
3
4
5
6
Extension (mm)
Specimen #
6

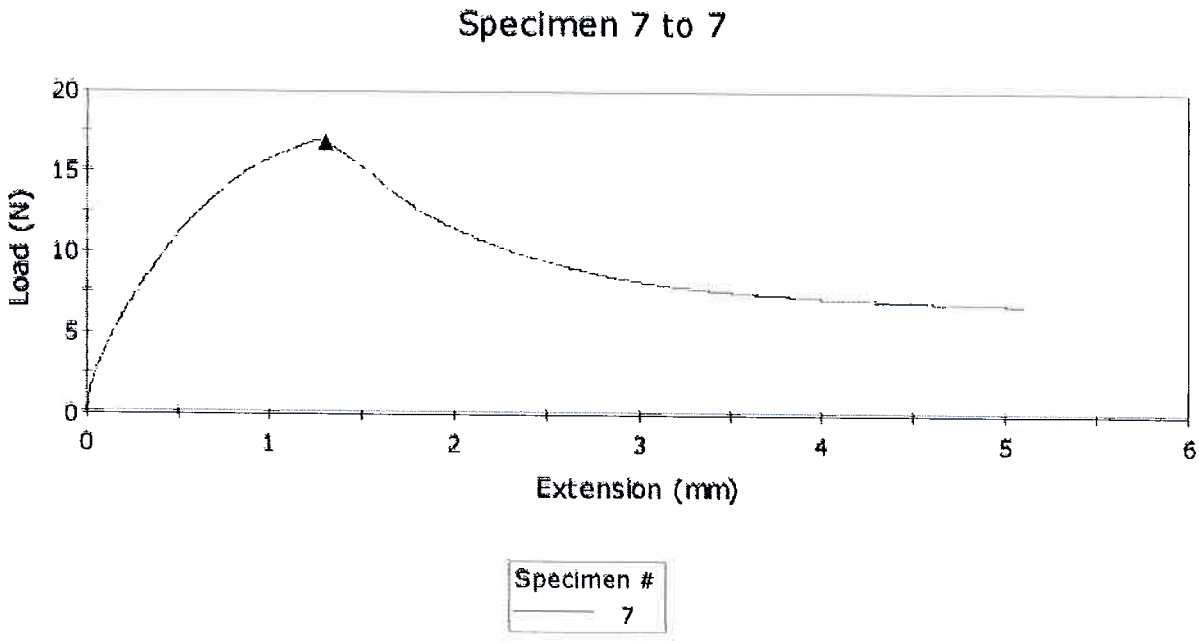
Specimen 7 to 7
Load (N)
20
15
10
5
0
0
1
2
3
4
5
6
Extension (mm)
Specimen #
7

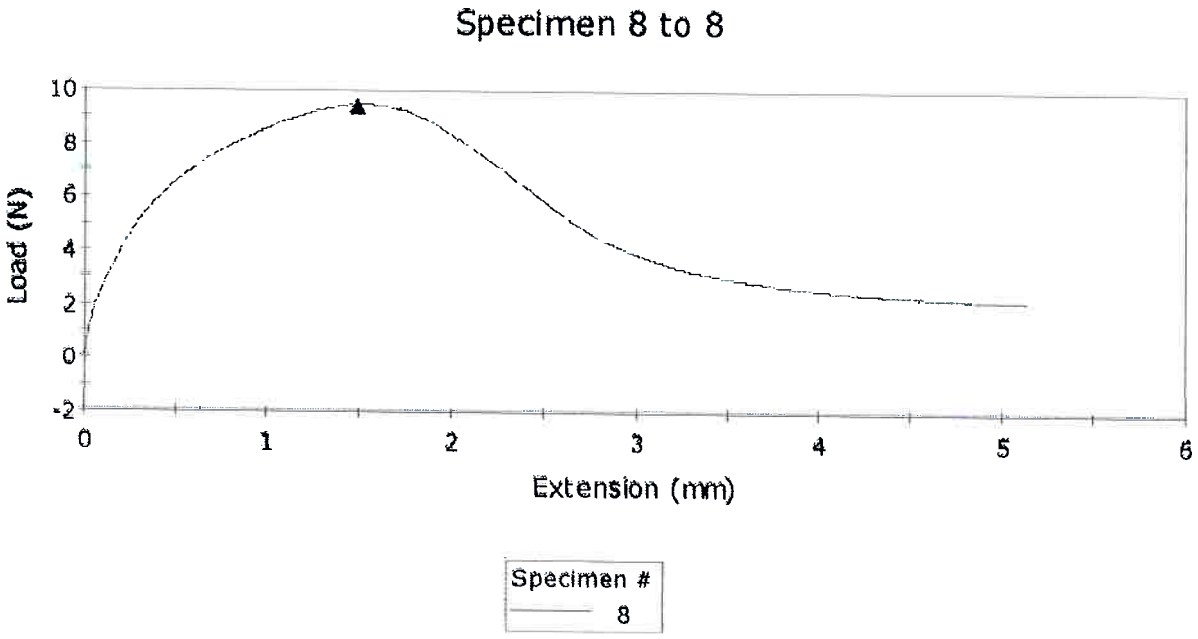
Specimen 8 to 8
Load (N)
10
8
6
4
2
0
-2
0
1
2
3
4
5
6
Extension (mm)
Specimen #
8

Table 11- Remarkable points of the tensile curves

	Maximum Load (N)	Tensile stress at Maximum Load (MPa)	Tensile extension at Maximum Load (mm)
1	12.40634	0.09769	2.02694
2	11.88276	0.09197	1.42012
3	13.22492	0.10580	2.21350
4	18.34984	0.14494	1.77350
5	11.70864	0.09105	1.60700
6	15.71234	0.12372	1.42025
7	16.81181	0.12972	1.30019
8	9.42491	0.07162	1.48694

III.3. Dolsan samples

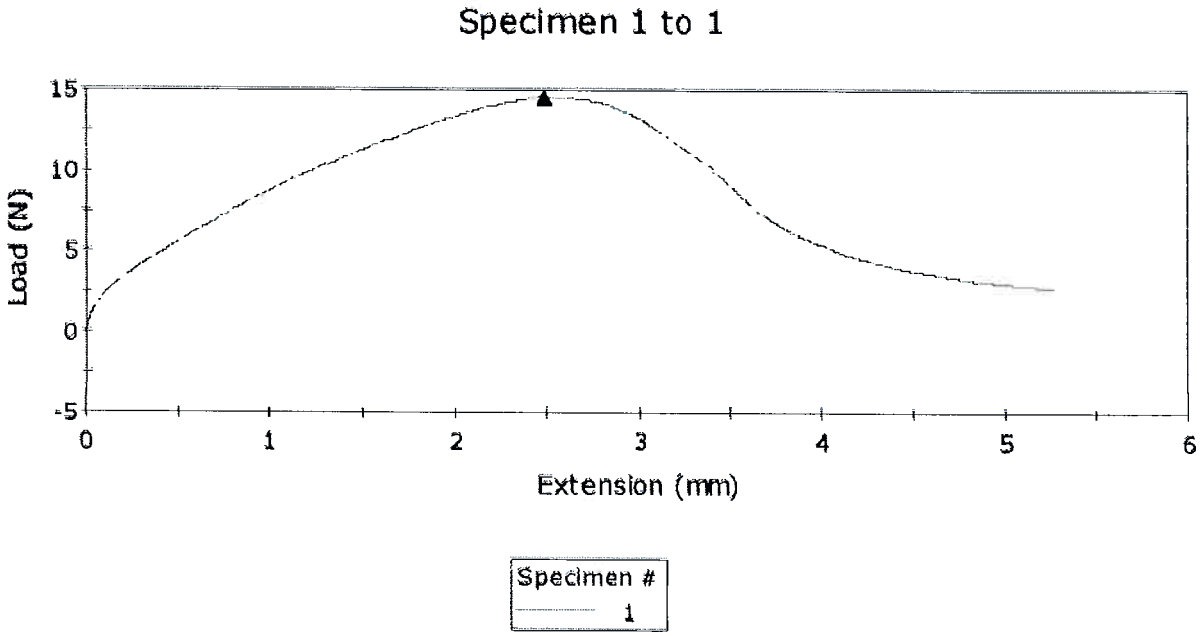

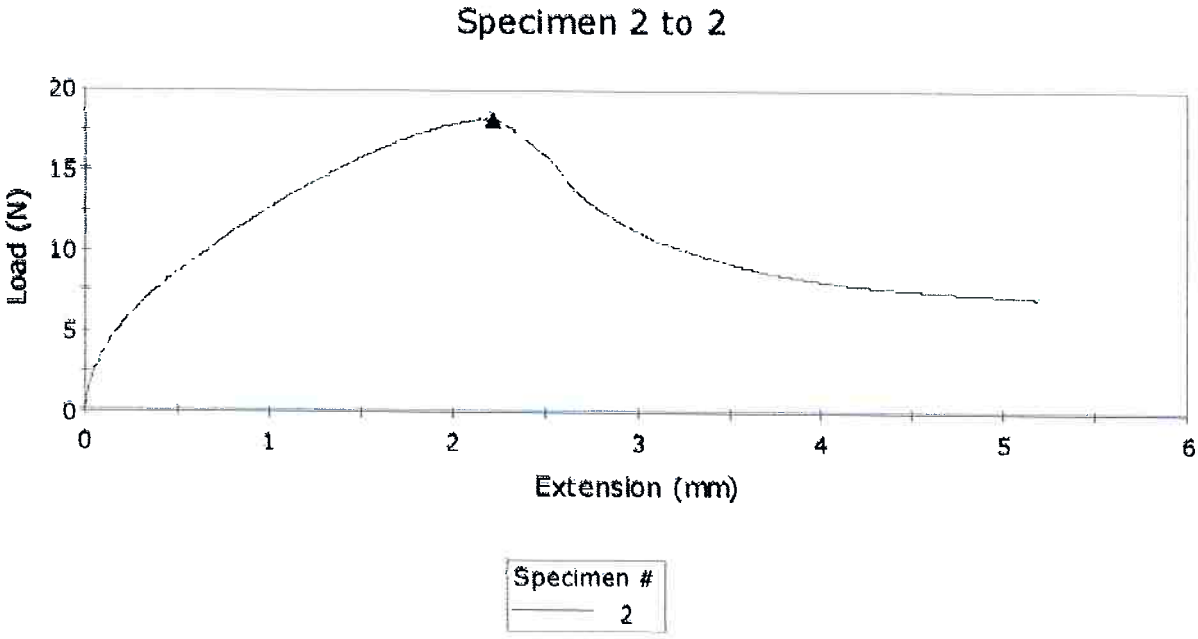
Specimen 2 to 2
Load (N)
20
15
10
5
0
0
1
2
3
4
5
6
Extension (mm)
Specimen #
2

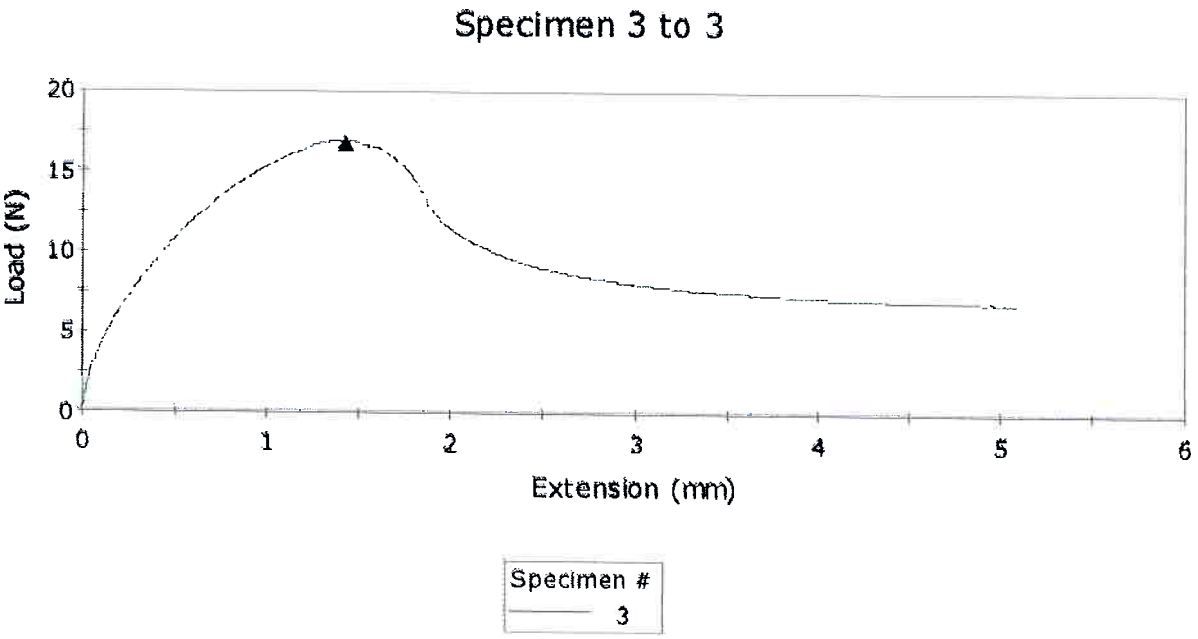
Specimen 3 to 3
Load (N)
20
15
10
5
0
0
1
2
3
4
5
6
Extension (mm)
Specimen #
3

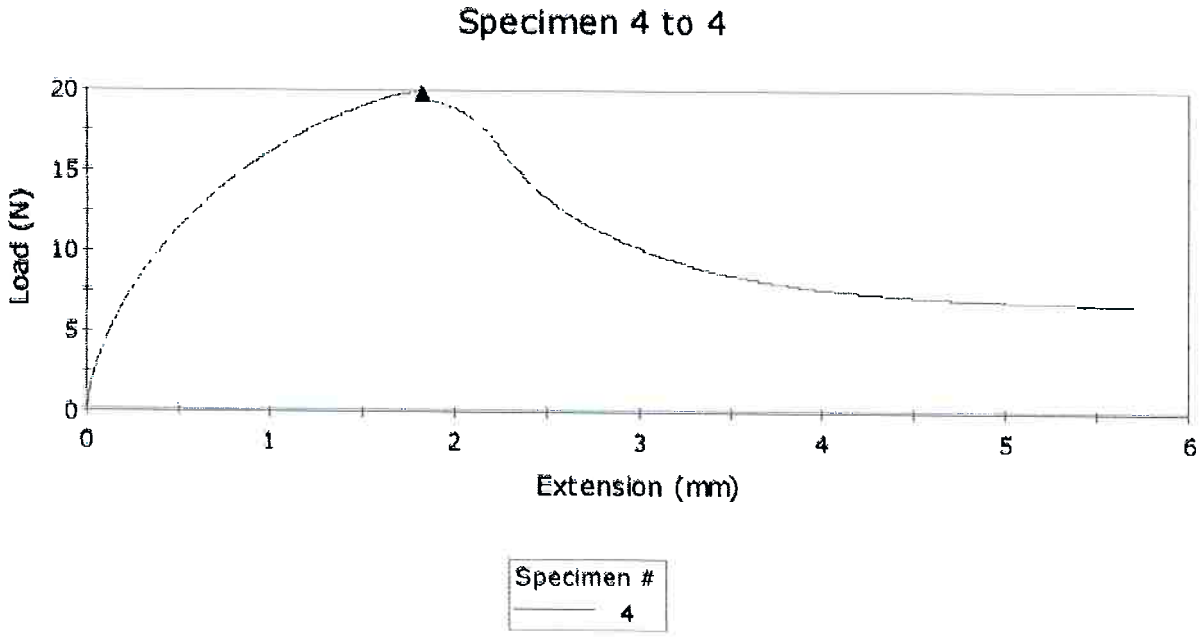
Specimen 4 to 4
Load (N)
20
15
10
5
0
0
1
2
3
4
5
6
Extension (mm)
Specimen #
4

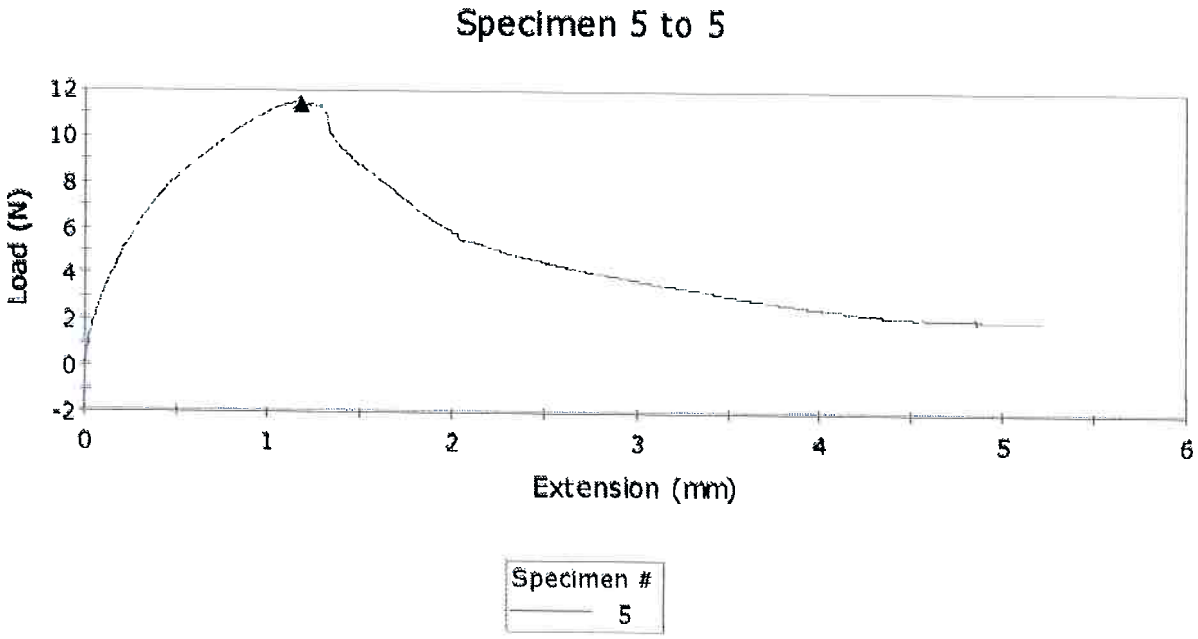
Specimen 5 to 5
Load (N)
12
10
8
6
4
2
0
-2
0
1
2
3
4
5
6
Extension (mm)
Specimen #
5

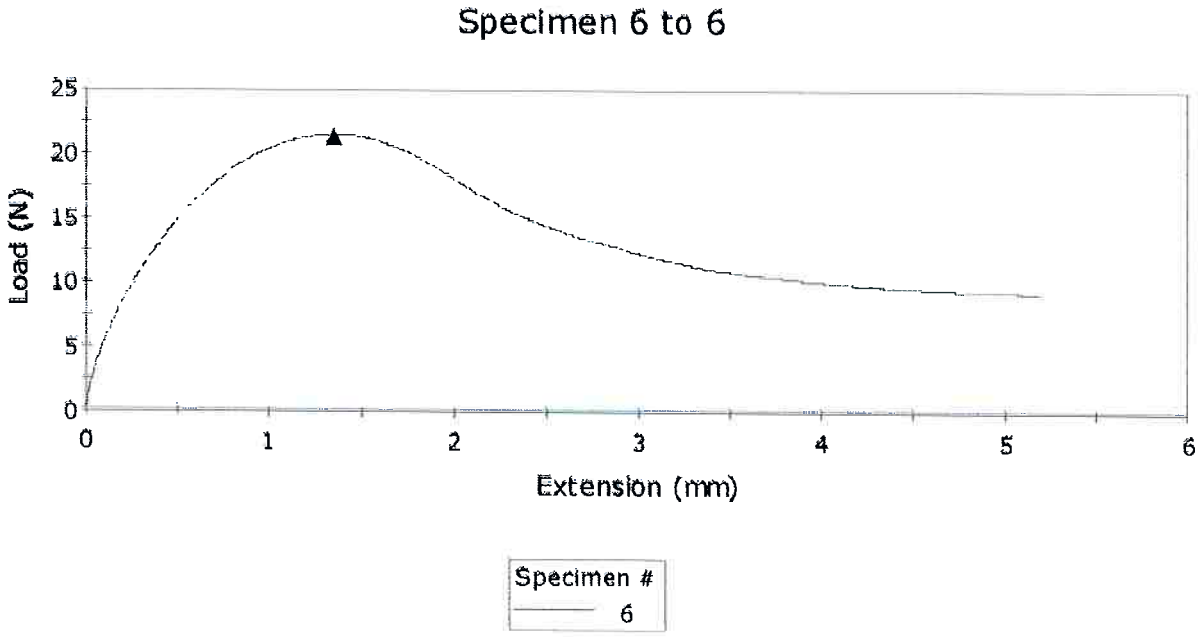
Specimen 6 to 6
Load (N)
25
20
15
10
5
0
0
1
2
3
4
5
6
Extension (mm)
Specimen #
6

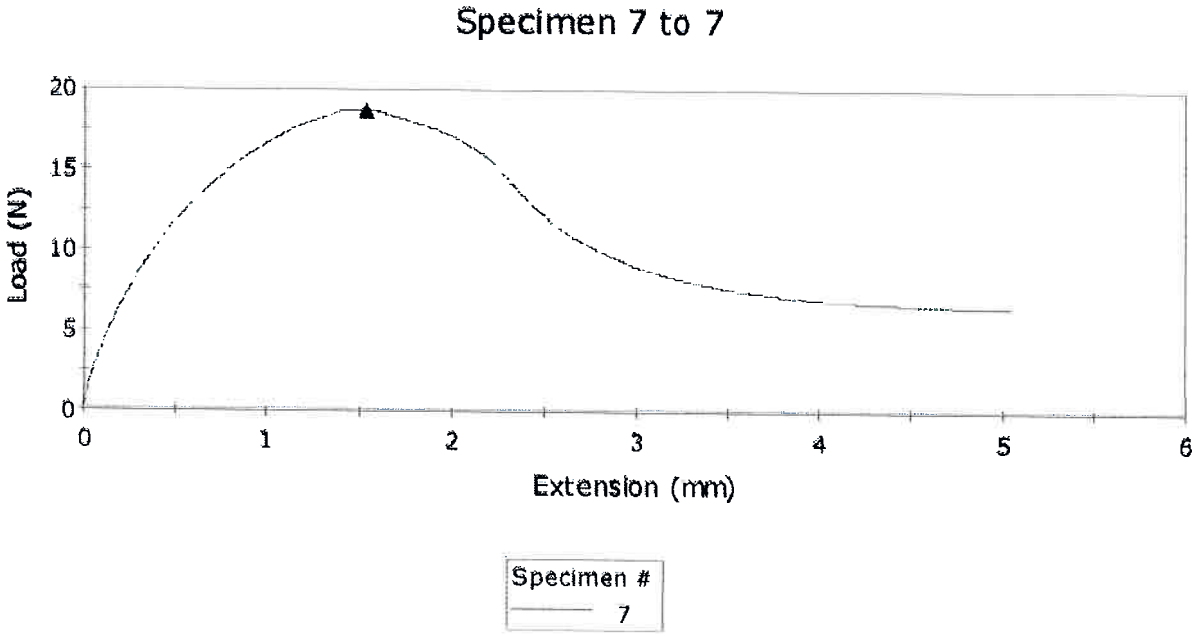
Specimen 7 to 7
Load (N)
20
15
10
5
0
0
1
2
3
4
5
6
Extension (mm)
Specimen #
7

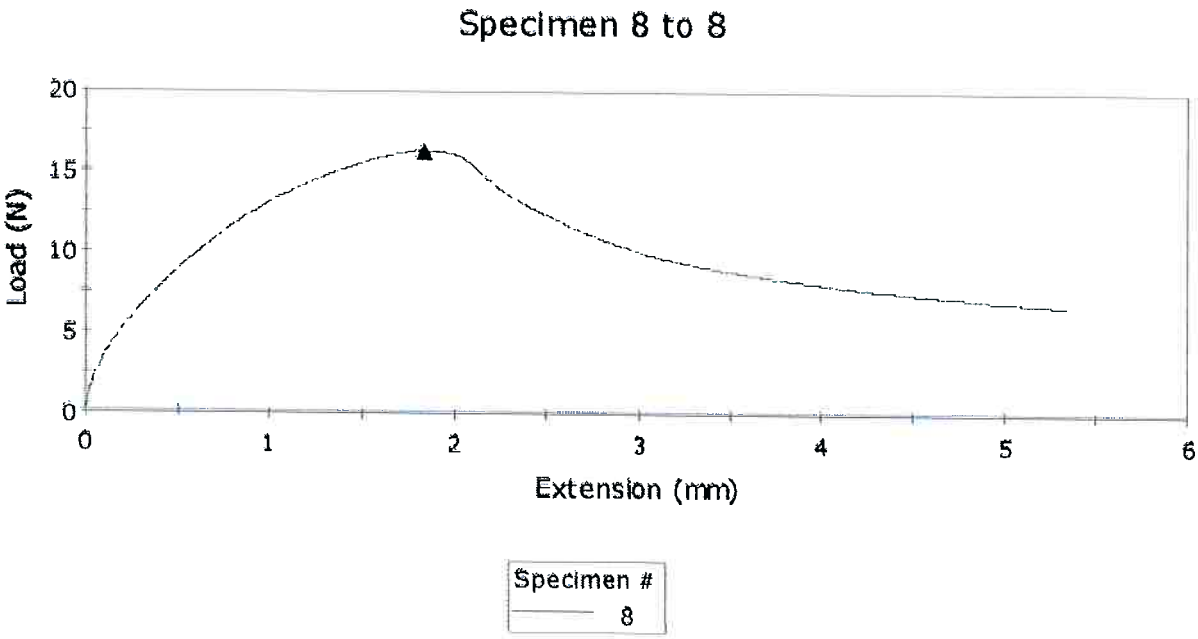

Table 12- Remarkable points of the tensile curves

	Maximum Load (N)	Tensile stress at Maximum Load (MPa)	Tensile extension at Maximum Load (mm)
1	14.44385	0.11743	2.48669
2	18.08539	0.14020	2.22006
3	16.75715	0.12505	1.42669
4	19.71389	0.14327	1.82669
5	11.37842	0.09843	1.18006
6	21.31298	0.16996	1.34675
7	18.56692	0.13897	1.53344
8	16.22867	0.11526	1.84025

Annex IV.Bending test data

For each of the three compositions, the bending test curves of 12 samples are displayed in the following without any modification. For space convenience, only the important points are presented.

IV.1. Reference

Bending test of planar sheet with a speed rate of 1,5 $mm.mn^{-1}$

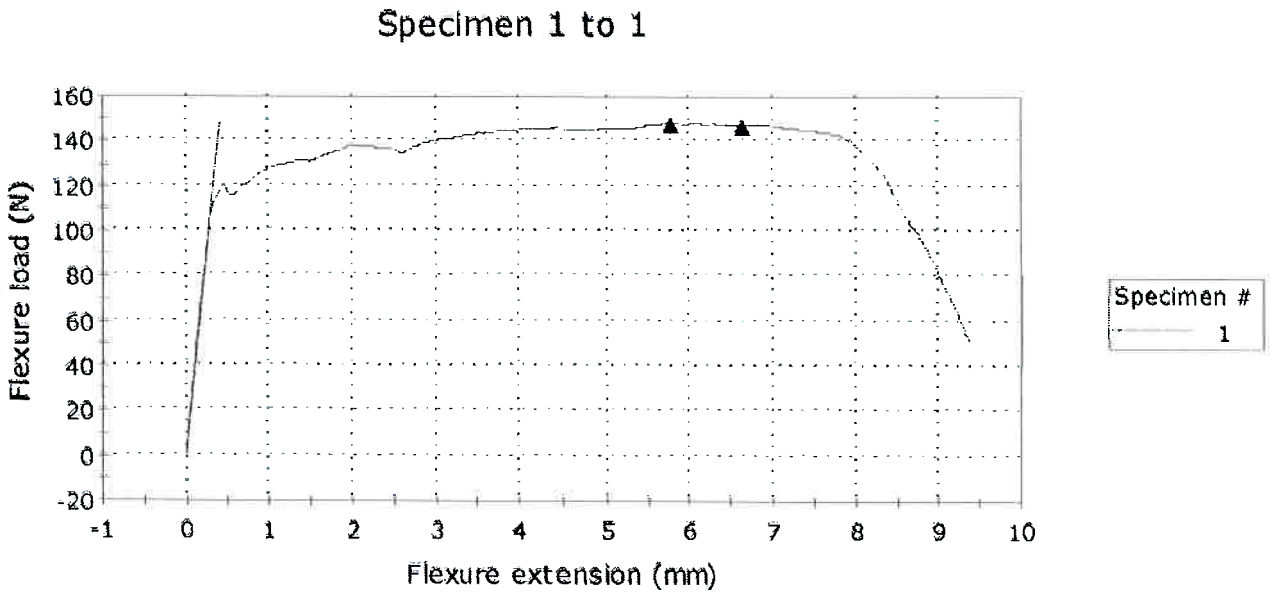

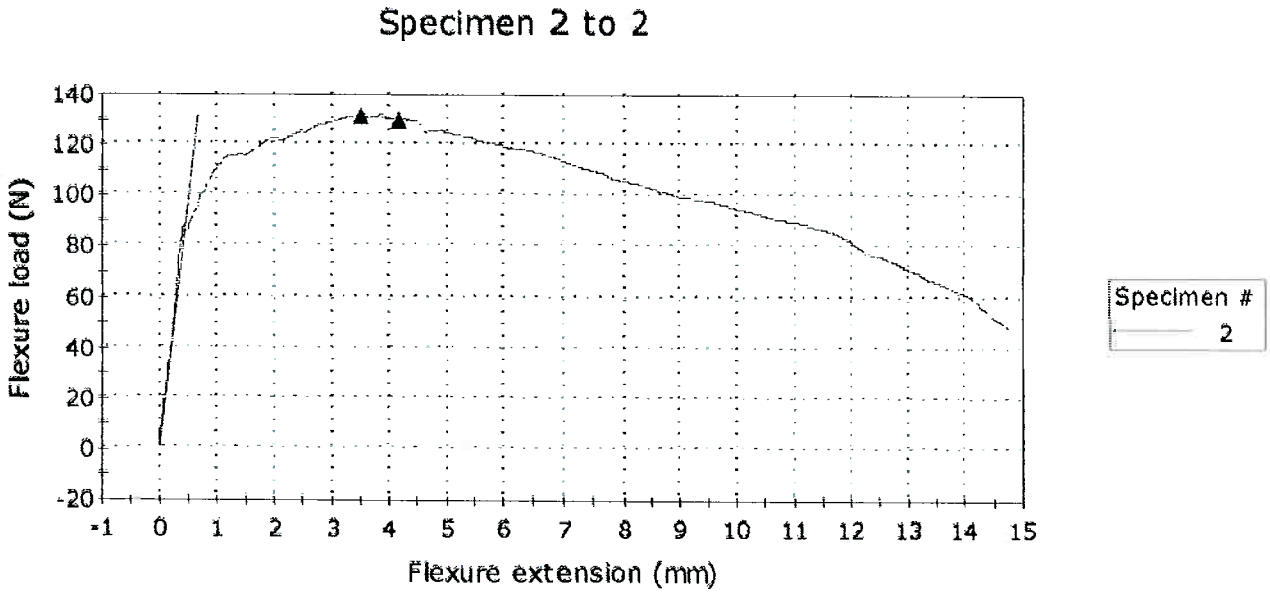

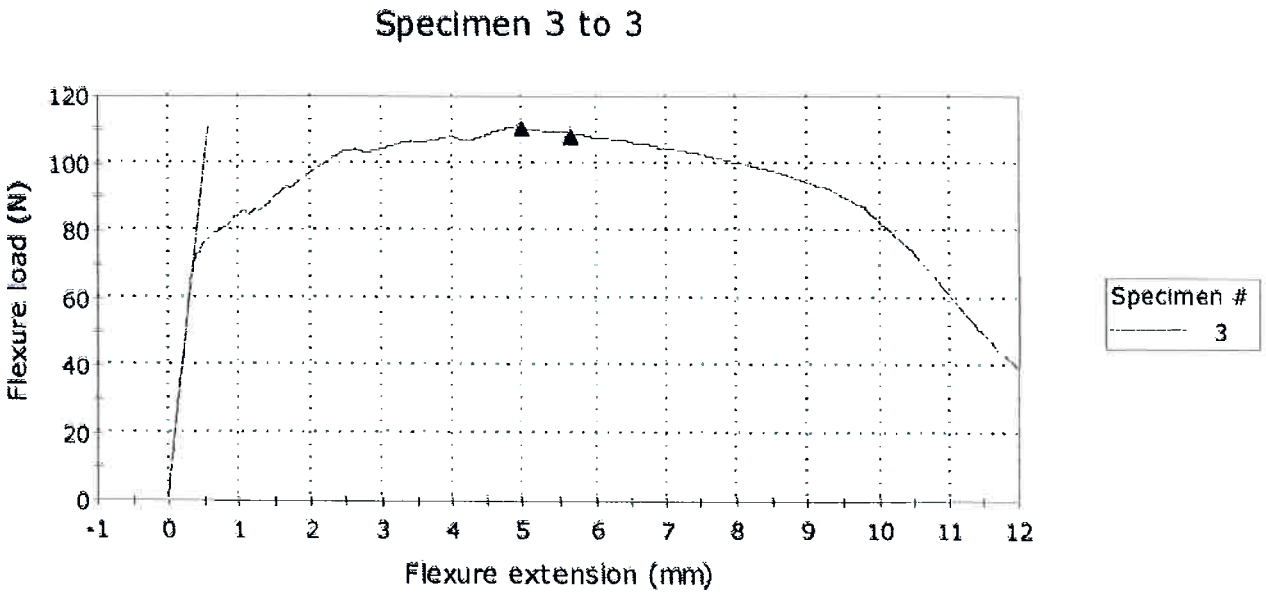
Specimen 3 to 3
Flexure load (N)
120
100
80
60
40
20
0
-1
0
1
2
3
4
5
6
7
8
9
10
11
12
Flexure extension (mm)
Specimen #
3

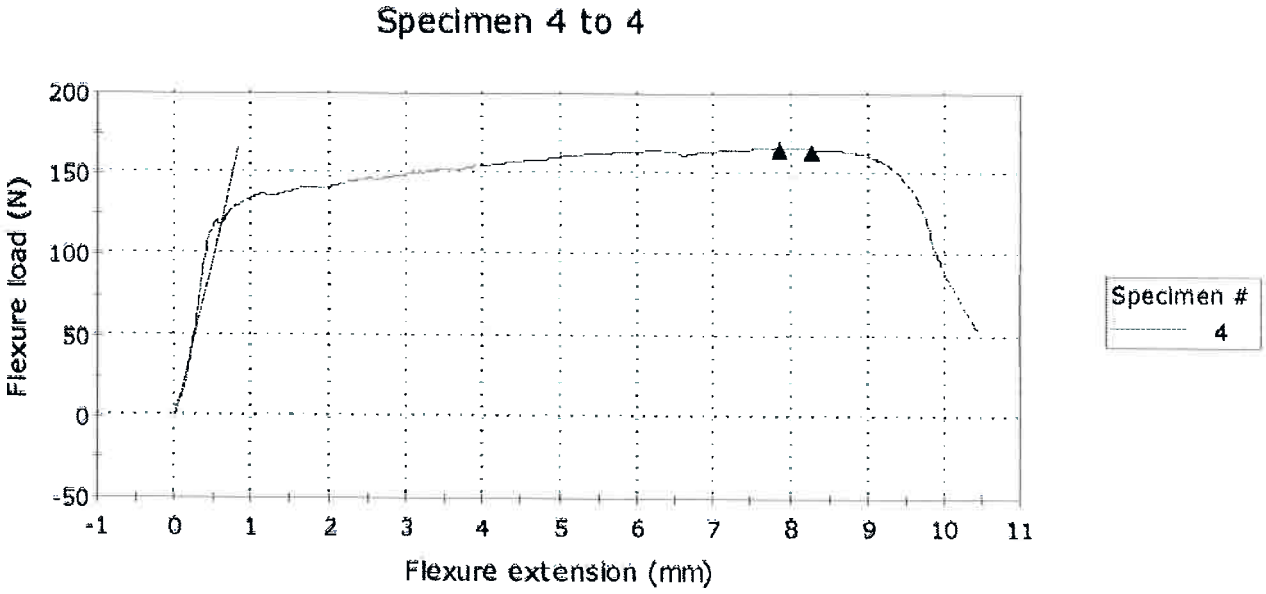
Specimen 4 to 4
Flexure load (N)
200
150
100
50
0
-50
-1
0
1
2
3
4
5
6
7
8
9
10
11
Flexure extension (mm)
Specimen #
4

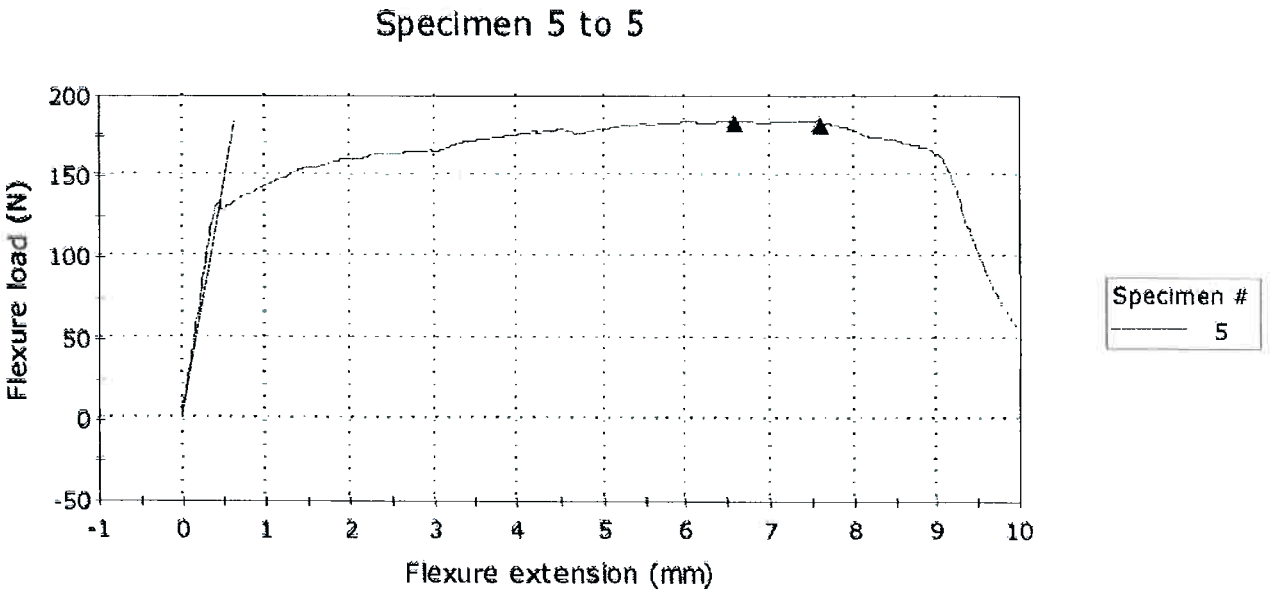
Specimen 5 to 5
Flexure load (N)
200
150
100
50
0
-50
-1
0
1
2
3
4
5
6
7
8
9
10
Flexure extension (mm)
Specimen #
5

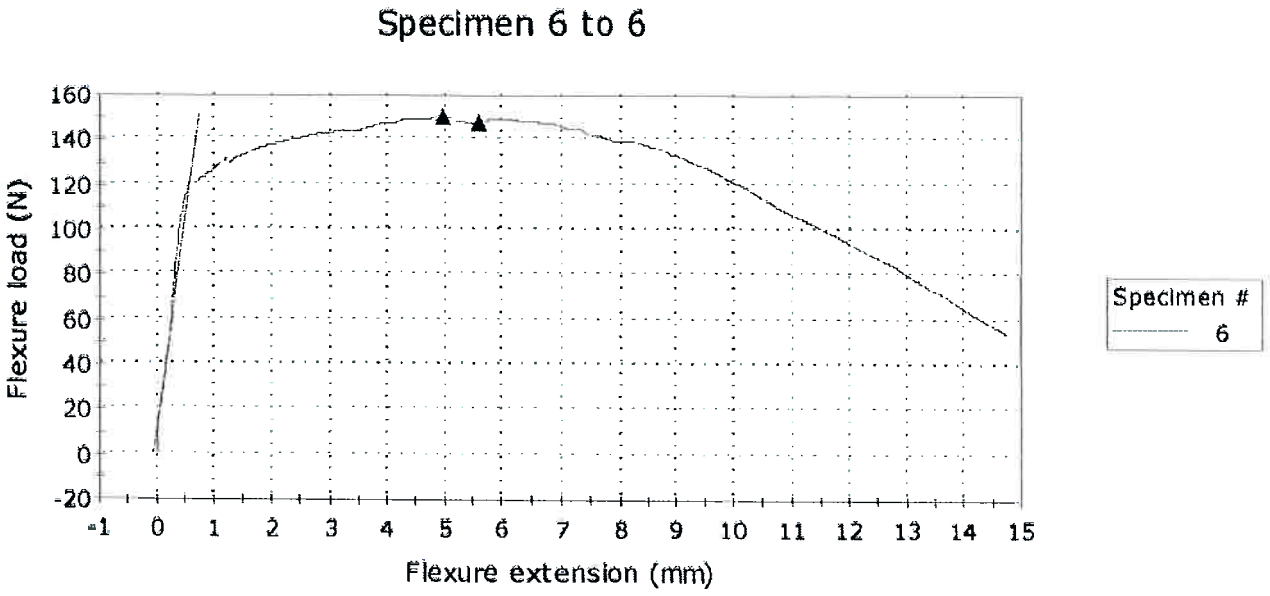
Specimen 6 to 6
Flexure load (N)
160
140
120
100
80
60
40
20
0
-20
-1
0
1
2
3
4
5
6
7
8
9
10
11
12
13
14
15
Flexure extension (mm)
Specimen #
6

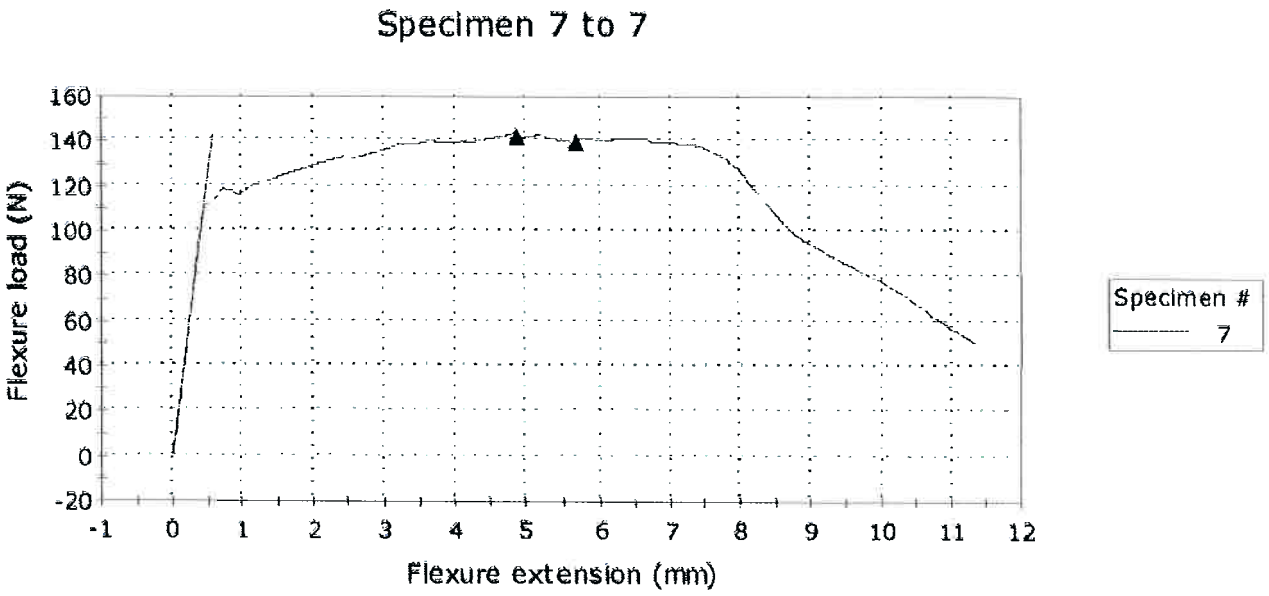
Specimen 7 to 7
Flexure load (N)
160
140
120
100
80
60
40
20
0
-20
-1
0
1
2
3
4
5
6
7
8
9
10
11
12
Flexure extension (mm)
Specimen #
7

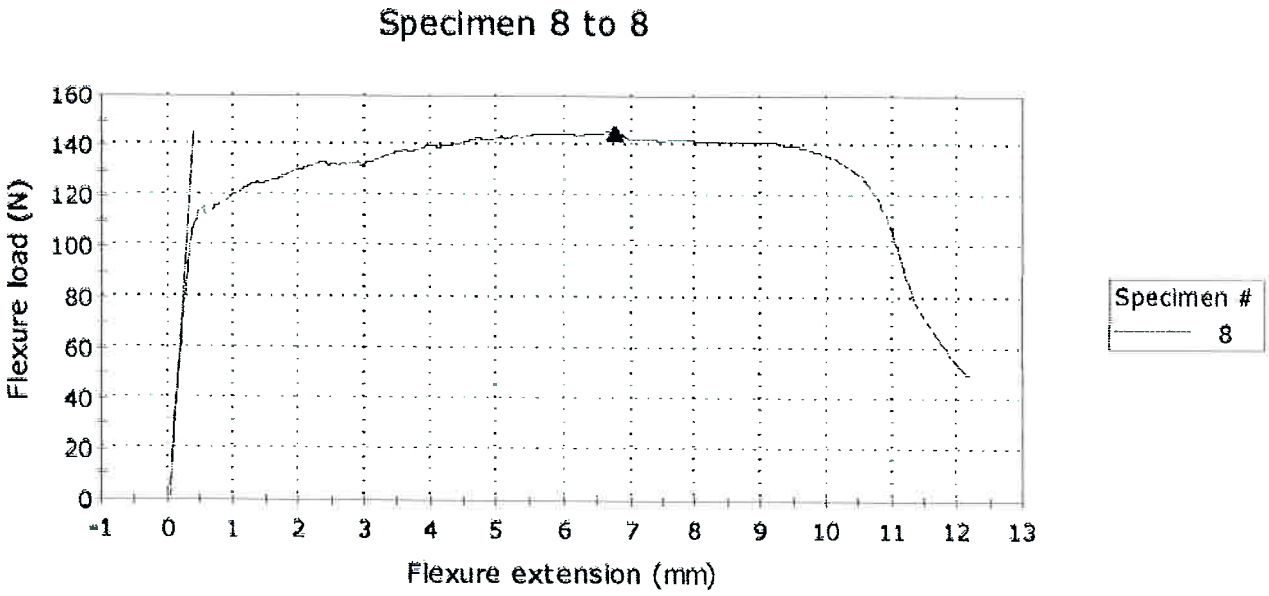
Specimen 8 to 8
Flexure load (N)
160
140
120
100
80
60
40
20
0
-1
0
1
2
3
4
5
6
7
8
9
10
11
12
13
Flexure extension (mm)
Specimen #
8

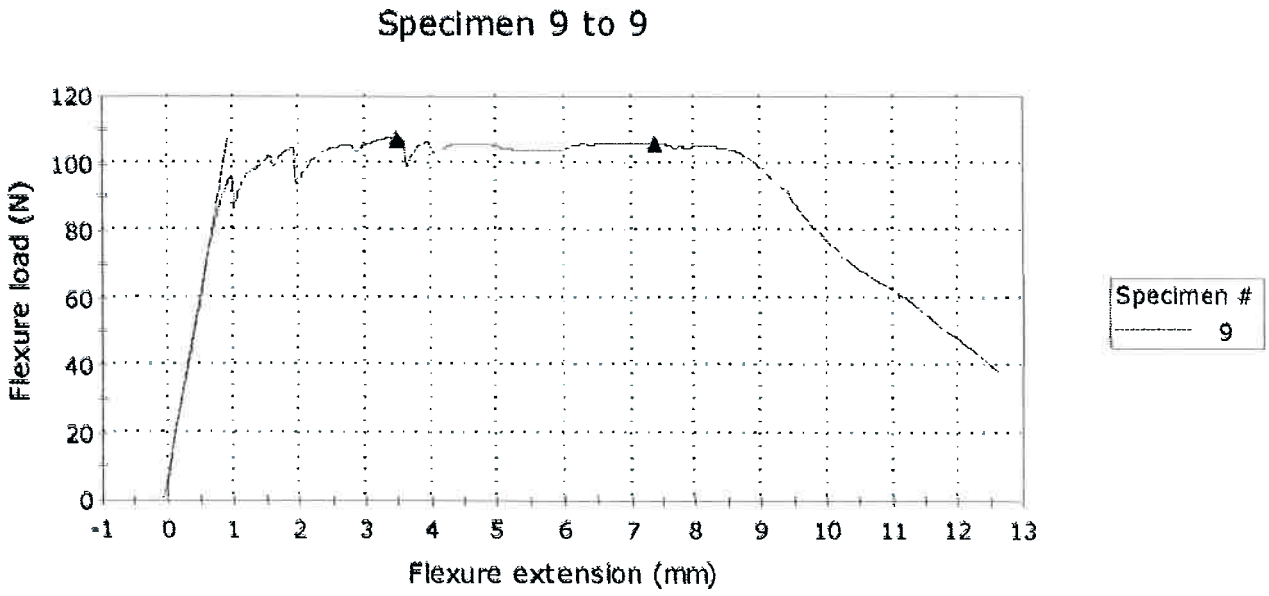
Specimen 9 to 9
Flexure load (N)
120
100
80
60
40
20
0
-1
0
1
2
3
4
5
6
7
8
9
10
11
12
13
Flexure extension (mm)
Specimen #
9

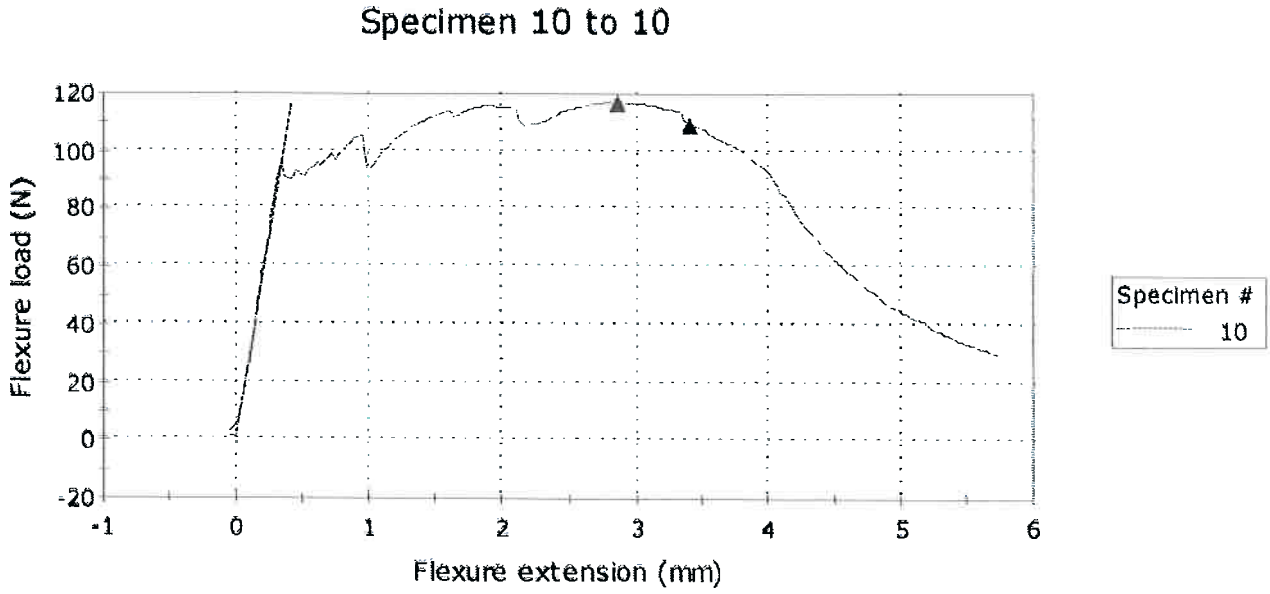
Specimen 10 to 10
Flexure load (N)
120
100
80
60
40
20
0
-20
-1
0
1
2
3
4
5
6
Flexure extension (mm)
Specimen #
10

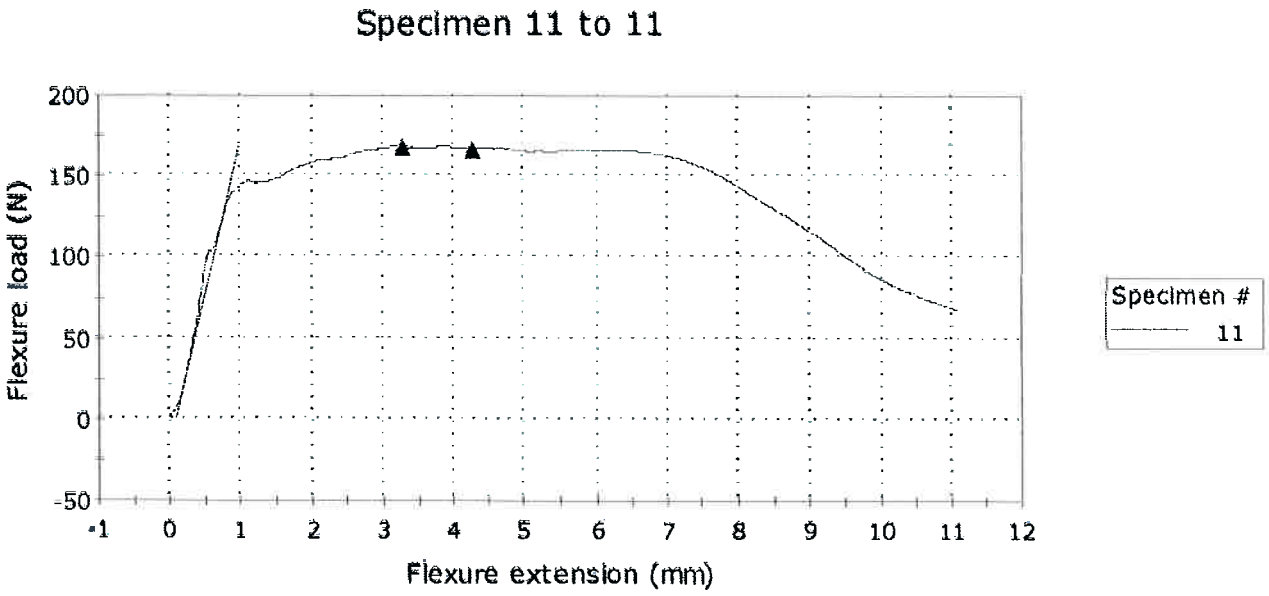
Specimen 11 to 11
Flexure load (N)
200
150
100
50
0
-50
-1
0
1
2
3
4
5
6
7
8
9
10
11
12
Flexure extension (mm)
Specimen #
11

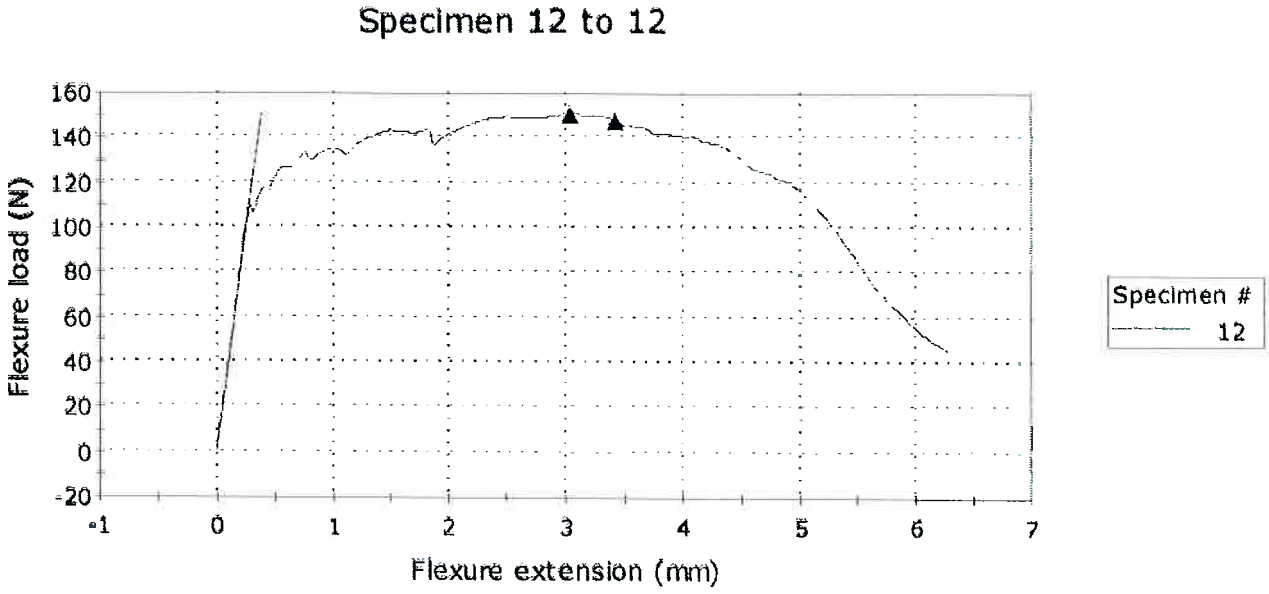
Specimen 12 to 12
Flexure load (N)
160
140
120
100
80
60
40
20
0
-20
-1
0
1
2
3
4
5
6
7
Flexure extension (mm)
Specimen #
12

Table 13- Remarkable points of the bending test

	Flexure stress at Maximum Flexure load (MPa)	Modulus (Segment 0.5 MPa - 3 MPa) (MPa)	Maximum Flexure load (N)	Flexure extension at Maximum Flexure load (mm)
1	10.15451	14128.89696	147.26676	5.76580
2	9.39657	7964.20496	131.57068	3.52135
3	7.86867	8123.25730	110.17695	5.00111
4	11.81703	8485.24074	165.46190	7.84332
5	11.02528	9235.24997	182.94780	6.59443
6	10.11175	7027.84030	149.70714	4.96956
7	10.23002	10190.18312	141.80759	4.88639
8	11.19030	17090.46362	144.67604	6.72535
9	8.38602	5101.53441	107.10812	3.49664
10	8.51795	11505.01169	116.74111	2.84700
11	10.81323	6522.24499	168.03178	3.28209
12	9.84723	13801.78902	150.20354	3.03471

IV.2. Tolsa samples

Bending test of planar sheet with a speed rate of 1,5 mm.mn^{-1}

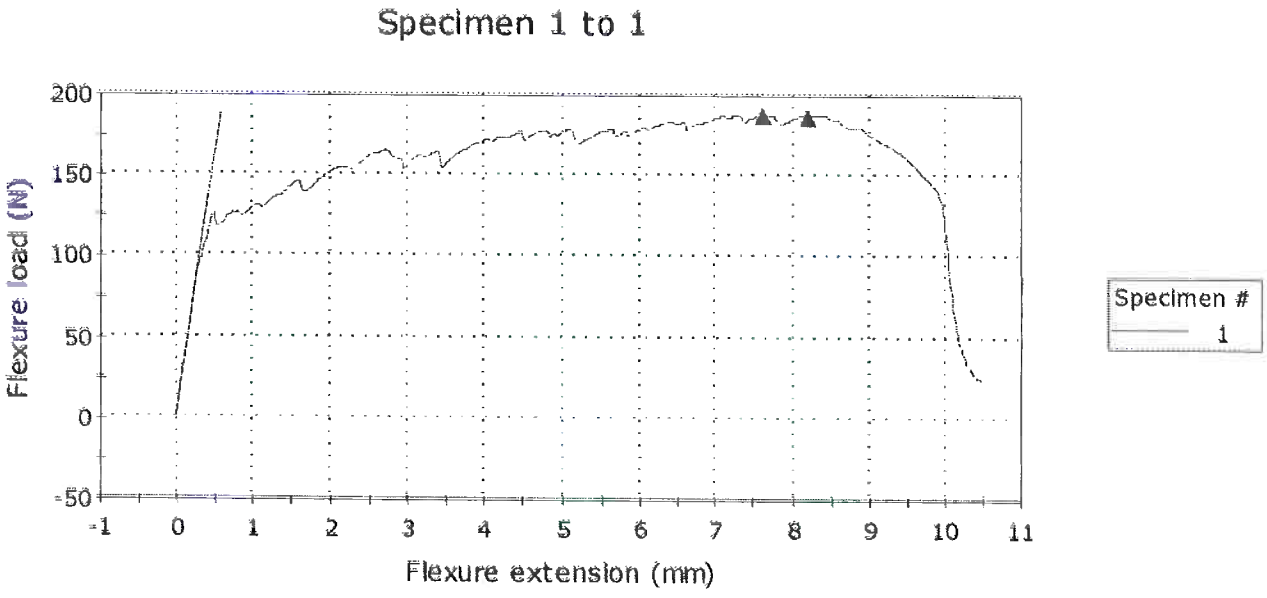

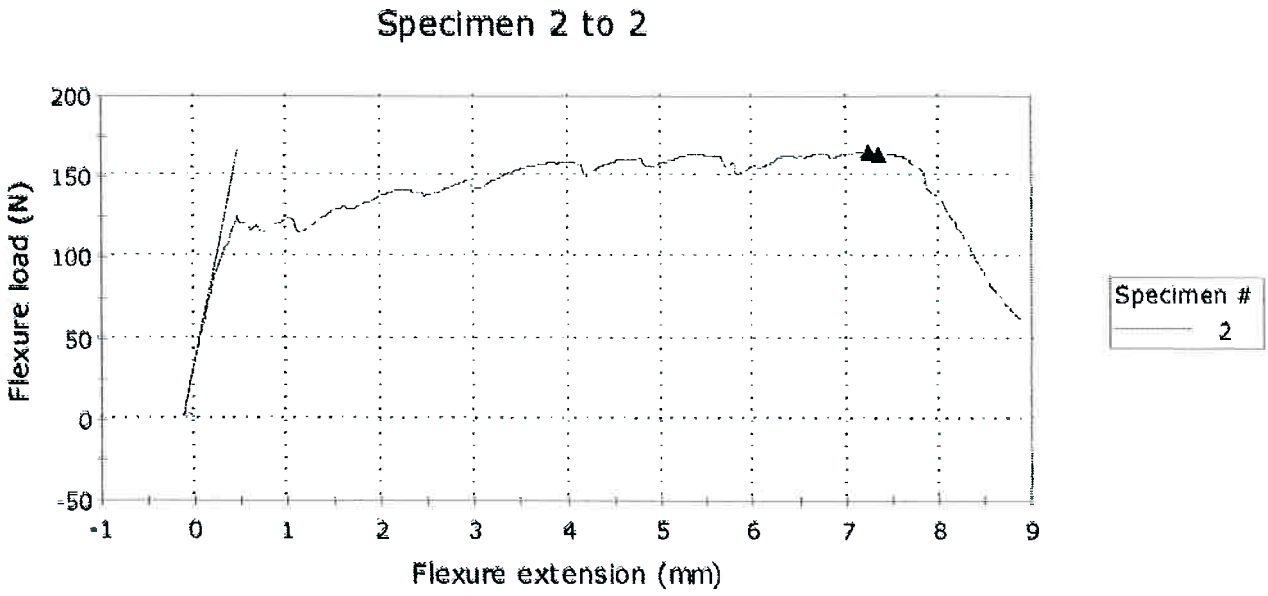
Specimen 2 to 2
Flexure load (N)
200
150
100
50
0
-50
-1
0
1
2
3
4
5
6
7
8
9
Flexure extension (mm)
Specimen #
2

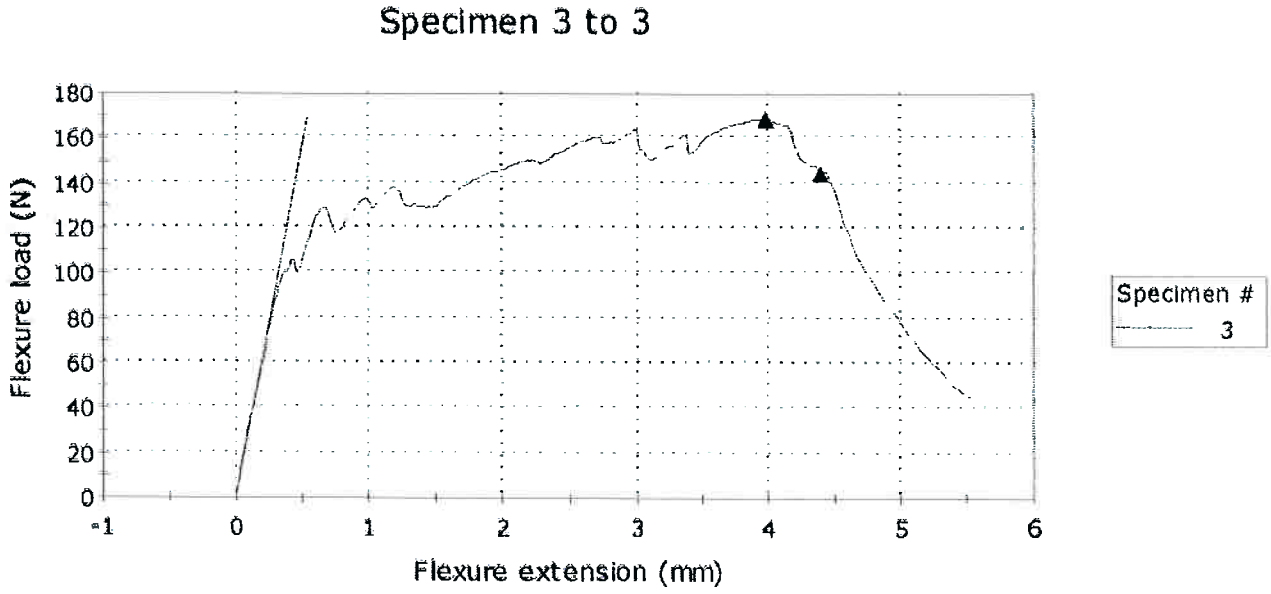
Specimen 3 to 3
Flexure load (N)
180
160
140
120
100
80
60
40
20
0
-1
0
1
2
3
4
5
6
Flexure extension (mm)
Specimen #
3

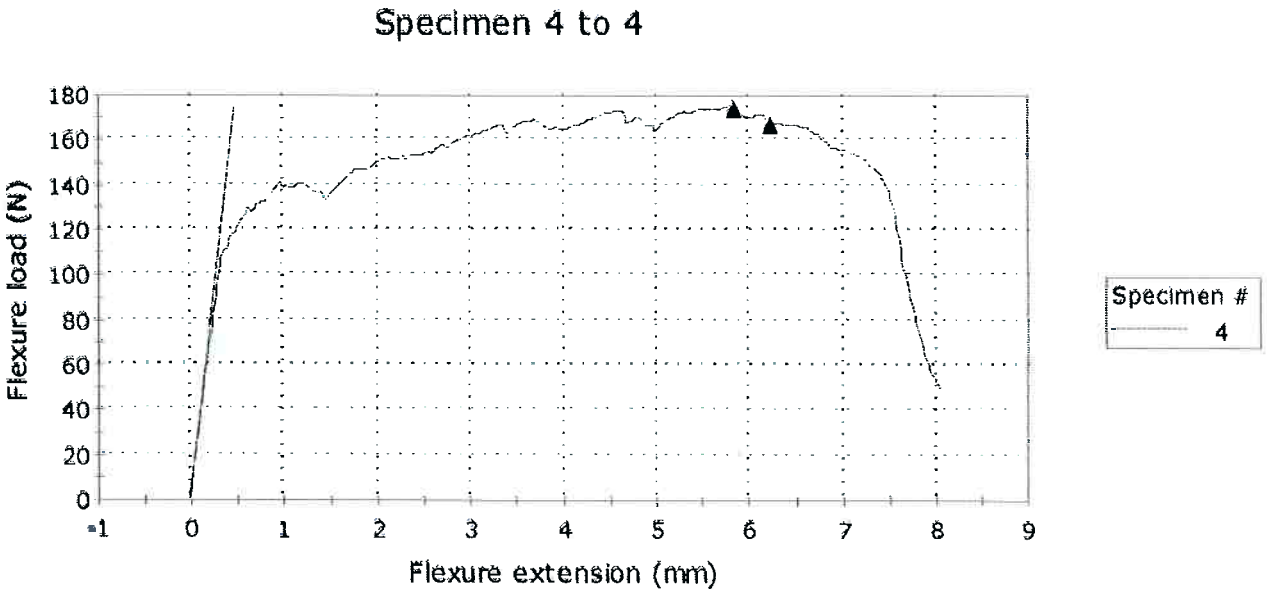
Specimen 4 to 4
Flexure load (N)
180
160
140
120
100
80
60
40
20
0
-1
0
1
2
3
4
5
6
7
8
9
Flexure extension (mm)
Specimen #
4

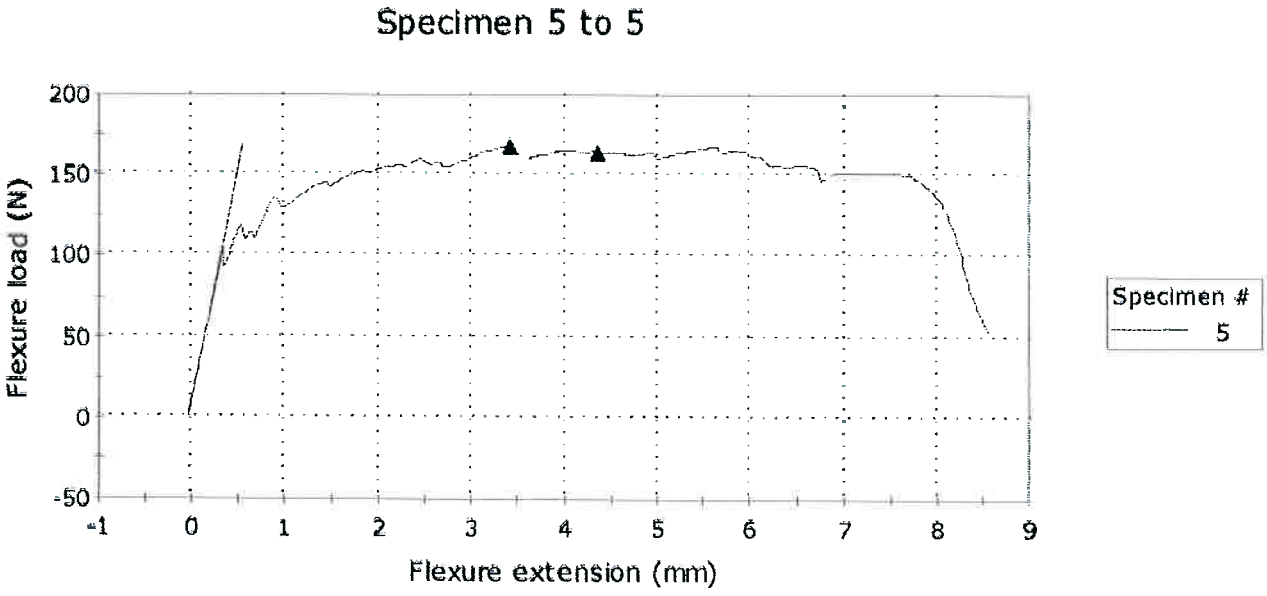
Specimen 5 to 5
Flexure load (N)
200
150
100
50
0
-50
-1
0
1
2
3
4
5
6
7
8
9
Flexure extension (mm)
Specimen #
5

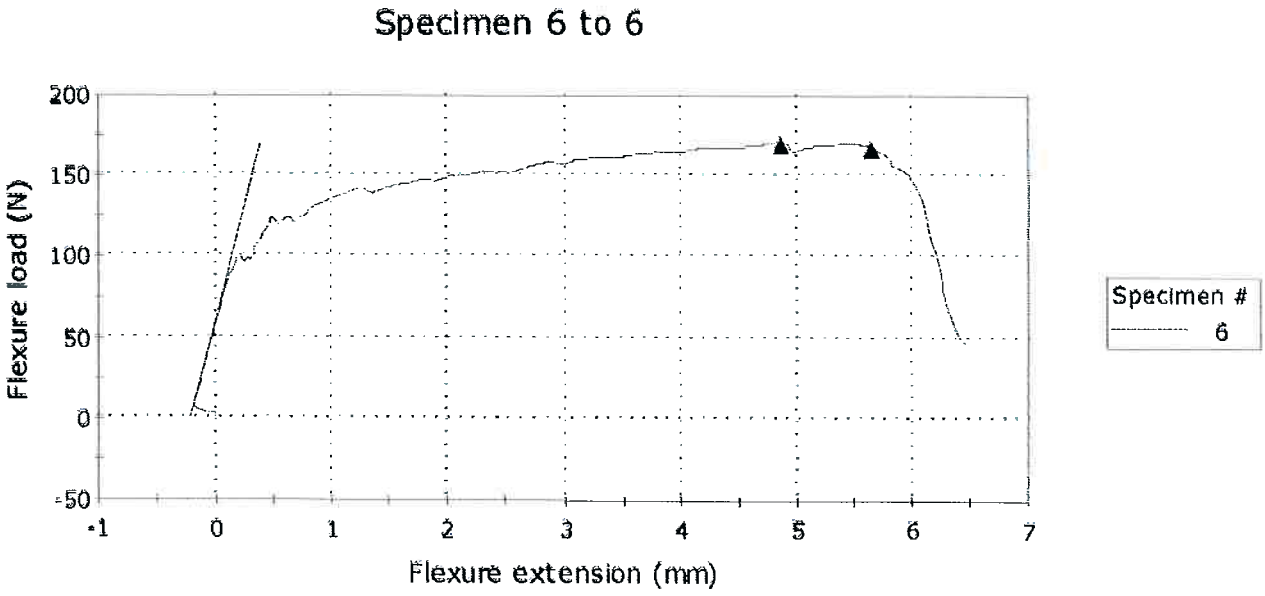
Specimen 6 to 6
Flexure load (N)
200
150
100
50
0
-50
-1
0
1
2
3
4
5
6
7
Flexure extension (mm)
Specimen #
6

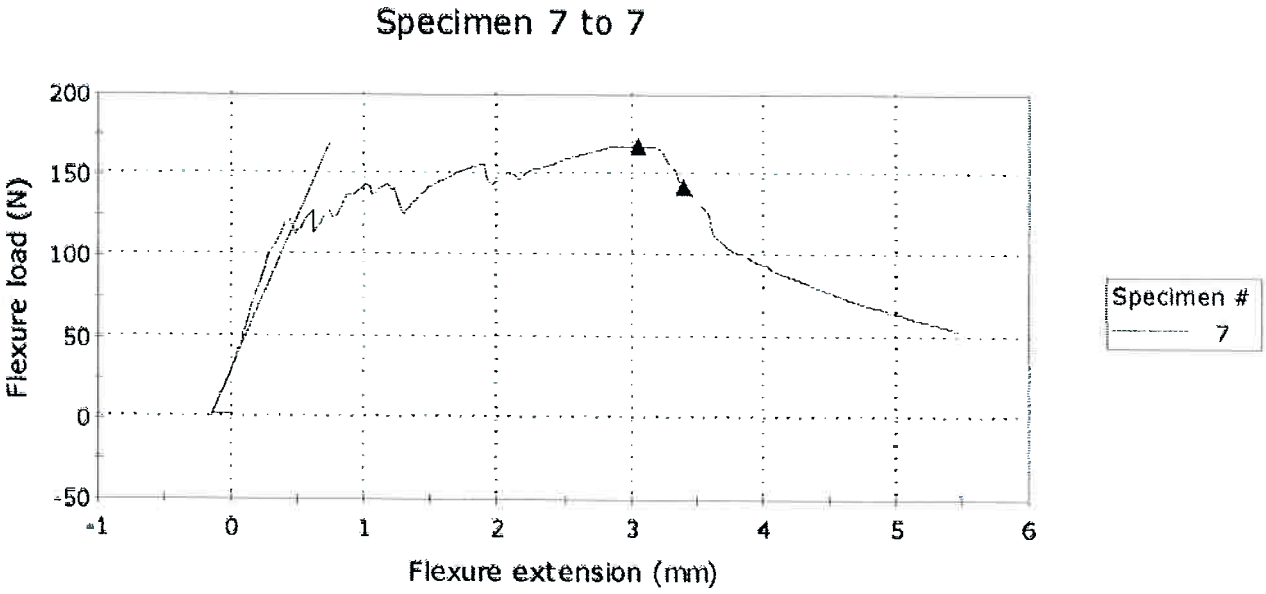
Specimen 7 to 7
Flexure load (N)
200
150
100
50
0
-50
-1
0
1
2
3
4
5
6
Flexure extension (mm)
Specimen #
7


Specimen 8 to 8
Flexure load (N)
160
140
120
100
80
60
40
20
0
-20
-1
0
1
2
3
4
5
6
Flexure extension (mm)
Specimen #
8

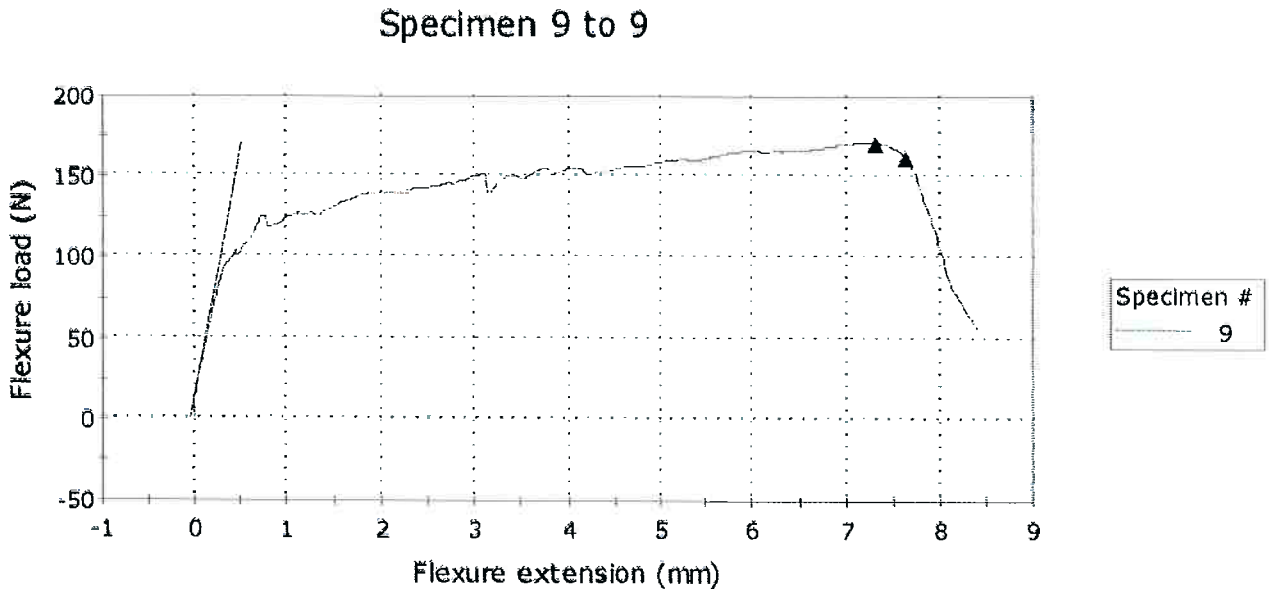
Specimen 9 to 9
Flexure load (N)
200
150
100
50
0
-50
-1
0
1
2
3
4
5
6
7
8
9
Flexure extension (mm)
Specimen #
9

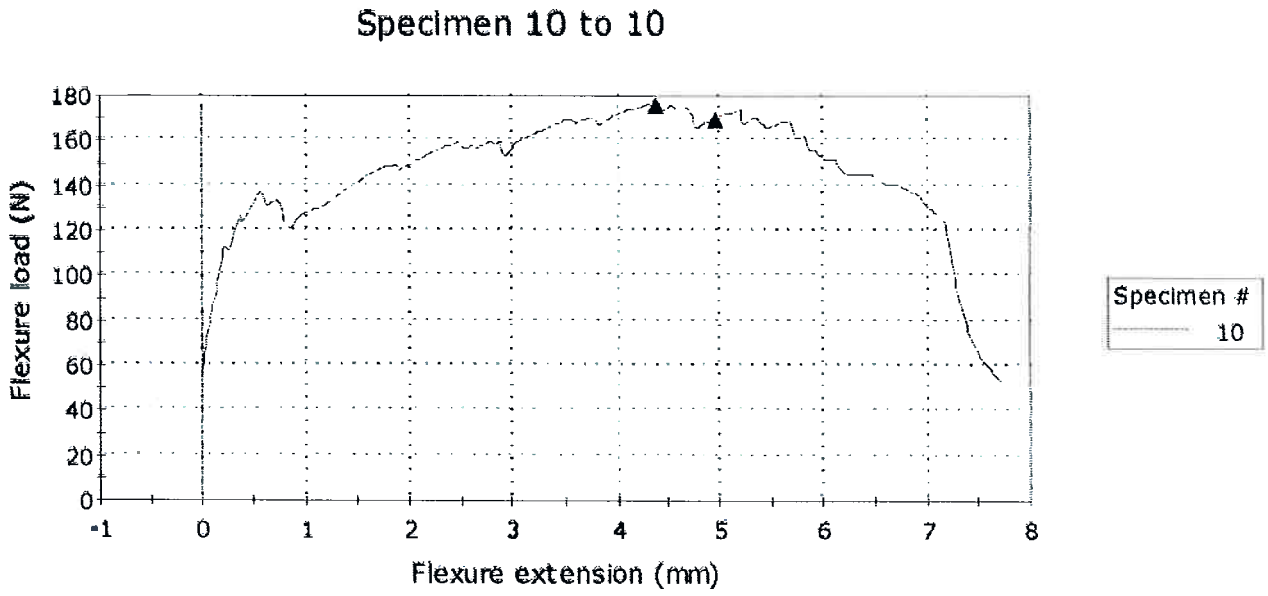
Specimen 10 to 10
Flexure load (N)
180
160
140
120
100
80
60
40
20
0
-1
0
1
2
3
4
5
6
7
8
Flexure extension (mm)
Specimen #
10

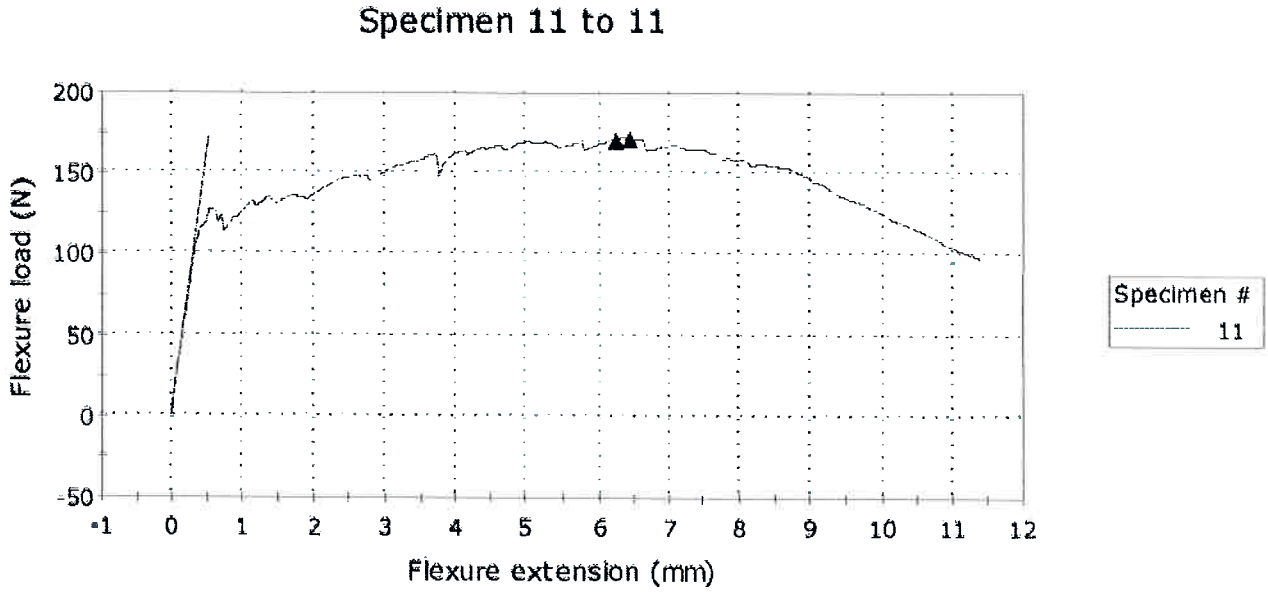
Specimen 11 to 11
Flexure load (N)
200
150
100
50
0
-50
-1
0
1
2
3
4
5
6
7
8
9
10
11
12
Flexure extension (mm)
Specimen #
11

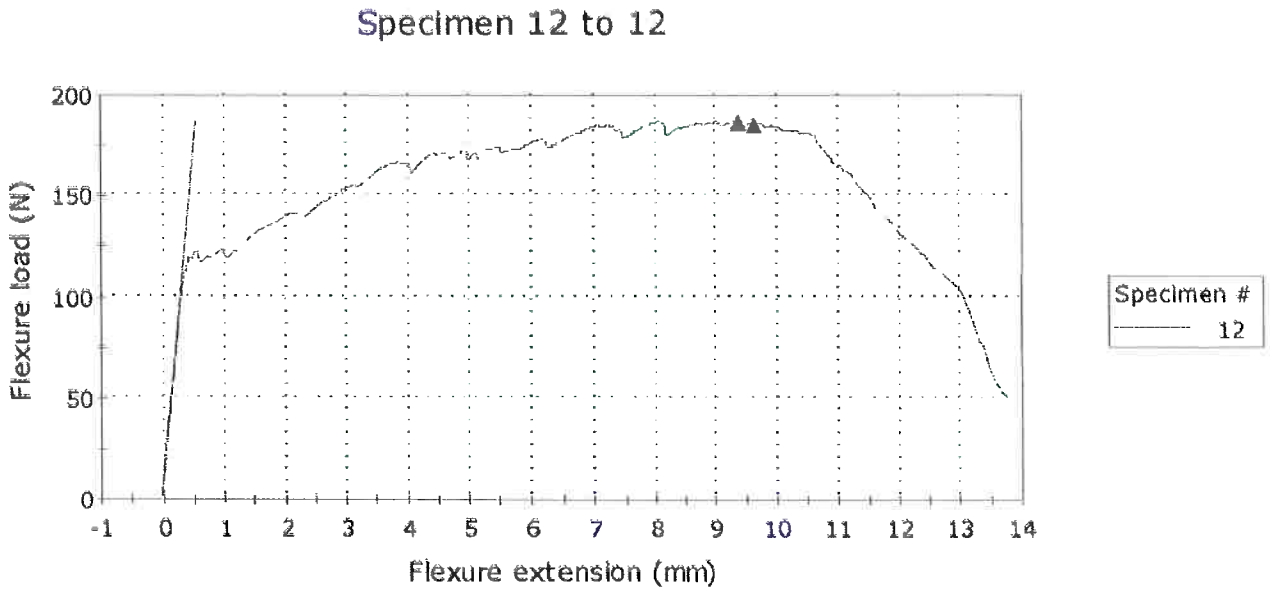

Table 14- Remarkable points of the bending test

	Flexure stress at Maximum Flexure load (MPa)	Modulus (Segment 0.5 MPa - 3 MPa) (MPa)	Maximum Flexure load (N)	Flexure extension at Maximum Flexure load (mm)
1	13.79836	13720.90098	187.51445	7.63185
2	12.11688	11924.32224	164.66376	7.24289
3	12.37586	12720.38979	168.18325	3.98244
4	13.54522	17336.89496	173.91527	5.83020
5	11.21014	10542.63324	167.76402	3.44349
6	12.00082	11329.05691	169.48019	4.86427
7	12.16623	7891.42286	167.06465	3.04391
8	11.10707	19716398.31262	154.58456	3.29747
9	12.41845	12822.08279	169.85892	7.30790
10	12.82184	-5906141.28849	175.96525	4.37214
11	12.20885	13003.39152	171.08266	6.43941
12	13.93494	14761.22082	186.49691	9.37841

IV.3. Dolsan samples

Bending test of planar sheet with a speed rate of 1,5 $mm.mn^{-1}$

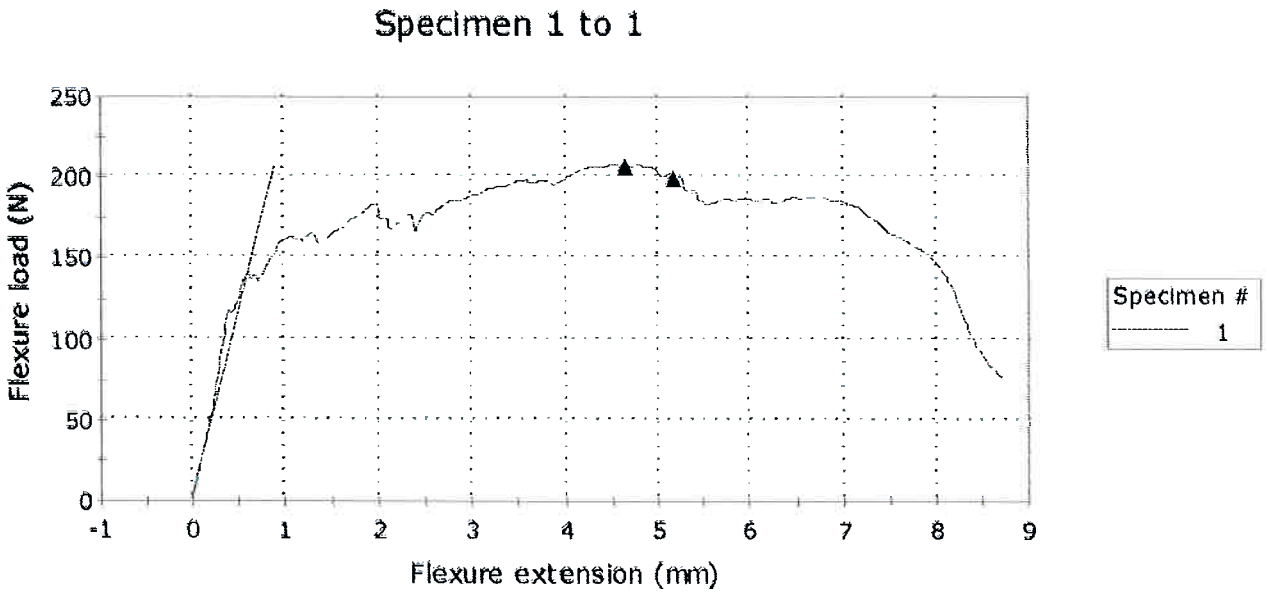

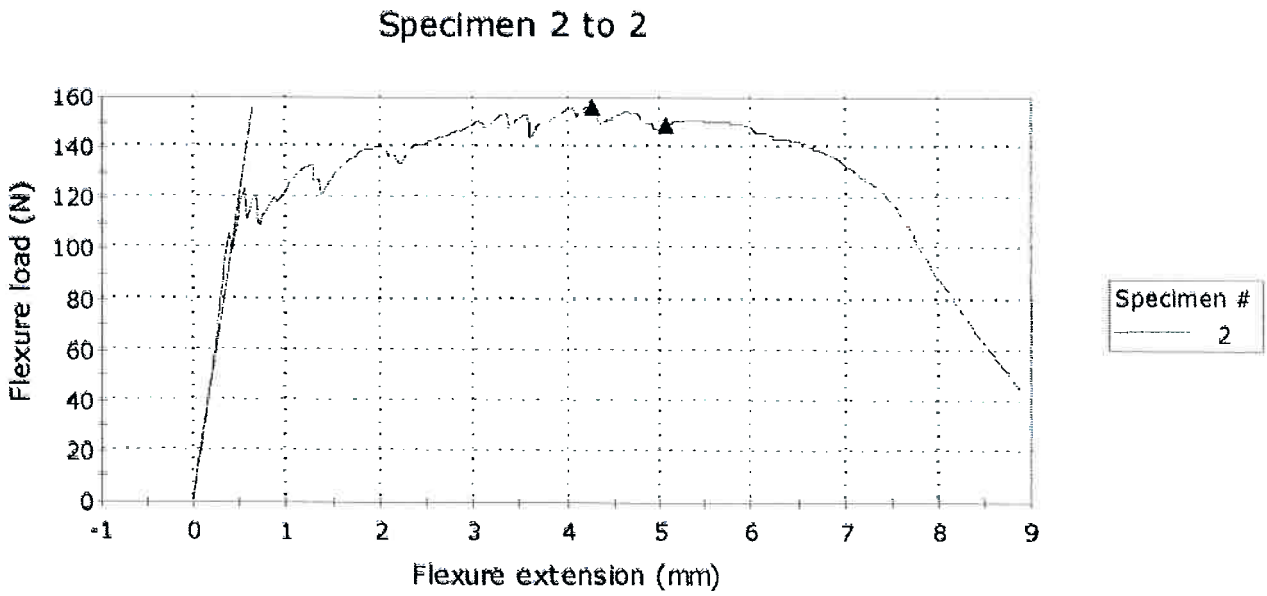

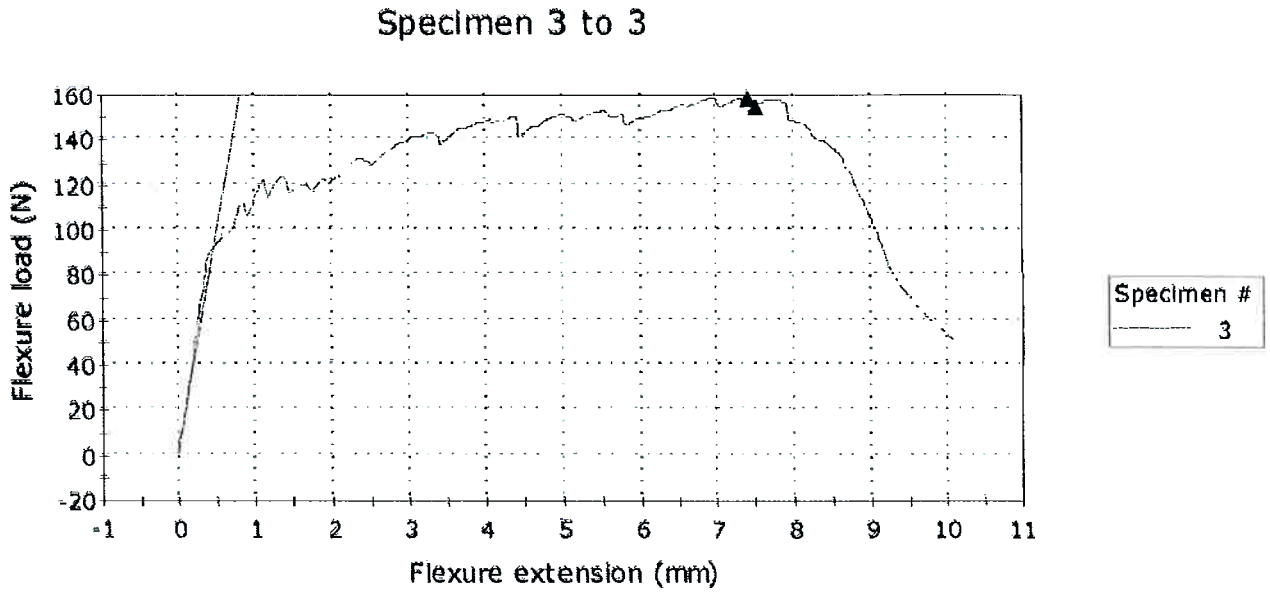
Specimen 3 to 3
Flexure load (N)
160
140
120
100
80
60
40
20
0
-20
-1
0
1
2
3
4
5
6
7
8
9
10
11
Flexure extension (mm)
Specimen #
3

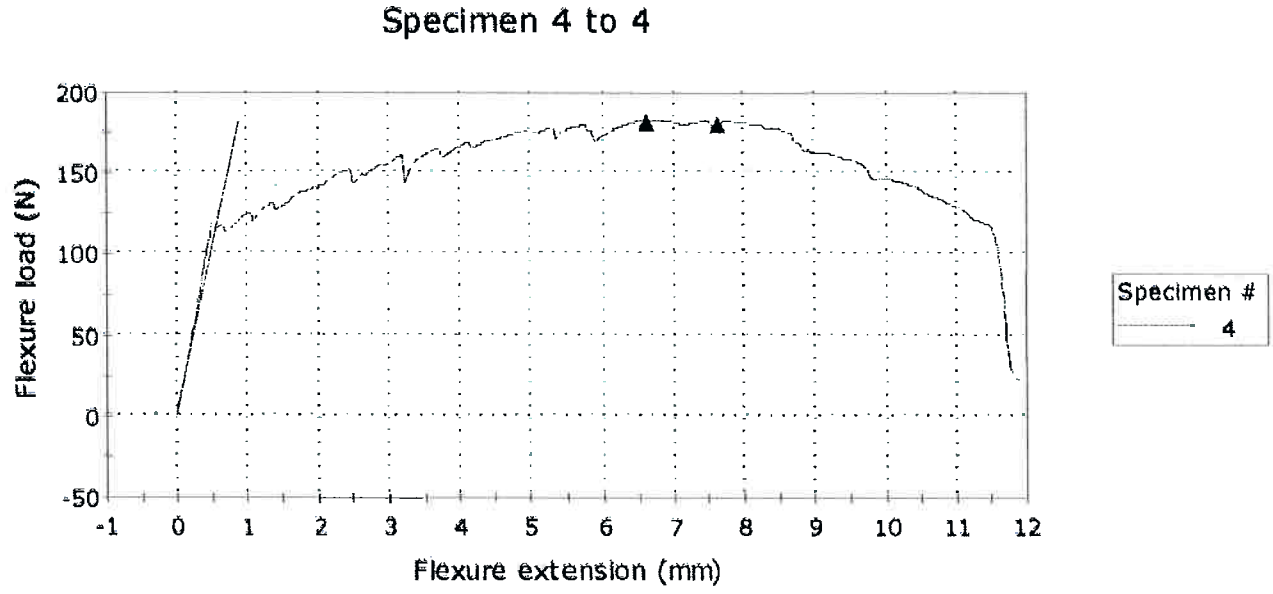
Specimen 4 to 4
Flexure load (N)
200
150
100
50
0
-50
-1
0
1
2
3
4
5
6
7
8
9
10
11
12
Flexure extension (mm)
Specimen #
4

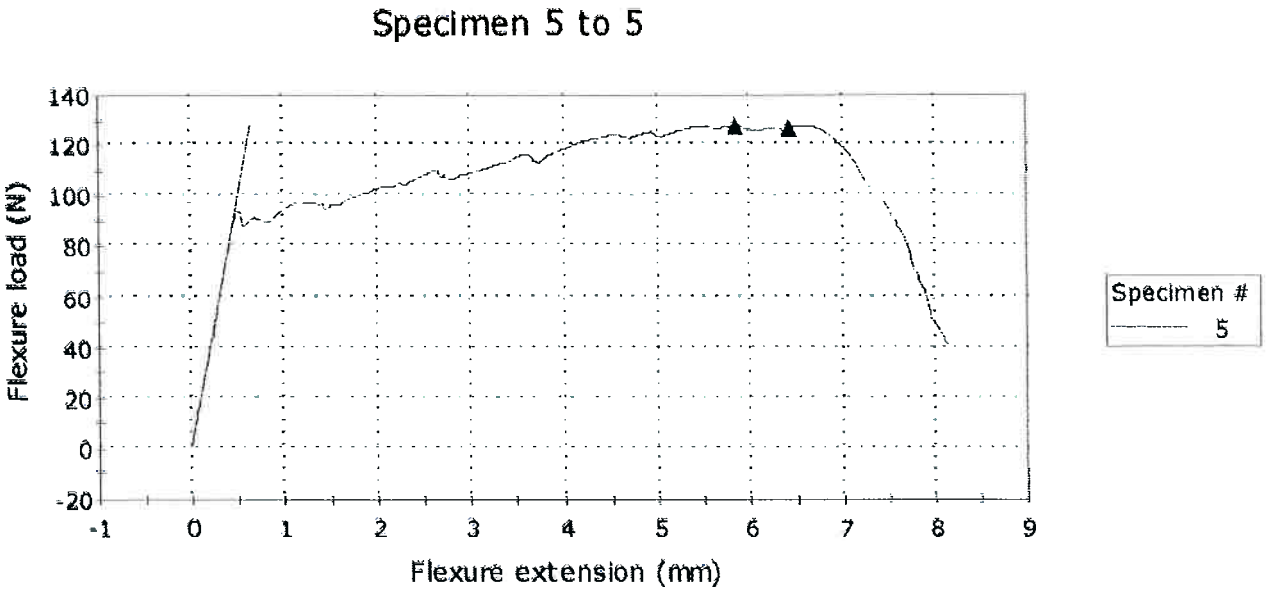
Specimen 5 to 5
Flexure load (N)
140
120
100
80
60
40
20
0
-20
-1
0
1
2
3
4
5
6
7
8
9
Flexure extension (mm)
Specimen #
5

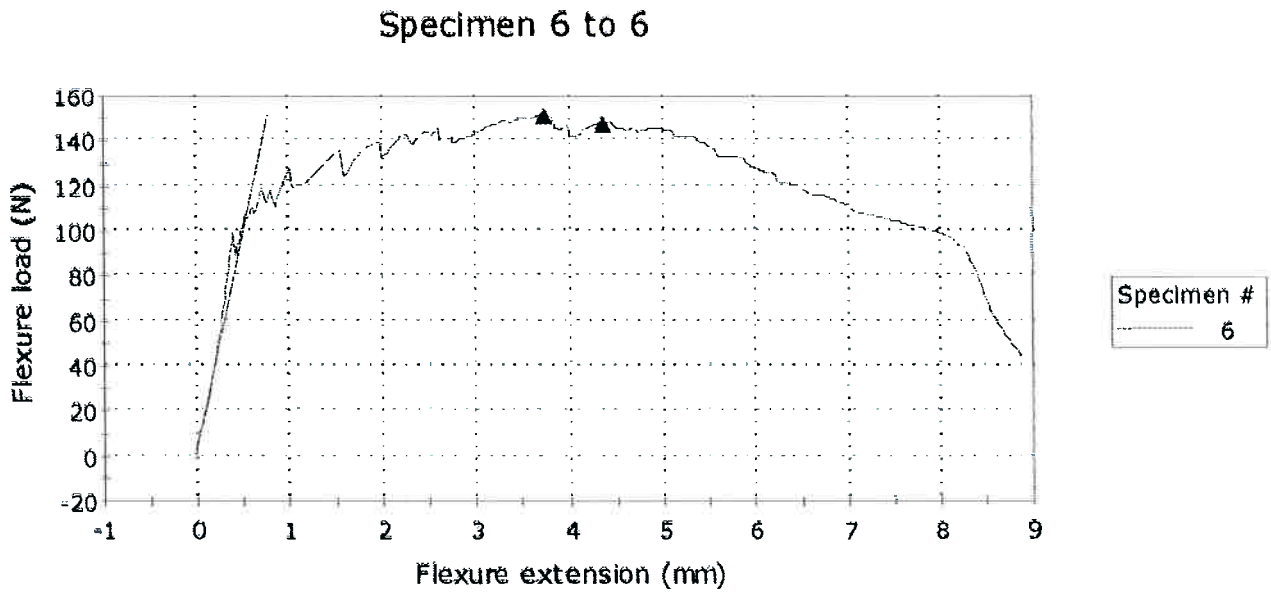
Specimen 6 to 6
Flexure load (N)
160
140
120
100
80
60
40
20
0
-20
-1
0
1
2
3
4
5
6
7
8
9
Flexure extension (mm)
Specimen #
6

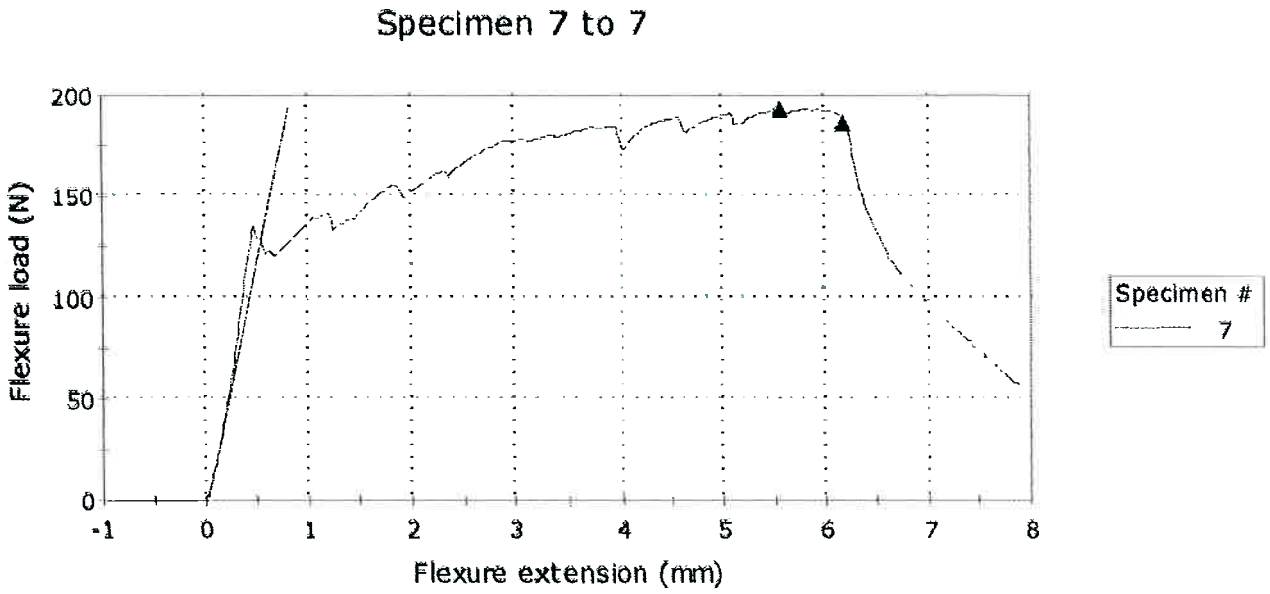
Specimen 7 to 7
Flexure load (N)
200
150
100
50
0
-1
0
1
2
3
4
5
6
7
8
Flexure extension (mm)
Specimen #
7

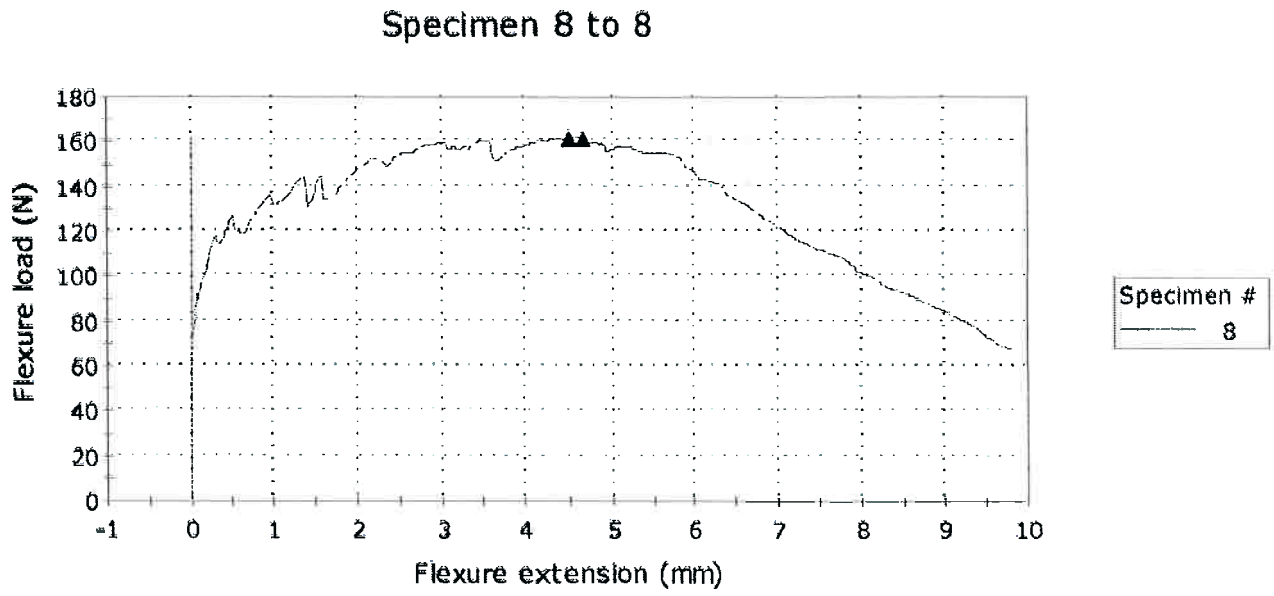
Specimen 8 to 8
Flexure load (N)
180
160
140
120
100
80
60
40
20
0
-1
0
1
2
3
4
5
6
7
8
9
10
Flexure extension (mm)
Specimen #
8

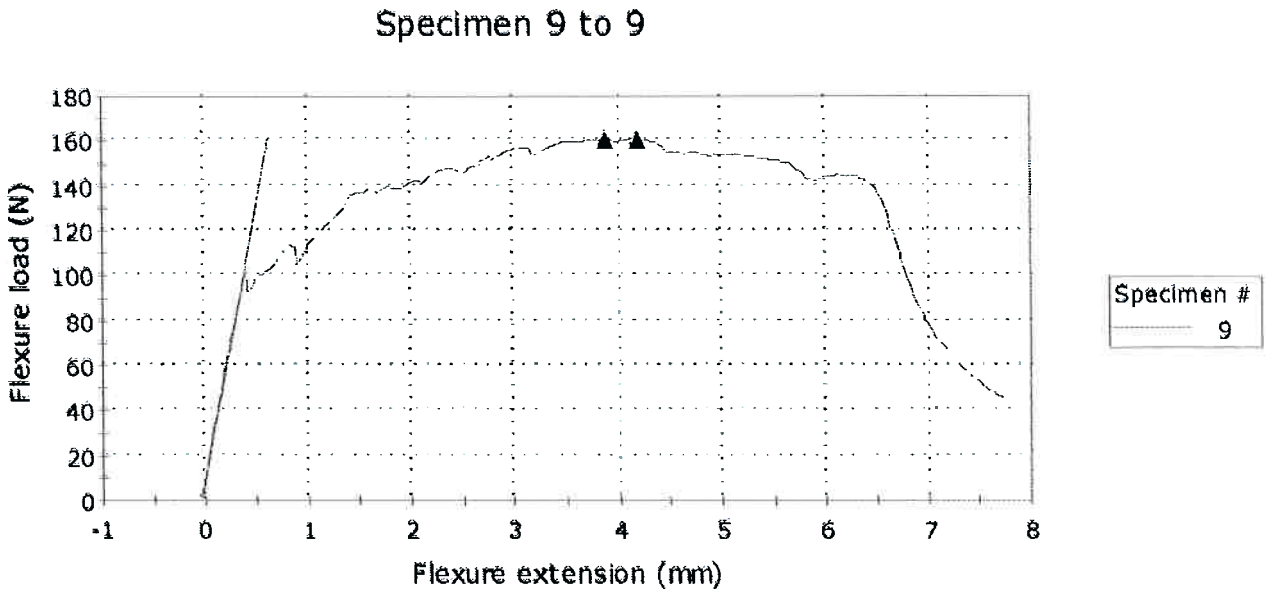
Specimen 9 to 9
Flexure load (N)
180
160
140
120
100
80
60
40
20
0
-1
0
1
2
3
4
5
6
7
8
Flexure extension (mm)
Specimen #
9

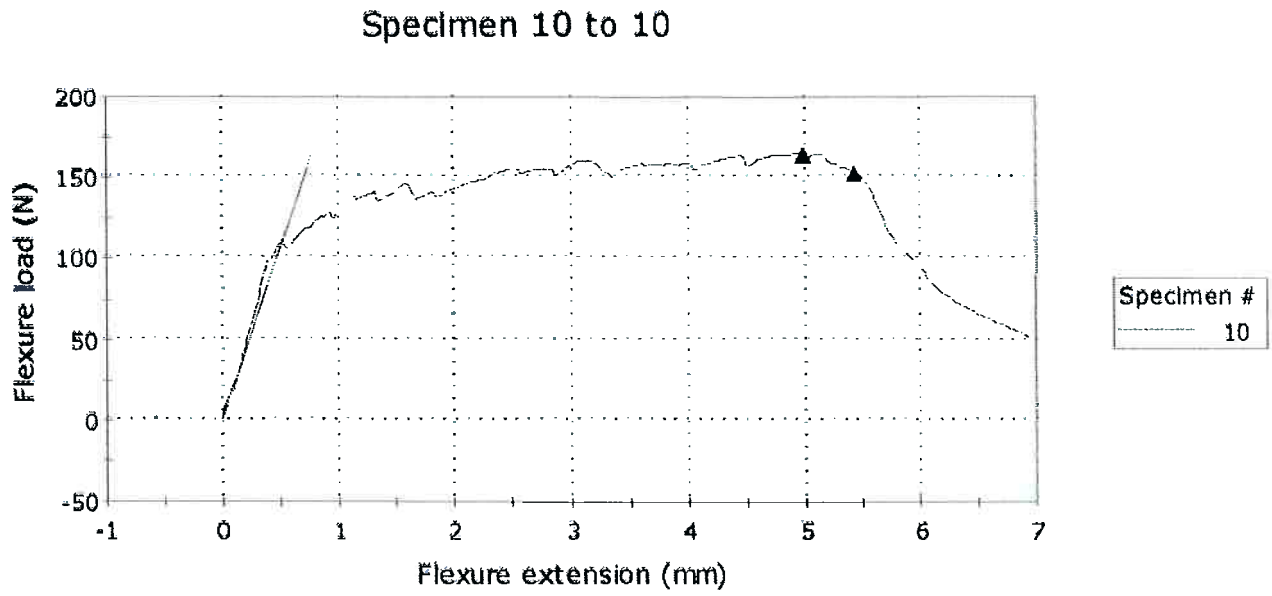
Specimen 10 to 10
Flexure load (N)
200
150
100
50
0
-50
-1
0
1
2
3
4
5
6
7
Flexure extension (mm)
Specimen #
10

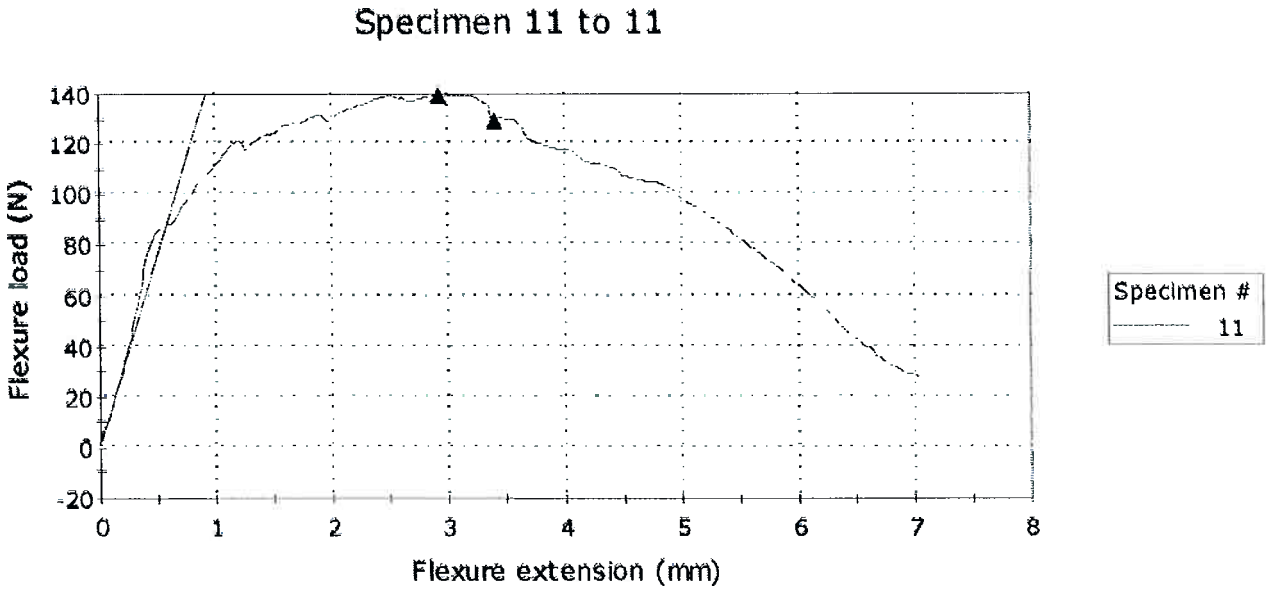
Specimen 11 to 11
Flexure load (N)
140
120
100
80
60
40
20
0
-20
0
1
2
3
4
5
6
7
8
Flexure extension (mm)
Specimen #
11

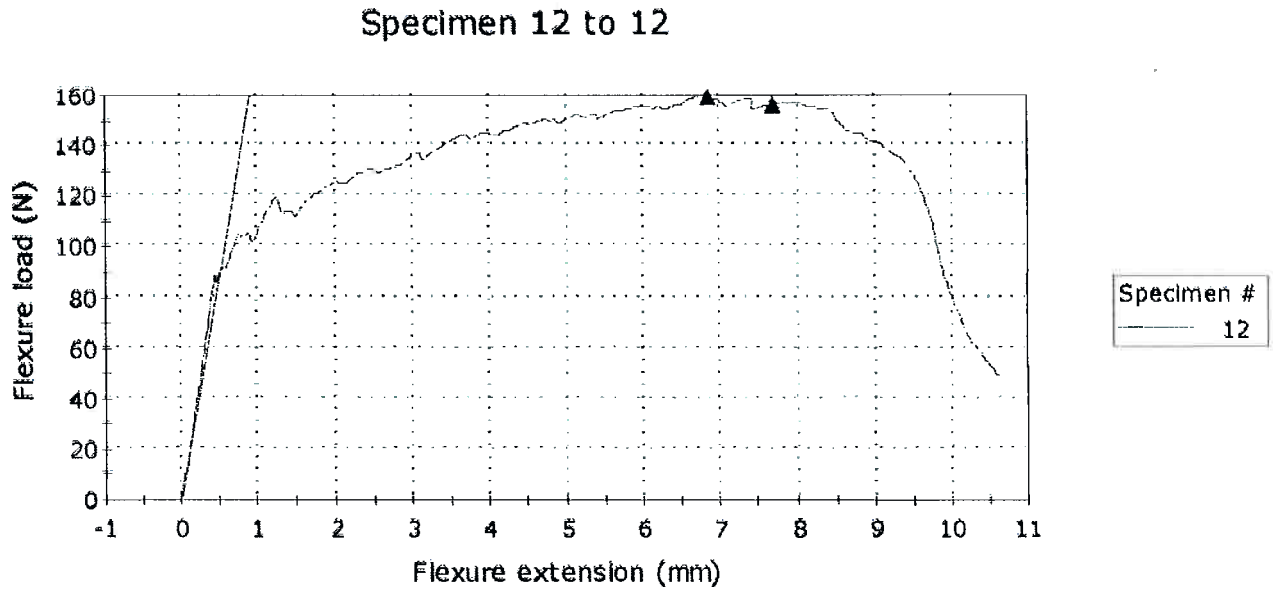
Specimen 12 to 12
Flexure load (N)
160
140
120
100
80
60
40
20
0
-1
0
1
2
3
4
5
6
7
8
9
10
11
Flexure extension (mm)
Specimen #
12

Table 15- Remarkable points of the bending test curves

	Flexure stress at Maximum Flexure load (MPa)	Modulus (Segment 0.5 MPa - 3 MPa) (MPa)	Maximum Flexure load (N)	Flexure extension at Maximum Flexure load (mm)
1	15.27650	9809.24777	207.02326	4.62718
2	12.21530	11097.34192	155.64406	4.26868
3	12.77422	9283.98816	157.91237	7.40628
4	13.77730	9083.73393	181.87079	6.61209
5	10.71133	10357.99358	126.87805	5.83735
6	11.68457	8876.43023	150.75356	3.73920
7	13.61192	9743.49350	192.58139	5.55895
8	11.10215	-5682433.21387	161.63610	4.65652
9	12.69274	11606.41342	160.19982	3.87455
10	11.81425	8787.42389	164.10904	4.98911
11	11.12802	7341.87221	139.01781	2.92896
12	12.98968	8920.96455	159.34664	6.85665